Shear characterisation of a novel woven solar cell integrated textile for tensile structures application

MSc Thesis Report

Stephanie Ramos

Delft University of Technology

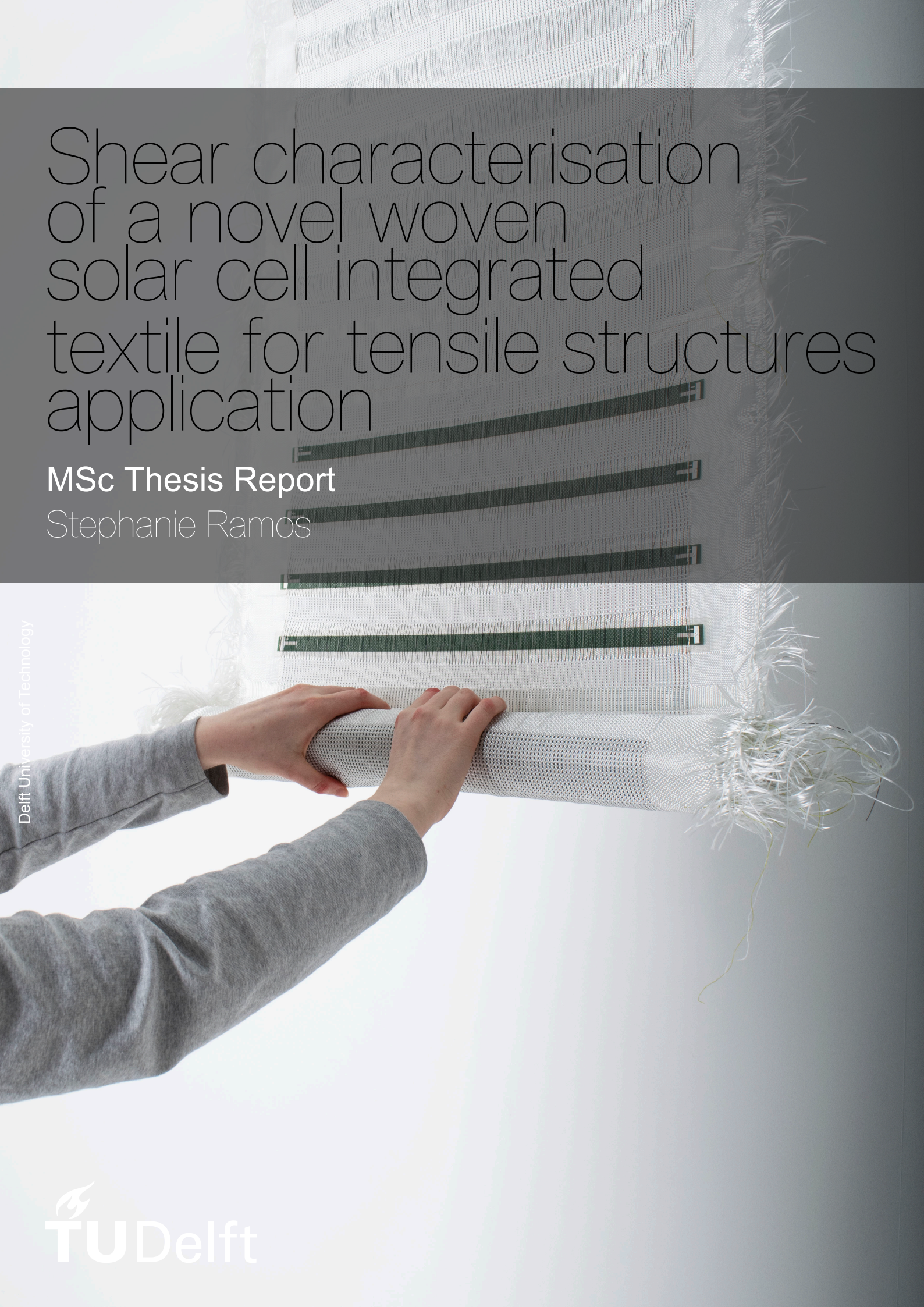

TU Delft

page left blank on purpose

Shear characterisation of a novel woven solar cell integrated textile for tensile structures application

by

Stephanie Ramos

to obtain the degree of Master of Science at the Delft University of Technology,
to be defended publicly on Monday 30th January, 2023 at 13:45.

Student number: 5138760
Project duration: March, 2022 – December, 2022
Thesis committee:

Dr. M.A. Popescu,	TU Delft, Chair of Committee
Dr. F. Kavoura,	TU Delft, Supervisor
Dr. R. Esposito,	TU Delft
Ir. R. Houtman ,	Tentech, Supervisor

This thesis is confidential and cannot be made public until December 31, 2023.

Cover: Suntex weaving trial 2, Pauline Van Dongen Studio

An electronic version of this thesis is available at http://repository.tudelft.nl/.

TU Delft PAULINE VAN DONGEN TEN TECH

Preface

This project allowed me to apply my knowledge to an unfamiliar material/field and helped me gain confidence in my engineering competencies. I have found it interesting since the first time I heard of it and I immediately wanted to challenge myself and contribute to the development of this new material. I am now sure the knowledge gained during these months will be useful for my future projects.

Coming to the end of the research I must look back and think of all the difficult steps that got me here. It is a nice opportunity for self-reflection over life achievements during the period of this research but also an opportunity to take a step back and look at this process from a different perspective and think about how to improve personally and professionally.

I would like to mention the people that contributed to this research and take the opportunity to thank them. My defence committee for all the support and precious feedback. Rogier for the opportunity, the support and the guidance. Evi, Firas, Ahmed and Ewout for each small and big contribution. Pauline, Ellen and Anna for the support and the knowledge you shared with me. Giorgos for all the technical support during experiments.

This report concludes my student life at the faculty of Civil Engineering at Delft University of Technology. It is the last chapter of an exciting and interesting but very difficult journey. The past two years, at TU Delft, have allowed me to grow professionally and personally, in ways I could have never imagined. I am proud of what I have achieved and I feel excited for the next chapter of my life and prepared for the challenges the future holds for me. This achievement, however, is not only mine. I must mention a few people that have been around and made this adventure more meaningful on a personal level.

I am extremely grateful to my family who has supported me not only financially but most importantly emotionally. Obrigada Mãe. Luitza, the one that has always believed in me and has always been there for me. Joris, the person that has slowly become my family and my anchor: I am forever grateful for your support. Cecilia, the person that brings a little bit of lightness into my life, thank you. Sofia, Amey and Firas, our conversations, shared emotions and fun times helped me keep sane over the past years. My *schoonfamilie* that helped me feel at home, far from my own, thank you. U-BASE for allowing me to meet amazing people, and finally all my amazing friends: thank you for all the fun I had over the past years. I will always keep those memories close to my heart.

Lastly, thank you Stephanie from the past and good luck Stephanie from the future.

Stephanie Ramos
Delft, January 2023

Abstract

Tensioned membrane structures are increasingly in demand, because of their ability to cover large spaces with minimum use of material. The material's mechanical properties play a key role in the design of such structures. The shear behaviour is one of the main influential properties of woven textiles during complex deformations, such as the ones in doubly curved structures where the change in curvature challenges the shear-bearing capacity of the textile during its service life.

This study provides a methodology to characterise a novel uncoated woven solar cell integrated textile for tensile structure application. It consists of investigating the limit angle, that avoids damage to the inserted solar strips, and the determination of the shear stiffness of the material. To evaluate the applicability of the material, different mechanical properties are assessed. Mono-axial, picture frame and bi-axial tests were used to determine the strength, elasticity and shear modulus. All results, have been validated by comparison with existing experimental data of similar architectural textiles.

When investigating the damage to the Organic Photo Voltaic (OPV) strips, the limit angle is defined by the space needed to avoid stresses caused by the weave in the strips. In case of large shear deformations, the OPV can undergo compression stresses due to the shortening of the float length. The imposed limit of 5mm has not been reached during testing. Hence, the OPV strips will not undergo any compressive stress up to 27 degrees of shearing angle.

The textile strength was assessed according to EN 13934-1 (Textiles — Tensile properties of fabrics - Part 1: Determination of maximum force and elongation at maximum force using the strip method). The warp strength results in 280 daN/5cm, while the weft strength results in 340 daN/5cm. Warp strength results in smaller than 300 daN/5cm, considered a lower boundary needed for practical architectural applications (architectural textiles type I). Suggestion on possible strength improvements were made: optimisation of mono-filaments in the warp direction is needed to achieve higher strength.

Norms for the assessment under biaxial stress for uncoated textiles applied as structural membranes do not exist. The elastic modulus of the novel uncoated textile was assessed following the normative for coated materials as a guideline, EN 17117 - 1 (Rubber or plastics-coated fabrics - Mechanical test methods under biaxial stress states - Part 1: Tensile stiffness properties). The elastic modulus of the studied textile results in $E_w = 310kN/m$ in the warp direction and $E_f = 290kN/m$ in the weft direction. The obtained results can be adopted in preliminary designs as they are in the expected range for a type I textile, which is $E = 250 - 350kN/m$. However, the low number of tested specimens makes the results not reliable; therefore it is recommended to test the material with project-specific bi-axial cycling loads as the parameter is related directly to the load history.

The assessment of the shear behaviour of an uncoated material is not yet normalised and its presence in literature is scarce. One of the difficulties faced during the research was understanding the shear angle behaviour of the textile after performing the tests. A change of curvature was observed in all specimens for an angle between 5 and 10 degrees. The behaviour can be due to different reasons: the improperly designed frame or the paint applied for the Digital image Correlation (DIC) measurement could have influenced the results. The material could also have an initial higher resistance to shear which decreases once the yarns start to elongate and the crimp becomes consecutively lower. Further investigations are recommended to conclude.

A bilinear regression analysis was applied to assess the material's shear modulus following literature examples. It was concluded that the material's shear modulus results in $42kN/m$ for shear angles between 0 and 2.5 degrees, and $17kN/m$ for angles between 2.5 and 27 degrees.

Membrane structures are a relatively new type of construction, therefore, technical guidance and recommendations on matters of design, specification and testing information tend to be available for more specific rather than general purposes. Especially for tensile structures, the common practice is to use coated textiles due to their high strength and weather-resistant properties. The desire to use an innovative and uncoated material, such as Suntex, for tensile structures applications comes with difficulties in terms of characterisation. Membrane properties determined in preliminary tests are helpful to be used in the early stages of the design. However, in a later stage, when the design is fixed, it is better to determine the mechanical properties based on the project and its specific load range.

This research introduces a method of investigation of shear properties of uncoated textiles that can be followed to evaluate other uncoated textiles. In addition, it is now possible to start a preliminary design of a tensile structure with the newly developed material. It is the first step in the introduction of the new building material.

Keywords: textile architecture, solar textile, tensile structures, shear behaviour, mechanical properties, uncoated textile.

Contents

1 Introduction

1.1. Problem Statement

The built environment has a significant impact on many sectors of the economy, on local jobs and on quality of life. It requires vast amounts of resources and accounts for about 50% of all extracted material. The construction sector is responsible for over 35% of the EU's total waste generation. Greenhouse gas emissions from material extraction, manufacturing of construction products, as well as construction and renovation of buildings are estimated at 5-12% of total national GHG emissions. Greater material efficiency could save 80% of those emissions [9]. In order to achieve Paris Agreement, buildings must become climate-positive by producing their own renewable energy, and become climate-proof through intelligent thermal management [14].

Solar energy, today's cheapest energy source, holds great promise for a sustainable future. One of the characteristics of solar systems is that they are decentralised with the installations for the production of energy located closer to the place of energy consumption. This factor has become particularly appealing in light of the uncertainty of the global energy market in 2022. However, solar panels on the roofs of homes and offices alone, especially in high-rise buildings, are insufficient to meet the energy demand [10].

New generations of thin-film solar cells mark a turning point in solar harvesting possibilities for buildings. These solar films are lightweight and flexible and can be custom fit for many more applications, such as applying them on existing building surfaces, including low-load-capacity roofs and curved surfaces, or integrating them into other flexible materials like textiles.

Textile is an inherently sustainable building material because it is lightweight. Its flexibility provides great design freedom and its transparency makes it very suitable for facade cladding, maintaining views to the outside while providing solar shading and many other architectural applications [14].

Combining thin-film solar technology with textiles is not new and the solutions range from highly experimental lab-stage research to more applied approaches that are already commercially available. The simplest, most common approach is to attach the flexible solar panel to the surface of the textile, for example through glueing, sewing or laminating. However, these assembly processes are difficult to scale industrially and present limitations for architectural applications in terms of mechanical properties, modularity and design potential. To date, this method is used commercially within an architectural context by the US-based company Pvilion.

Suntex, an architectural textile currently under development, takes a different approach. Thin-film solar panels and electrical circuits are integral to the construction of the textile by being directly combined in the weaving process. With the aim of being both a standardised and easily customized architectural textile that increases the energy-harvesting potential of otherwise untapped surface area [14].

Figure 1.1: A woven solar integrated textile currently under development [Pauline van Dongen Studio]

An iterative process between stakeholders' wishes and market needs must be followed when developing a construction material of any kind. The necessary steps to put a new material into the market include research and testing on strength, stiffness, stress, temperature and much more. Usually, all the material characteristics are mentioned in Eurocodes, which also provide common rules and standardisation for the design of constructions [32].

When focusing on textiles, testing standards are missing, especially regarding shear testing and acknowledgement of shear characteristics. Textiles are considered membranes as their out-of-plane bending stiffness is zero and membrane structures usually lack information on shear stiffness. Yet, when designing a double curvature tensile structure, shear stress must be considered because of the different orientations of the curvatures.

This thesis focuses on the material characterisation of a woven solar cell integrated textile to understand its applicability in tensile structures, especially double curved structured. This chapter introduces the knowledge gap, background knowledge and the scope of the research.

1.1.1. Woven Textile

The term *woven* refers to how the fabric is formed: by weaving, meaning interlacing two or more threads at right angles to one another. Those threads are called *yarns*. A yarn is made of continuous or stretchable fibres with diameters typically in the order of micron meters (μm).

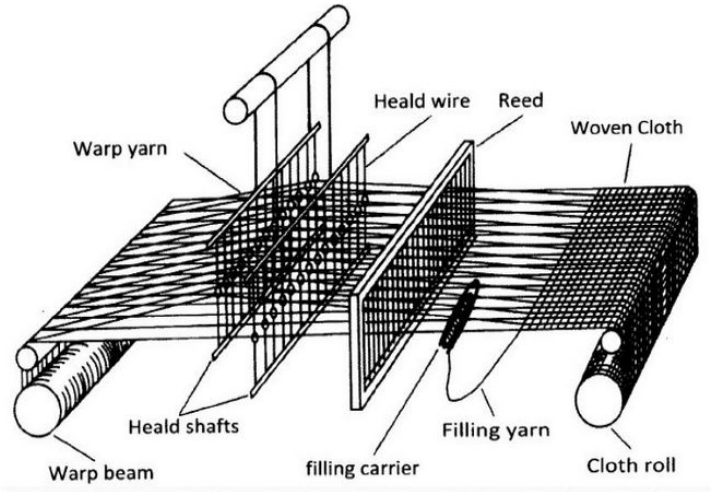

Figure 1.2: Weaving loom [4]

Woven fabrics are often created on a loom (Figure 1.2), and made of many yarns woven on a *warp* and a *weft* direction. Warp being the yarns along the length of the fabric and weft the yarns perpendicular to the warp as seen in Figure 1.3.

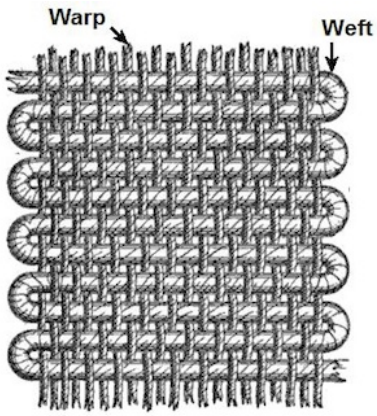

Figure 1.3: Woven textile structure [4]

Figure 1.3, refers to a plain weave pattern. Many other types of patterns can be done by interlacing warp and weft differently. Some examples:

- Plain Weave: the simplest, most basic type of weave pattern, assembled by the weft thread running through the warp thread in an 'over and under' sequence.
- Basket Weave: similar to plain weave but uses two or more warp and weft threads combined and woven as one. This creates a more textured fabric with an emphasized checkerboard appearance.
- Twill: This type of weave creates a pattern of diagonal lines, or ribs, by passing the weft yarn under and over several warp yarns in an alternating pattern.

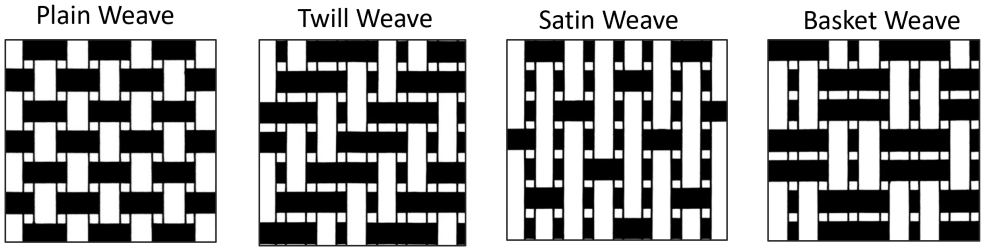

Figure 1.4: Example of weave patterns [4]

The development of weaving began in ancient Egypt around 34th BC. Textiles were first produced for home goods, people produced them to meet their own needs. Industrialised production began in Leiden, The Netherlands, around the 14th century AC. During the Industrial Revolution, textiles could be produced more cheaply and in much larger quantities thanks to the mechanically driven loom and various technological inventions that led to a different role for the worker in the process [38].

To this date, weaving still requires lengthy and precise human labour for many stages. An example of a weaving process is reported below. It regards the analysed textile of this thesis, the aim is to clarify the forming process. Suntex is not yet in the stage of mass production therefore many stages of the weaving process are naturally slower as the weaves are hand-made.

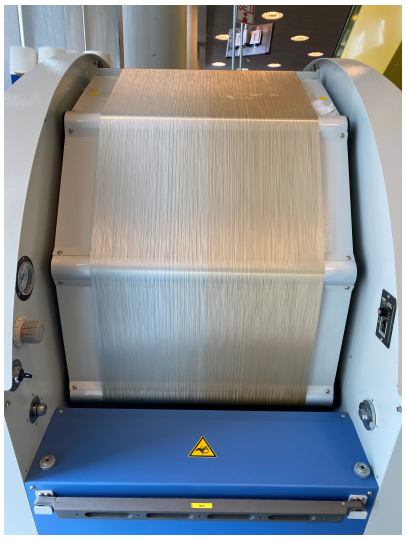

Figure 1.5: The yarn rotates around a spinning machine and the warp is created

Figure 1.6: Each yarn of the warp has to pass through one heald of the correspondent shaft (see Figure 1.2)

Figure 1.7: They have then to pass through the beater (or reed), this process is also done manually

Figure 1.8: The beam containing the warp, all the shafts and the beater is then transferred to the weaving machine

Figure 1.9: Here the warp droppers need to be applied to each yarn

Figure 1.10: The height of the warp droppers represents the tension along each yarn

Figure 1.11: Weaving of weft can finally begin, in the case of Suntex the solar panels are added manually

Figure 1.12: The textile is ready

1.1.2. Textile Architecture and Tensile Structures

Textile architecture means building with textiles, ropes and steel. In most cases it consist of a primary and secondary structure. The primary structure is the supporting structure which is in most cases a steel structure but can also be made of aluminium, timber or concrete. The secondary structure is the textile membrane or foil structure [32]. It has its roots in the oldest forms of human habitation and will be a significant part of the architectural future. Nowadays as more high performance textile are available, new functions and different applications of textile in architecture arise [25].

Using textile has numerous advantages:

- possibility of covering large areas of light with a reduced structural cost;
- fast and relatively simple building of temporarily structures;
- ease to adapt and move;
- the overall weight of the structure is reduced;
- contributes to the indoor climate;
- the translucency allows light to pass through;
- contributes to the acoustic isolation.

From an engineering point of view, fabric structures are thin membranes of constant thickness which, by virtue of their surface shape and inherent large deflection behaviour, are able to support the imposed loads required by building codes [19]. A few examples of textile architecture can be observed in the images below.

Figure 1.13: Allianz Stadium, Nice - France [31]

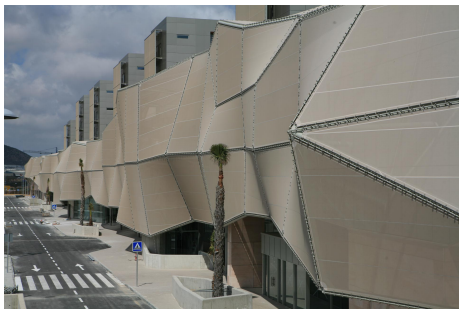

Figure 1.14: Hospital Santa Lucia, Cartagena - Spain [31]

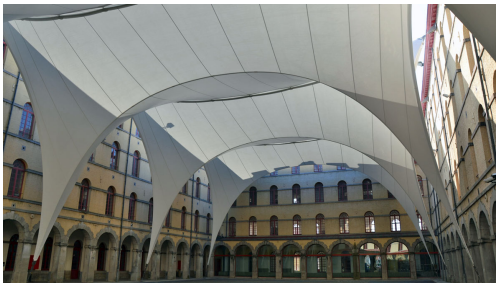

Figure 1.15: Arts Conservatory Royal Du Carré Des Arts, Monastere - Belgium [36]

Figure 1.16: Leidsche Rijn bus stop, Leiden - The Netherlands [36]

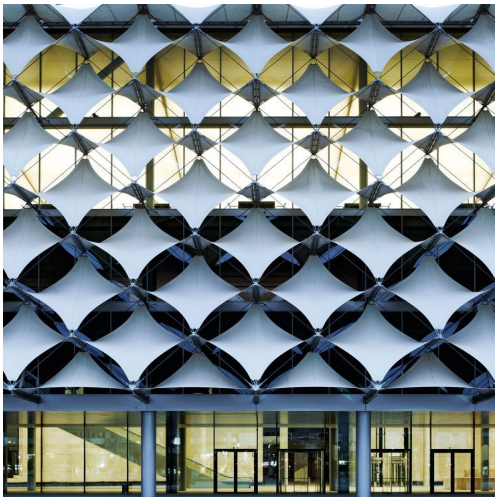

Figure 1.17: King Fahad National Library, Riyadh - Saudi Arabia [12]

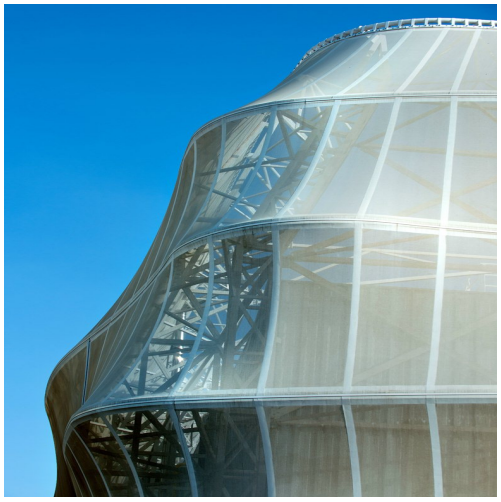

Figure 1.18: Video production Magical Media, Lleida - Spain [12]

This thesis focuses on one of the many applications of textile architecture, called *Tensile Structures*. A tensile structure is a construction of elements carrying only tension and no compression or bending. Tensile structures have their own technology, principally based on the behaviour of the material. It is a multidisciplinary cross-application engineering integrating architecture, structural mechanics, chemicals, materials science and computer technology.

Tensile structures have unique properties that most conventional building elements often do not possess simultaneously, such as low self-weight, high flexibility, translucency and the capability of forming architecturally expressive shapes. Moreover, they are known to be 'optimal' since they are only loaded in tension and adapt their shape to the flow of forces. Hence, they use a minimal amount of material to cover a space [32]. Designers of tensile structures concern themselves with three primary structural factors: choice of surface shape, levels of prestressing and surface deformability [19].

The first examples of modern tensile structures were designed thanks to the research activities of Frei Otto and Buckminster Fuller who are considered the fathers of lightweight structures' design. The geometry determination and the structural verification were based on physical models of different scales, mostly based on the property of soap surfaces [5]. The geometry of a membrane's surface is not defined by imposing on it a mathematically based surface of revolution as in the case of shells, rather it needs to be defined by its internal equilibrium of prestresses within a predetermined boundary support. We can think of a physical analogy being the soap film and Frei Otto experiments, where the film can only be formed within the boundary whose geometry permits tensile equilibrium, as seen in Figure 1.19.

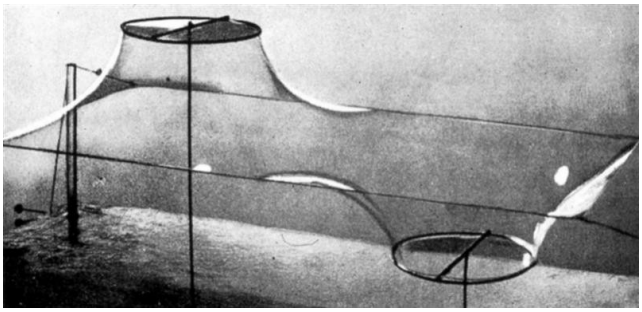

Figure 1.19: Frei Otto experiments: film de savon - an example [15]

Therefore in terms of designing fabric structures, the designer is essentially involved in choosing a set of “boundary conditions” in the process of defining the membrane’s shape. Boundary conditions are in effect the disposition of all elements that contact and provide support to the membrane, for instance, ridge and edge cables, masts, arches, beams etc. The process of determining the shape and form of the structure is commonly referred to as “form-finding”. It is an iterative process where changes and adjustments are made to the disposition of supporting elements.

The choice of the initial boundary conditions for an anticlastic surface can often be guided by the use of the relationship

$$T = pR \tag{1.1}$$

where:
T = membrane tension
p = pressure applied perpendicular to the surface
R = radius of curvature of the surface.

By using Equation 1.1 several simplifying assumptions are being made. Nevertheless, it can be a useful starting point for design as well as a simple means of checking the output of more elaborate computations. Where geometric constraints are placed upon a design, for example, flatter surface and therefore larger radii of curvature, then larger values of membrane tension will be required to control the size of the membrane’s deflections. In the limit where the surface becomes flat (radius = ∞), then applied tension and the material’s stiffness (EA) are the only parameters controlling deflection.

Membrane tension can also be considered as a type of prestress applied to the structure by pulling the membrane from opposite sides. Prestresses contribute significantly to a membrane’s stiffness. The chosen level of prestressing will normally be a compromise: low enough to reduce the work done during installation whilst sufficiently high to maintain a sufficient prestress after losses due to the creep of the membrane material over time. Actual values of prestress used in practice generally represent a small proportion of a membrane’s ultimate strength. [32]

Unlike in more conventional forms of building construction, deformability is seen as a useful and important characteristic of a tensile structure. Due to its relatively low surface stiffness (both in-plane and out-of-plane), changes in geometry are the primary response to an externally applied load coupled with changes in stress distribution throughout the structure’s surface. The developed strains within membrane material are larger than those in steel, for instance, therefore the fabric will exhibit larger deflections and geometric changes under load.

One of the benefits of textile structures is that the stresses do not rise linearly with the loads due to the geometric changes that occur on the surface. For instance, wind flowing around a conical membrane causes a “pin-ended” mast to lean into the wind allowing changes to surface curvature on the windward face to attenuate the rise in membrane stresses in that zone, but also with membrane curvatures on the leeward side acting to stabilise the mast. Heavy localised loading such as wind pressure on eaves and ridges is supported by a much larger area than simply the contact area of the pressure due to changes in surface geometry within the membrane.

Typical shapes are *synclastic*, flat and forms. Generally, synclastic structures are pneumatically and flat and anticlastic structures are mechanically prestressed. Most contemporary fabric structures have as their basis an anticlastic surface geometry. Anticlastic surfaces are those in which the centres of curvature are located on opposing sides of the surface, also called *double curvature structures*.

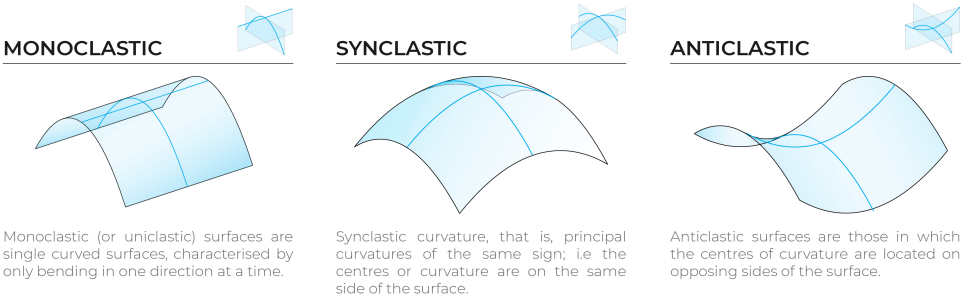

Figure 1.20: Membrane geometry

A few examples of double curvature structures can be observed in the images below.

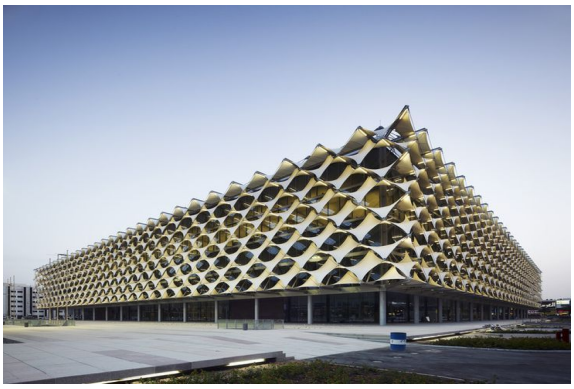

Figure 1.21: King Fahad National Library, Riyadh - Saudi Arabia [12]

Figure 1.22: Temporary exposition 2016, Amsterdam - The Netherlands [36]

Figure 1.23: The Wave car park, Cardiff - Wales [quintinlake.com]

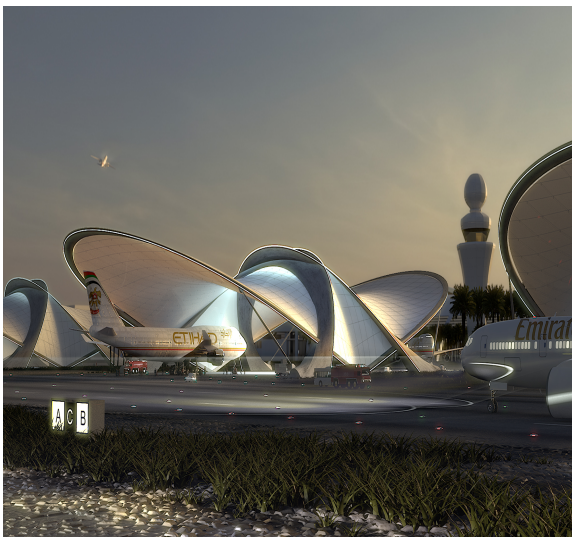

Figure 1.24: Aircraft shading, Abu Dhabi - United Arab Emirates [sl-rasch.com]

1.1.3. Textile Regulations Overview

In Europe, technical guidance and recommendations on matters of design, specification and testing of tensile structures have not yet been summarised in one document and information tends to be available for more specific rather than general purposes [19].

Today, only a few national design codes for several types of membrane structures, such as air halls, are available in some European countries (Germany, Italy and France). The industry desires a comprehensive European design code to provide verification techniques representing the latest state-of-the-art and recognized research. That is necessary to achieve a common pool of design approaches and a harmonized safety level [32]. The steps to a Eurocode for Membrane Structures have been taking place since 2013 and, according to the proposed timeline of the Joint Research Center of the European Commission, it should be ready by 2024 [32]. A review of the existing regulations on the European and Dutch levels is shown in Figure 1.25 - Figure 1.26.

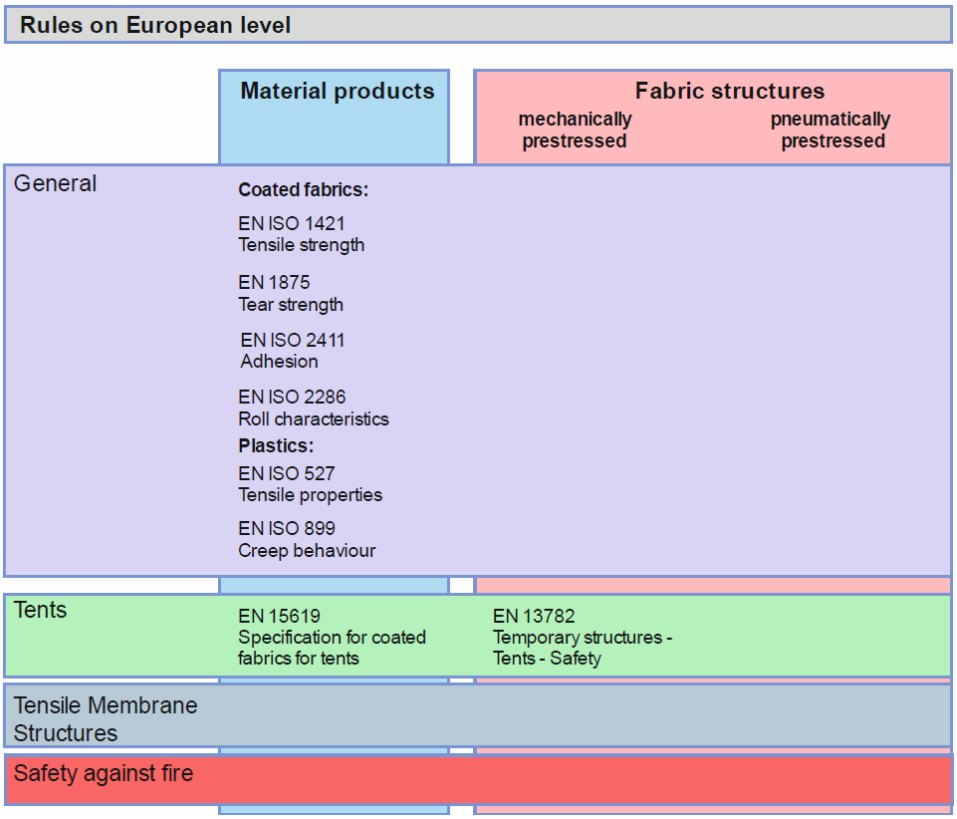

Figure 1.25: Current regulations on European level [32]

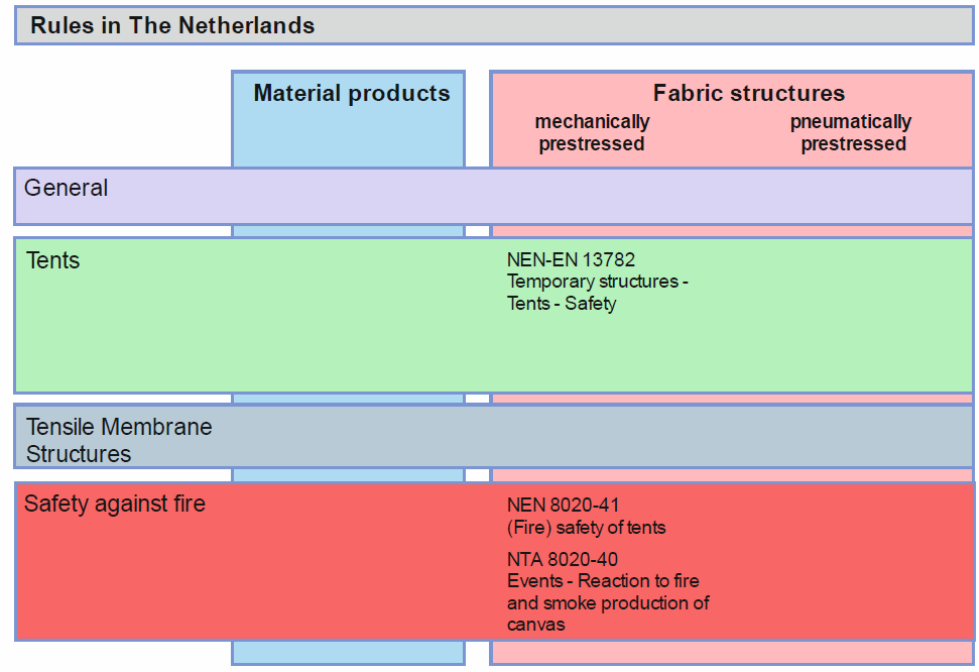

Figure 1.26: Current regulations on Dutch national codes [32]

Architectural fabrics are often woven from yarns made from Polyester (PES), Glass fibre or Polytetrafluorethylene (PTFE). Typical coating materials are Polyvinylchloride (PVC), Polytetrafluorethylene (PTFE) and silicone. The most used material combinations are:

- PVC (Polyvinylchloride)-coated Polyester(PES) fabrics (PES/PVC-fabrics),
- PTFE (Polytetrafluorethylene)-coated Glass fabrics (Glass/PTFE-fabrics).

While uncoated fabrics are usually made of:

- Polytetrafluorethylene (PTFE) or
- Polyvinylidenfluorid (PVDF).

Their tensile properties are regulated on EN ISO 13934 *Textiles — Tensile properties of fabrics* [17].

1.2. Research Questions and Objectives

The materials commonly used in fabric structures consist of a woven textile encapsulated in a polymeric coating. There are, for instance, different constructions of weave, and different weaving techniques which can include control of yarn straightness and tension which affect the strain behaviour of the finished product. Such factors need to be understood and accommodated in the engineering design and specification processes for each project [19]. Hence the need to investigate the behaviour of a newly developed textile to determine its applicability in textile architecture and tensile structures.

The main goal of this research is to determine the material characteristics of an uncoated woven solar cell integrated textile in pursuance of its application for tensile structures. To achieve this goal the research has been divided into sub-question, based on the necessary information needed to answer the main question.

How can the shear behaviour of an uncoated woven solar cell integrated textile be characterised for its application in tensile structures?

The process of answering the main research question has been divided into sub-questions:

1. Can an uncoated woven solar cell integrated textile undergoes shear deformation without damaging the solar cells?

2. What are the parameters needed for the design of a tensile structure?

    - What is the warp and weft strength of the studied textile?
    - What is the elastic modulus of the studied material?
    - What is the relation of the shear angle of a textile to its shear stiffness and what is the shear stiffness of the studied textile?

These sub-questions are important to understand the applicability of the studied material and to characterize the shear behaviour of the studied material. The applicability is mainly evaluated by comparison with a typically used textile, of which information is already available in the literature.

1.3. Research Methodology

To reach the above-mentioned objectives the following strategy has taken place.

Firstly, to understand what information was necessary and what was achievable from this research, a deep understanding of textile mechanics and a literature review about the shear behaviour of fabrics and available norms was carried out (chapter 2). As a result, to evaluate the applicability of the new textile, it is necessary to know its warp and weft strength, its elastic modulus and its shear modulus. It has been decided to perform laboratory experiments to obtain the desired information.

Uniaxial tensile strip tests are routinely carried out by manufacturers to determine the tensile strength of the fabric and are clearly defined by standards (EN ISO 1421 and EN ISO 13934-1). To identify the warp and weft strength of the studied material a tensile test was carried out on three specimens for each direction according to the code standards. Shear testing is less common and little is known about the behaviour of architectural fabrics sheared under bi-axial stress; designers generally use rules of thumb to estimate the shear characteristics of the fabric [23]. As the textile is uncoated the most suitable type of shear test is a picture frame test (section 2.2). Regarding the elastic modulus, the expertise and common practices of the engineers at Tentech have been adopted to obtain an indication of its value.

Specimens were prepared for the tests with an iterative process aimed to understand the best way to cut the available samples and tests were executed (chapter 3). Once results were available a regression analysis was performed to evaluate the shear modulus of the material (chapter 4).

All results have been validated by comparison with existing experimental data of similar architectural textiles.

1.4. Thesis Structure

The thesis report is structured as follows.

Chapter 1 contains an introduction to the problem, covering the overall background knowledge necessary to understand the research. It explains how a woven textile is formed (subsection 1.1.1) and what is textile architecture with a few image examples (subsection 1.1.2). An overview of textile regulations is given on subsection 1.1.3. The research questions and methodology is described in section 1.2 and section 1.3.

Chapter 2 contains a literature review about the shear behaviour of fabrics, available shear tests and the relation between shear angle and shear stiffness of a textile. The type of textile architecture involved in this research is tensile structures. This chapter also covers woven textile mechanics and how shear relates to the curvature of a tensile structure.

Chapter 3 regards the experimental program of the studied material. Experiments are related to warp and weft strength, elastic modulus and shear angle evaluation. The material is presented and experimental results and preparation such as sample cutting and pretension are shown.

On chapter 4 a regression analysis is carried out based on literature examples and experimental results. It is aimed to evaluate the shear stiffness of the studied material.

The answers to the research questions, main thesis contributions and recommendations for future work are treated in chapter 5.

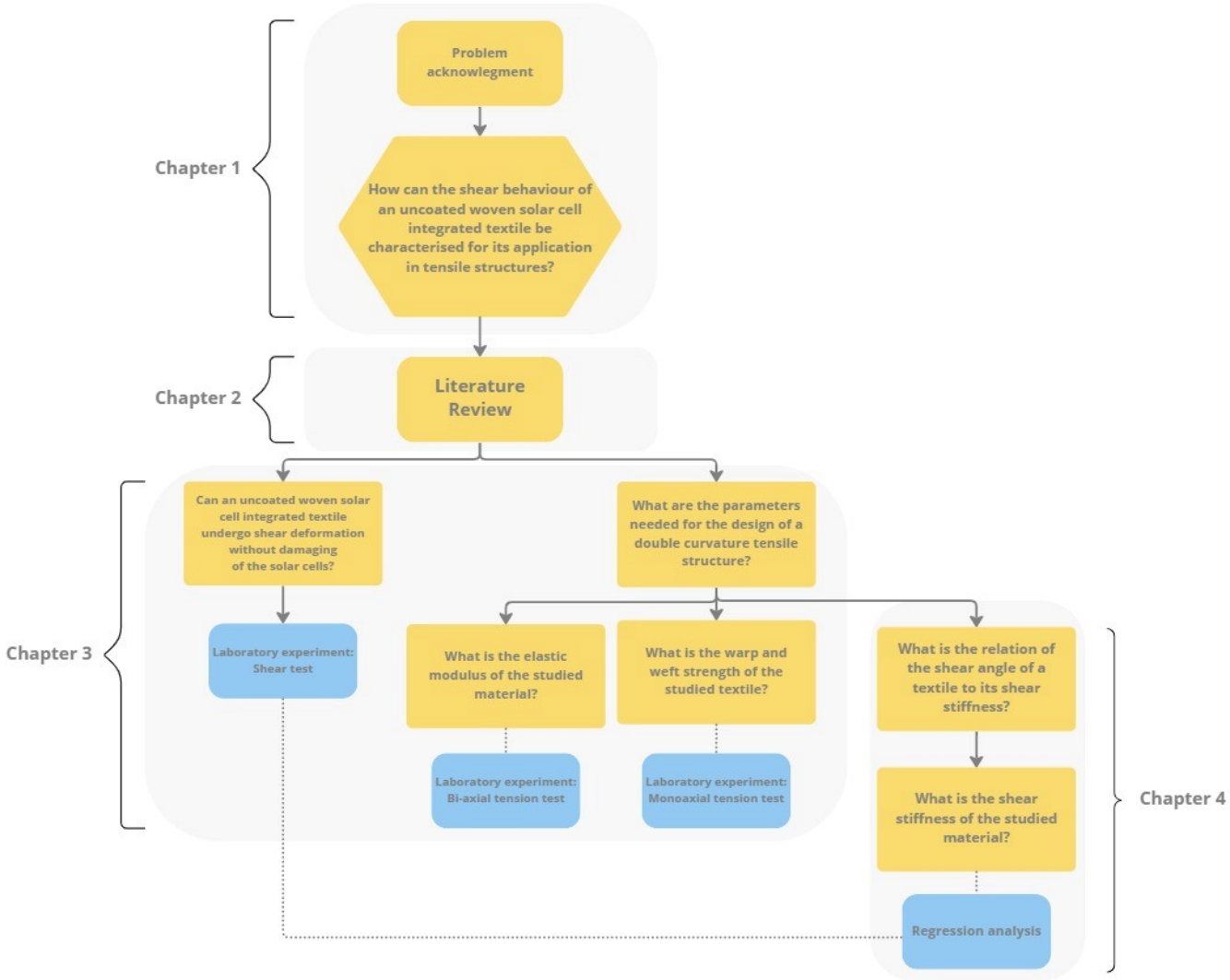

Figure 1.27: Research methodology and thesis structure

2

Literature Review

This chapter gathers information found in the state of art literature that is relevant to this research. The properties of woven fabrics are very different from conventional materials, such as bulk metals and polymers. Their irreplaceable advantages such as a high strength-to-weight ratio lead to the interest of the material community.

In literature, we can find different papers regarding the evaluation of the shear angle of engineering woven fabrics. Bias extension test, picture frame test and bi-axial frame test are the most common methods. On [3], [11] and [29] we can find examples of relation between shear angle and shear modulus by using regression analysis. However, the current knowledge of the shear behaviour of fabrics is limited and design is based on past experience. From the literature is clear that when approaching a new material, in order to know if it is compatible with the market, the norm is to test all its properties. Unfortunately, typically this is done with coated fabrics only. The state of the art is: specimen design, test procedure, constitutive relationships and valid failure criteria of composite fabrics are unavailable while desirable.

2.1. Shear Behaviour of Textiles

Woven fabrics are subjected to a wide range of complex deformations during usage but shear deformation is the dominative deformation mode in forming. The trellis-like manner in which the woven fabrics readily deform is the essential mechanical difference between woven fabrics and other sheet materials.

In woven fabrics, in-plane shear deformation is induced due to the occurrence of double curvature or more complex geometries. In-plane shear together with bending of woven fabrics crucially determines the fabric drape, which is defined as the ability of the fabric to fit onto a three-dimensional object [30]. Shear deformation also happens as a result of large deflections due to active loads such as the ones in response to wind pressure and snow load [8].

In order to understand the shear deformation of textiles it's necessary to mention the shear angle, shear stiffness and how those parameters interfere with the degree of curvature in which a structure can deform. Woven fabrics can conform to different forms by mainly shearing. This involves mainly in-plane rotation of the fibre bundles at the cross-overs of the weave, but also fibre slip and fibre buckling. Good draping involves the fitting of a fabric over a surface without wrinkling and tearing [29].

In general, when the tensile load on the fabric is not parallel or perpendicular to the yarn's directions, the warp and weft yarns are not perpendicular to each other and shear stress appears. During shear deformation, the contact between neighbouring yarns results consecutively in:

- Increase of shear stiffness
- Shear interlocking
- Wrinkling

Wrinkling is defined as buckling of the fibre bundles, which happens when the fabric is sheared locally over a certain limiting angle, the shear locking angle.

In what is considered to be the first analytical treatment on the subject of the fitting of woven cloth to surfaces [26], it was established that cloth conforms to given shapes by the fabric mesh changing from squares to rhombi which is the result of shearing strains (Figure 2.1). Although the study was related to cloth conforming to rigid surfaces and several simplifying assumptions were made to make the problem tractable, it was theoretically demonstrated that fabrics, flat in their unstressed state, must undergo shear straining to conform to shapes that do not have zero Gaussian curvature.

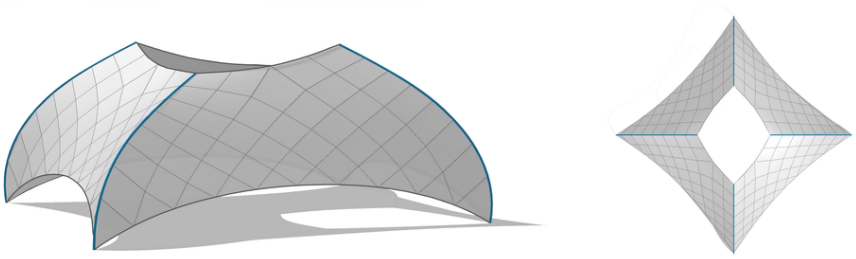

Figure 2.1: Fabric under shear: grey lines represent warp and weft directions. When the fabric is undergoing shear stresses warp and weft are not perpendicular to each other. [27]

The response of fabrics to shear is important in tensile fabric structures. This is because shear strains must exist for the necessary non-developable forms to be generated from fabric patterns that are flat in their unstressed state. Despite the importance of the shear response of fabrics in the application of tensile fabric structures, it has received little attention. Understanding and quantifying the shear behaviour of architectural fabrics is important to designers, as large shear deformations are inherent in tensile fabric structures, both during installation and under imposed loading [8].

In regards to the evaluation of the shear behaviour, there are many published researches. In literature, not only the differences and limitations of various measuring methods have been examined but also mechanical and geometrical models that simulate the shear of the woven fabrics have been developed. Woven materials can not be considered isotropic or homogeneous, as they can display non-linear and unpredictable behaviour under multiple stress states. Therefore a theoretical analysis can become very complex and experimental determination of the material behaviour becomes necessary [30]. Moreover, modelling the forming process for engineering fabrics and textile composites using a mechanical approach, such as the finite element method, requires characterisation of the material's behaviour under large shear deformation. [21].

The three major experimental methods by which the shear behaviour of thin fabrics can be evaluated are as follows:

- Kawabata Evaluation System for Fabrics (KES-F);
- Bias extension of sample cut at 45° relative to warp or weft directions;
- Picture frame method in which the fabric is held in a frame.

None of the mentioned methods can be used as a standard test method in the determination of the in-plane shear behaviour of fabrics. This is due to the fact that all the stated methods suffer from

limitations and uncertainties in exerting pure shear stress on the fabric during the test. It is therefore necessary to evaluate which test is more suitable to perform on each specific textile. Later on in this chapter all types of tests will be introduced and compared.

In [33] it is reported that a shear angle of more than 25 degrees can lead to fabric wrinkling. It was found that the shear behaviour of the fabrics along the principal directions is dependent upon the structural parameters of woven fabrics in the weft direction. The dependency of fabric shear behaviour on fabric weft density in most of the experimental samples was found to be the most important result among the findings of this work. Results confirmed that the increase in fabric weft density and weft yarn count leads to an increase in fabric shear rigidity along the principal directions.

2.1.1. Shear Angle

The stages of fabric shearing are typically three: the initial region, where shear is due to the flexural deformation of the tows; the mid-region, where shear resistance becomes dominated by a bearing load type contact; and the last region, where there is a rapid load increase due to jamming of the fabric structure. As the fabric undergoes these deformation phases, the material architecture must change so that the different phases can be accommodated.

Shear of fabrics refers to a change in the angle between perpendicular yarns. As shown in Figure 2.2, warp and weft are initially perpendicular to each other and yarn axes rotate during shear deformation. The rotation can be measured by the shear angle, which is the angle reduction from 90 degrees to an acute angle until the shear interlock limit is reached.

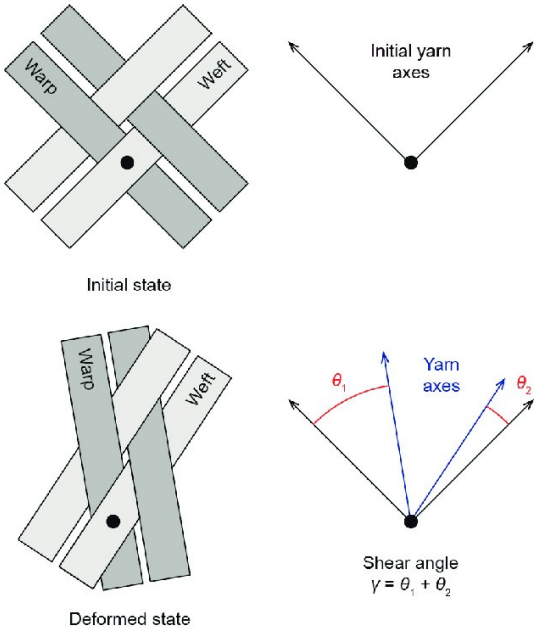

Figure 2.2: Shear deformation of yarns: changing of shear angle.[3]

Due to the woven nature of architectural fabrics contact between neighbouring yarns during shearing leads to an increase in shear stiffness, shear lock-up and subsequent wrinkling [23].

Shear interlock is a phenomenon at which an upper bound is reached when yarns of both directions become kinematically locked, as the shear rotations increase. Locking refers to the point at which the tows are no longer able to freely rotate and they begin to apply a compressive force on each other as the fabric is further deformed. The force required to deform the fabric begins to increase significantly as the locking angle is reached and surpassed. When the compression of the tows reaches a maximum, wrinkling begins to occur and the fabric begins to buckle out of plane. Wrinkling in a formed part is considered a defect, therefore undesirable [7].

Wrinkling is associated with the level of the compressive stresses which develop during the shearing of fabrics, the thickness of fabric, its stiffness and its microstructure [29]. At the microstructural level, wrinkling of fabric during shear is associated with the maximum locking shear. In plain weaves, it is assumed that the maximum shear angle at shear locking is associated with the disappearance of the macro-pores between fibre yarns.

2.1.2. Shear Stiffness

Because the fibres in woven webbings are not continuous or connected along the two principle directions, calculating the shear properties analytically can be very complex. Due to this limitation, mechanical testing is necessary to determine the shear behaviour [30]. The shear modulus of fabrics calculated from tests can be used as input data for finite elements, elastic solid mechanics simulations of draping and more [29].

When conducting biaxial tensile tests, fabrics show a highly nonlinear and anisotropic stress-strain behaviour, which strongly depends on the load ratios warp/weft and the loading history. Furthermore, the stress-strain-behaviour is highly dependent on the crimp interchange of the yams and the initial crimp value depends on the stress in the warp and weft direction that is applied during the weaving process.

The number of intersections per unit area of the fabrics is determined by fabric weft density, which has been found to be the first most influential fabric structural parameter affecting fabric shear behaviour. The weft count which affects contact surface area at intersections was found to be the second most influential structural parameter affecting fabric shear behaviour. Thus, the three independent parameters, which quite naturally influence the total friction force between warp and weft yarns at intersections, affect the shear behaviour of woven fabrics. However, univariate test results vividly confirm that the number of intersections in comparison to the surface contact area of the intersections and fibre type is the paramount influential parameter that controls the frictional coefficients between warp and weft yarns at the intersections. An increase in the weft density and the weft count leads to an increase in the fabric shear rigidity along the principal directions.

2.1.3. Degree of Curvature

The mechanical behaviour of fabrics is non-linear and time-dependent, with assumed or highly simplified material properties commonly used for analysis. The shape of a tensile structure is fundamental to its ability to resist applied loads. A canopy, for example, to resist both uplift and down-forces must be double-curved (anticlastic curvature) and prestressed. Boundary conditions determine the fabric shape and stress distribution [6].

The structural action of tensile structures depends on curvature rather than span, hence their efficiency for large-span structures. By consideration of ratios of geometric parameters and curvature (rather than span), the results of the analyses can be considered to be independent of scale.

A square hypar structure form-analysis is reported, an example from [6]. The hypar acts principally in tension between diagonally opposite corners, for the orthogonally patterned hypar this means that the fabric is acting in shear. As the shear stiffness of architectural fabrics is typically low (tensile elastic modulus divided by 20 is commonly used as a rule of thumb) an orthogonally patterned hypar will exhibit high deflections (Figure 2.3). The higher the height/side ratio, the bigger the curvature of the hypar. Figure 2.3 shows that shear stiffness, curvature and maximum deflection are related.

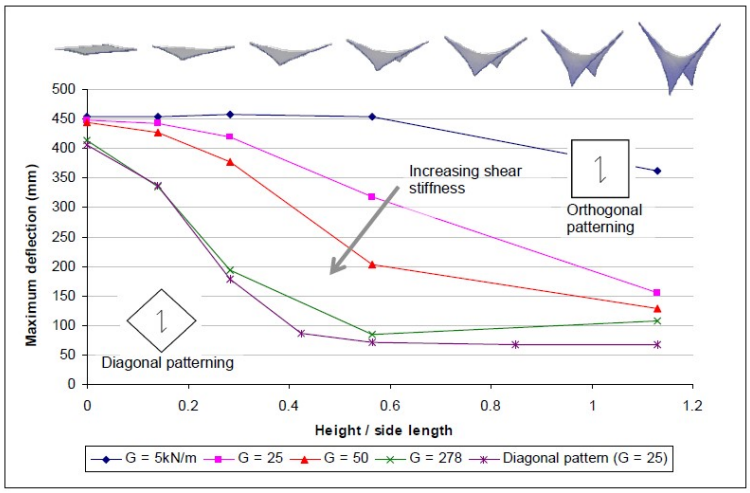

Figure 2.3: Square hypar. Variation of maximum membrane deflection due to wind uplift with form and shear modulus. Model parameters: $E_{warp} = E_{weft} = 1000kN/m$, $\nu = 0.8$. [6]

This effect is less significant for flatter structures (i.e. as height/side lengths tend to zero) when the fabric panel will be acting primarily as a two-way spanning flat panel (left-hand side of Figure 2.3). As the corner height and fabric curvature increase (right-hand side of Figure 2.3), the structure must span between diagonally opposite corners and the effect of fabric orientation and shear stiffness on deflections becomes pronounced.

Fabric structures do not have strict deflection limits such as those imposed on conventional building structures, but limits are defined by the need to avoid 'ponding', and in some cases to avoid clashes between the deflected fabric form and the supporting structure or other objects. Ponding is the build-up of snow, ice or water on the fabric canopy, in particular of meltwater in hollows formed by snow loading. It is therefore vital to ensure that fabric structures maintain positive drainage under all load conditions. This check is carried out following analysis with unfactored loads (due to geometric non-linearity), but this means that the subsequent design may only just avoid ponding with a factor of safety close to one, with no consideration of uncertainty and variability in the material properties, prestress levels, construction tolerances and the analysis itself. In addition, it is best practice to avoid inversion of the fabric curvature, as this may result in flapping and creasing of the material with subsequent damage and reduction in strength.

The stress that occurs under the load of the fabric is inversely proportional to the curvature of the shape. Therefore large curvature radius will compensate under load by curving more until it hits equilibrium. This mechanism is an inefficient way of load bearing and should be left to canopies less than 10m long. The span/sag ratio should be kept at less than 15. With increased spans, a lower ratio and/or cable reinforcement is needed [34].

2.2. Shear Testing of Textiles

Because the fibres in woven textiles are not continuous along the two principle directions, it is not possible to calculate analytically the shear properties based on the fibre elastic modulus and Poisson's ratio. Due to this limitation, mechanical testing is necessary to determine the shear behaviour [30]. The following are the most commonly performed tests.

Kawabata Evaluation System for Fabrics (KES-F)
An instrumental approach to measuring the low stress mechanical and surface characteristics of fabrics [13]. This type of test is mostly used for clothing and not engineered fabrics. For this reason, this paper is limited to a brief introduction of this method.
Kawabata Evaluation System of Fabric (KES-F) has the following four modules:

- KES-F1 for measurement of tensile and shearing characteristics;

- KES-F2 for measurement of bending characteristics;
- KES-F3 for measurement of compressional characteristics;
- KES-F4 for measurement of surface friction and roughness.

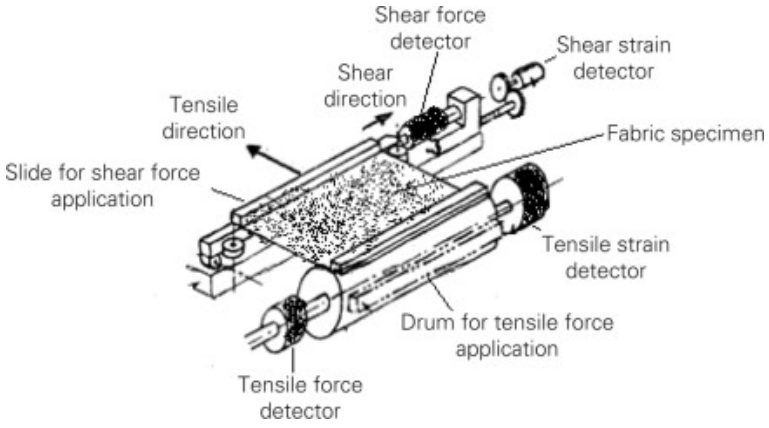

Figure 2.4: KESF-1 system [13]

Figure 2.4 shows the principle of the KESF-1 system (measuring tensile and shearing characteristics). The fabric specimen is clamped between two jaws (one attached to the drum for tensile force application and the other is attached with a slide for shear force application) and subjected to a constant tension of 10 gf/cm by a weight attached to the drum on which one jaw is mounted. Tensile force is applied by allowing the drum to rotate freely. The tensile force is measured by the tensile force detector by measuring the torque and the tensile strain is measured by the tensile strain detector from the data of the angle of rotation of the drum. The shear force is measured by a transducer connected to the other jaw (attached with slide) which moved sideways to apply the shear deformation. The shear force is measured by the shear force detector by measuring the force required to slide and the shear strain is measured by the shear strain detector from the data of the displacement of the slide [13].

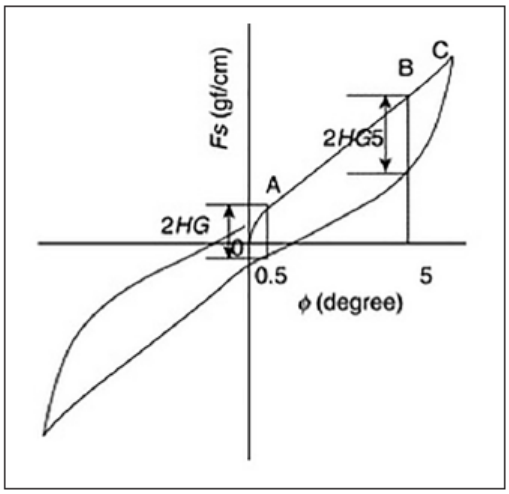

Figure 2.5: The typical shearing curve of woven fabric by the Kawabata apparatus
Fs is the shear force and ϕ is the shear angle. [13]

Bias Extension

The method in which a rectangular piece of woven material is clamped such that the warp and weft are orientated initially at 45° to the direction of the applied tensile direction. The initial length of the specimen must be more than or equal to twice its width, such as there exists a pure shear*zone C* (Figure 2.7) in the centre of the specimen.

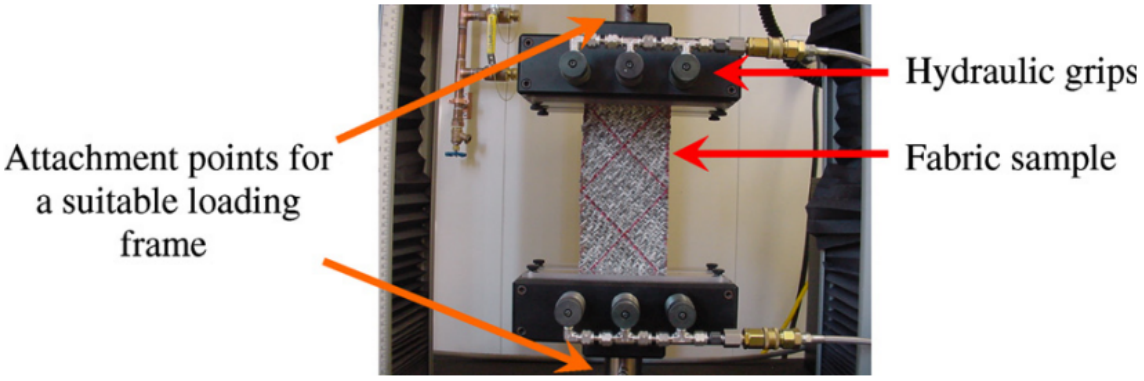

Figure 2.6: Example of bias extension test [7]

It has been shown that the shear angle in *region C* is assumed to be twice that in *region B*, while region A remains undeformed assuming yarns are inextensible and no slip occurs in the sample [7].

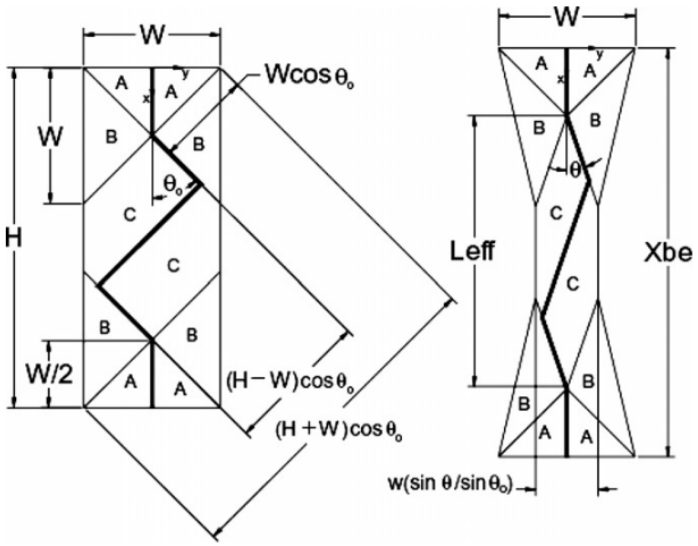

Figure 2.7: Illustration of a fabric specimen under a bias-extension test [7]

The shear angle in this case can be calculated as:

$$cos\theta = \frac{(H-\delta)-W}{(H-W)cos\theta_0} \tag{2.1}$$

- δ is the displacement during the test
- H, W as shown in Figure 2.7

The shear angle in region C can also be measured using image processing software based on pictures taken during a test. On [7] it is shown how Equation 2.1 accurately reflects the true shear angle - in zone C - in the fabric until it reaches $30°$.To obtain the shear force in the bias-extension test, some assumptions must be done and the (lengthy) process can be found in [7] as it is not relevant for this research.

Correctly predicting wrinkling during the forming of engineering fabrics is a difficult issue. The bias extension test can also be used to characterize wrinkling as a function of in-plane tension, but a correct prediction requires a small but finite value of the out-of-plane bending stiffness. It is extremely difficult to obtain the same information by performing a picture frame test. [21]

Picture Frame
The method in which the fabric is held in a trellis-like frame. Two diagonally opposite corners of the picture frame are pulled apart at a constant rate in a tensile testing machine. If it is assumed that the fabric is inextensible in the two fibre directions, there is only in-plane shear before wrinkling starts [29]. By using this test method, uniform shearing of the majority of the fabric specimen is obtained. Displacement and load data are recorded to aid in the characterization of pure shear behaviour. Shear deformation is no longer uniform once wrinkling occurs [7]. According to the kinematic analysis of the frame, the shear stress and shear angle can be determined.

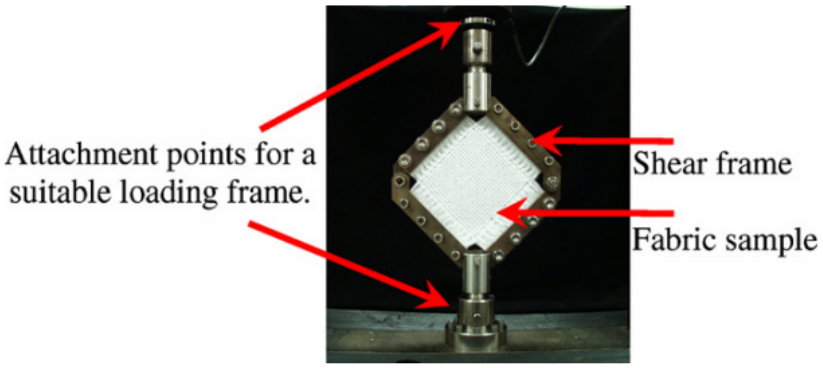

Figure 2.8: Example of picture frame test [7]

Frame design for this type of test can vary depending on the available loading system and the sample dimension. All corners must be pinned and when the fabric is loaded into the frame slippage must be prevented by using appropriate clamps.
With the fabric properly aligned and tightly clamped in the frame, the distance between two opposing corners is increased with the aid of the tensile testing machine, and therefore the tows begin to reorient themselves as they shear as seen in Figure 2.9.

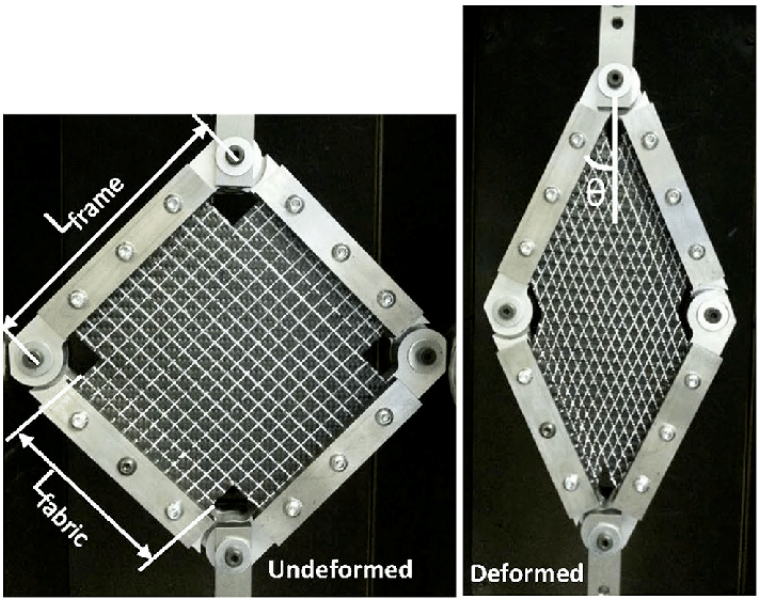

Figure 2.9: Picture frame deformation [7]

For example, [7] reports that by ‘mechanically conditioning’ the specimen, by shearing the fabric in the frame several times before starting the test, the variability in tension due to local deviations in orientation could be eliminated. This occurrence indicates the importance of the precise handling of both

the sample and the test fixture. Moreover, it is also possible to remove some yarns in the unclamped zones in order to avoid wrinkling.

With a picture frame test, is possible to obtain information and measure the shear angle of a textile (Figure 2.10). The shear angle is denoted as the shearing between the yarn of warp and weft. This is usually assigned to zero at the initial stage, when warp and weft are perpendicular to each other, and measured during the specimen deformation.

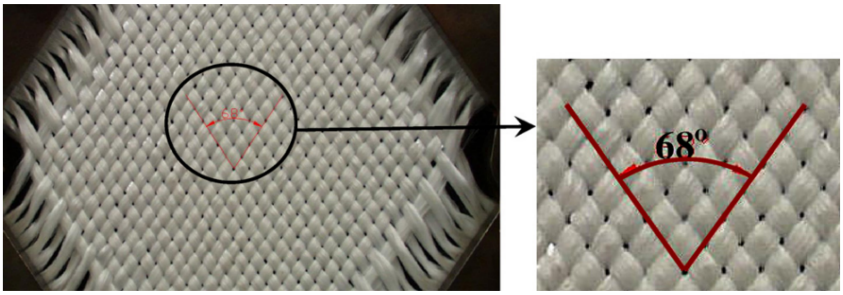

Figure 2.10: Shear angle: shearing of warp and weft yarns [7]

By measuring the displacement of the tensile machine, d, where the frame is attached and through trigonometric relations, the angle of the frame θ is calculated (Figure 2.10):

$$cos\theta = \frac{\sqrt{2}L_{frame} + d}{2L_{frame}} \tag{2.2}$$

The shear angle γ is calculated from the geometry of the picture frame as:

$$\gamma = 90° - 2\theta. \tag{2.3}$$

γ is also called the global shear angle. Note that this value is taken to be an average shear value over the entire specimen, the actual shear angle at any point on the fabric may vary.

There are optical methods available, which can determine the shear angle at any particular point on the fabric specimen. In [7] it was found that the difference between the measured shear angle and the calculated shear angle is about 9.3% and the maximum deviation occurs at larger shear angles, meaning the two methods are comparable and the difference is negligible before a shear angle of $33°$.

The force needed to deform the fixture must be measured accurately to determine the actual force required in shearing the fabric. The shear force F_s can be calculated from the measured pulling force and the current frame configuration as:

$$F_s = \frac{F}{2cos\theta} = \frac{F'' - F'}{2cos\theta} \tag{2.4}$$

Where F is the net load and θ is the angle of the frame (Equation 2.2). To eliminate the error caused by the weight and inertia of the fixture, the net load F should be obtained by subtracting an offset value F' from the machine-recorded value F" when the fabric is being deformed in the picture frame. A typical shearing curve obtained from the picture frame test can be seen below.

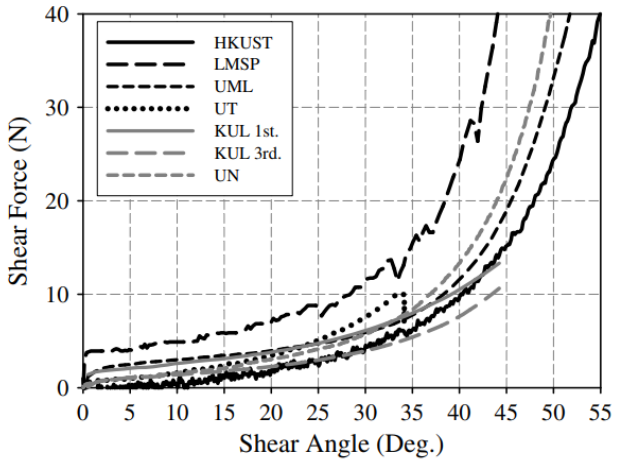

Figure 2.11: The typical shearing curve of woven fabric by the picture frame test. In this particular case it concerns a plain weave comparison between different types of yarns [7]

Assuming that the thickness of the fabric *H* does not change, before the locking angle has been reached, the shear stress τ_s is homogeneous [29]:

$$\tau_s = \frac{F_s}{HL_{frame}} \tag{2.5}$$

2.3. Relation between Shear Angle and Fabric Stiffness

As [7] mentions, research efforts in the woven fabric sheet forming are currently at a point where benchmarking will lead to major advances in understanding both the strengths and the limitations of existing experimental and modelling approaches. Test results can provide valuable information for the material characterization and forming process design of woven composites if researchers know how to interpret the results obtained from varying test methods appropriately.

In [29] the non-linear curves of shear stress in the fibre direction versus shear angle were fitted with polynomial functions which are symmetric about the origin. Moreover, a mathematical elasticity analysis was applied to the data of shear mechanical testing. The aim was to evaluate the orthogonal, in-plane, shear and normal stresses as a function of shear angle when taking into account the effects of changing fibre directions on the strain tensor and the effects of constraints in yarn extensibility. The modelling in combination with data fitting yielded values for the moduli and the inextensibility parameter for the three types of weaves (plain, satin and twill) before wrinkling. From that, it was concluded that the yarn inextensibility plays an important role in the elasticity analysis of the satin and twill fabrics. The shear stress varies non-linearly with shear angle due mainly to the change of the angle between the fibre directions during shear and its effects on the values of orthogonal stress and strain.

Another example is [11]. Firstly, the shear stress τ_s is plotted against the angle in radians, and then the obtained curves are assigned polynomial regressions equations. The derivative of those regression equations provides the shear rigidity modulus G_{12} as a function of the global shear angle γ in radian. Once assigned the regression equation to the applied shear force, one can calculate the shear stress. The expression of shear stress for a *balanced plain weave* (BPW) fabric in [11] is:

$$\tau_s = 1,879\gamma^5–3,090\gamma^4 + 1,972\gamma^3–0,520\gamma^2 + 0,074\gamma \tag{2.6}$$

By taking the derivative of this polynomial equation as a function of shear angle γ (radian), we obtain the shear rigidity modulus:

$$G_{12} = 9,395\gamma^4–12,36\gamma^3 + 5,916\gamma^2 + 1,04\gamma + 0,074 \tag{2.7}$$

This procedure of shear modulus rigidity determination for BPW is plotted in the form of a graphic representation as shown in the figures below.

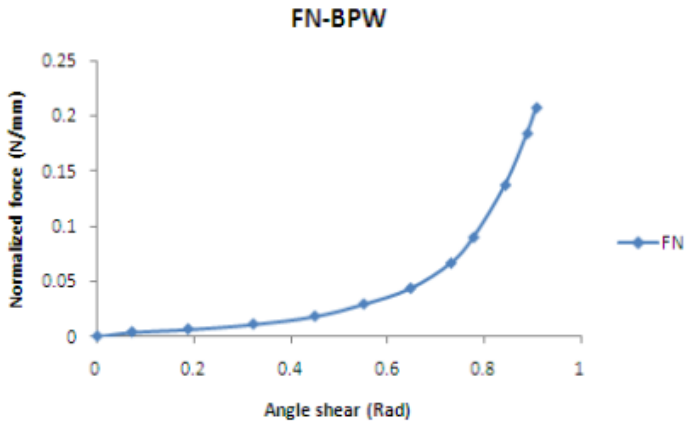

Figure 2.12: Normalized shear force for BPW fabric [11]

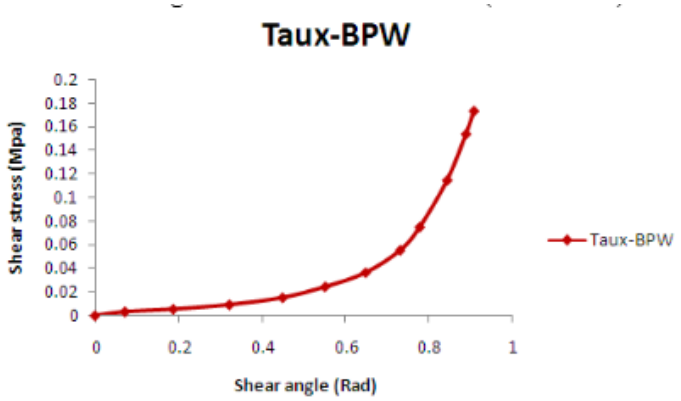

Figure 2.13: Expression of shear stress for BPW fabric [11]

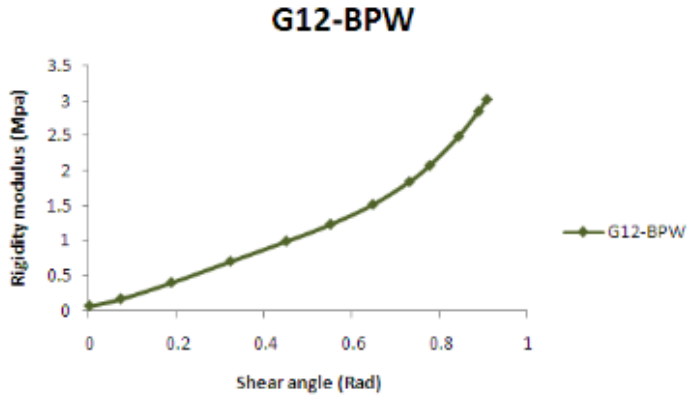

Figure 2.14: Rigidity modulus for BPW fabric [11]

3

Experimental Program

3.1. Overview

3.1.1. Material

Suntex is the studied material of this thesis therefore it has been subjected to different tests. Suntex is a woven solar integrated textile, meaning thin-film solar panels and electrical circuits are integral to the construction of the textile by being directly combined in the weaving process. The main scope of the developed material is of being both a standardised and easily customized architectural textile that increases the energy-harvesting potential of otherwise untapped surface area. The aim is to develop a textile for application in the textile architecture field. Key objective of Pauline Van Dongen's research in collaboration with Tentech is to "*create a new architectural textile, by interweaving thin film solar cells and electrically conductive yarn into a structural technical textile, so it can generate energy while providing shade, structure or an aesthetic update to a building*" [14].

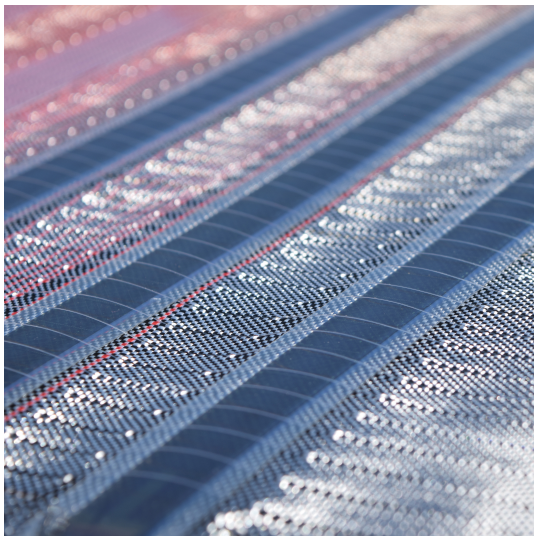

Figure 3.1: A woven solar integrated textile

Suntex combines five qualities:

- provides the building with energy generation;
- improves solar shading;
- gives a unique aesthetic appearance;
- promotes acceptance of solar technology;
- offers a positive climate impact.

A woven solar-integrated textile can be considered a new type of membrane material for Building Integrated Photovoltaics (BIPV). With this innovative, constructive fabric, enormous surfaces that are still unused can be outfitted with energy-generating potential.

All specimens used during testing are from *weaving trial 2*. The warp structure is made of rPet yarns (recycled polyester yarns) and mono-filaments which are similar to fish-line, the weft structure is made of rPet yarns. More information about the weave pattern and yarn selection can be found in Appendix A. The weaving of the two different materials is also divided into two different parts:

- regular plain weave where all the yarn on warp yarns are weaved with weft yarns
- a floating part where the weave pattern is plain rPet weave as the monofilaments are *floating* and not part of the weave so they can hold the OPV cells (Organic Photovoltaic) in place as seen in Figure 3.1.

PAULINE VAN DONGEN

SUNTEX MIT-RD-20-00359838

							Sample 1	
Company	**Product**	**diameter**	**dtex**	**Breaking Load (cN)**	**Elongation at break (%)**	**Tenacity cN/dTex**	**Warp**	**Weft**
Filva	HTR-B Monofilament	0,39 mm	1600	2745	97	1,72	TRUE	
Karl Grimm	High-Flex 3981, 7x1, copper with silver coating	0,42 mm	2325	2,8	-	1,18	TRUE	TRUE
MSP	rPET	0,32 mm	1100	8430	13,8	7,54	TRUE	TRUE

Figure 3.2: Yarn specification of Suntex weaving trial 2 (Appendix A)

3.1.2. Performed Tests

The two structural main performance criteria for fabric structures are stress and deflection. Due to the low shear stiffness of woven fabrics compared to their tensile stiffness, maximum stresses will usually occur in the weave directions (warp and weft) [6].

For the sake of assessing the material's applicability, it is essential to perform experiments for the evaluation of warp and weft strength. Experiments related to shear angle measurements are aimed to be subjected to regression analysis for shear stiffness evaluation (chapter 4). The elastic modulus has been assessed with a bi-axial test (section 3.5). All three parameters are likewise essential for applicability judgment.

In order to evaluate the strength of the studied material an extension test on both warp and weft direction has been performed according to ISO 13934-1 standard for uncoated fabrics [17]. The tensile test consists of three warp and three weft specimens. Description and results can be found in section 3.3.

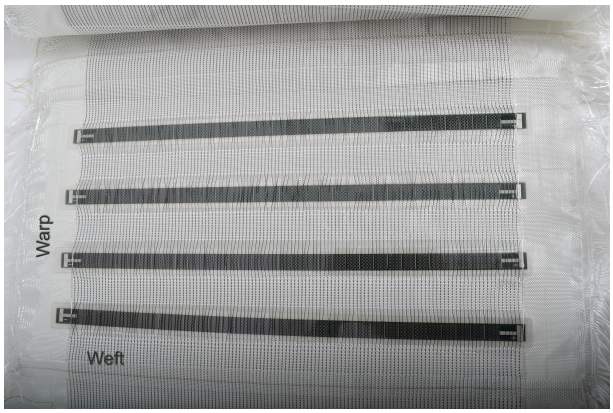

Figure 3.3: Warp being the longitudinal direction of the fabric and weft being the transverse direction, along the solar strips

The choice of which shear test to perform was quite simple. As illustrated in section 2.2, the Kawabata test is indicated for clothing/wearable textiles, therefore not applicable to the studied material. The bias extension test would result in the yarns sliding and the fabric being completely destroyed without producing results due to the lack of coating. Hence, the picture frame test was the most logical test to perform in this case. For this type of test, three specimens were tested. Description and results can be found in section 3.4.

How to determine tensile stiffness properties and elastic moduli for coated fabrics is detailed on EN 17117-1 [18]. In this case a similar procedure has been followed even if the studied material is uncoated. Regarding the elastic modulus, the expertise and common practices of the engineers at Tentech have been adopted to obtain an indication of its value. More specifically a bi-axial test has been performed on three cruciform specimens (the same specimens used for picture frame tests). The strain on warp and weft direction has been measured and the elastic modulus has been estimated (section 3.5).

3.2. Specimen Preparation

Only three samples were available from Suntex weaving trial 02, the studied material (Appendix A): A 42x35 cm, B 42x23 cm, C 42x48cm. The following was the planned cutting pattern:

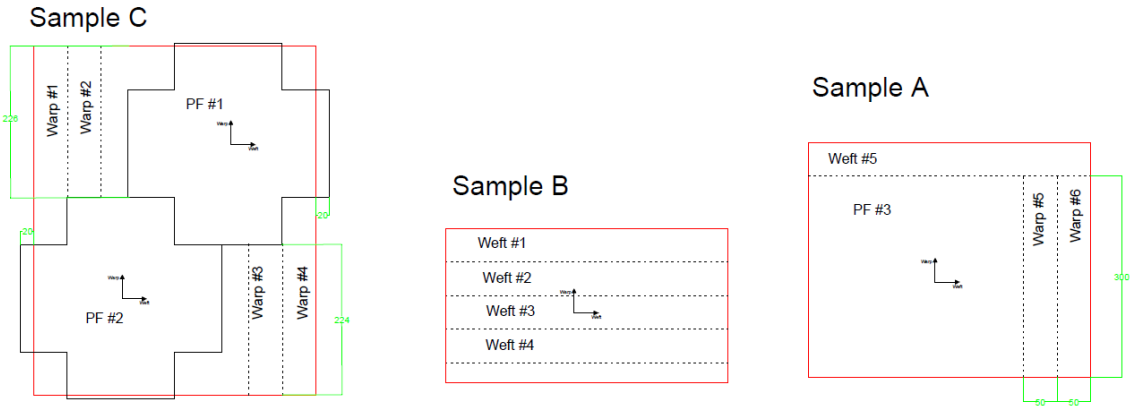

Figure 3.4: Planned sample cutting pattern. Warp is the vertical axis, weft is the horizontal axis.

Warp and weft specimens were used to test the tensile strength in both directions. The three picture frame specimens *(PF#)* were used for picture frame tests and bi-axial tensile tests for evaluation of shear and elastic modulus.

When performing a picture frame test, great care should be taken to make sure that the yarns of the specimen are orientated perpendicular to the edges of the frame. Any small misalignment will lead to tensile or compressive forces in the fibre directions, resulting in a large scatter in measured force readings. In order to obtain perfect alignment during testing, the specimen must be cut along its yarns. Great care should be taken when changing the cutting angle to make sure the border follows warp and weft directions. Regarding the mono-axial tensile tests, care should be taken on the dimension of the specimens and that the border follows the yarns likewise. For the bi-axial tensile test care should be taken on yarn alignment for correct measurement of the elastic modulus.

In order to make sure the only samples available were not going to be ruined during the preparation, trials were done using two different types of textiles. The first specimens produced were made of glass fibre fabric. At a later stage, specimens were formed out of a hand-woven sample and lastly, the mechanically woven sample was cut. The latter are the specimens used for testing.

The materials used for the preparation of the specimens are:

- Textile glue HT2 - Gutterman

- Textile glue latex based - Hema
- Epoxy resin two components - Resion ResinTechnology
- Textile scissors, rulers, markers

Figure 3.5: Textile glue HT2 - Gutterman

Figure 3.6: Textile glue latex based - Hema

Figure 3.7: Epoxy resin two components - Resion ResinTechnology

Figure 3.8: Set up

On the glass fibre sample, it was necessary to hand-saw the specimen borders on the fabric, to make sure each wanted yarn was divided from the unwanted ones. By following this procedure, it was possible to make sure each corner was at an exact right angle as the yarn pattern from warp to the weft and vice versa was followed. A textile glue was then applied to secure the sewn borders in place. Precision was necessary in order to avoid glue on the specimen parts that were going to be embodied in the test. Once the glue was dry the specimens could be cut, making sure to not pull any yarn and to be following the set boundaries [Figure 3.9 - Figure 3.12].

On the hand-woven Suntex sample, as the yarn density is higher compared to the glass fibre, sewing the geometry of the specimen wasn't necessary. In this case, drawing the geometry directly on the fabric was possible, as the yarns did not move so easily and they were clearly distinguishable from each other. By using a ruler and following the yarns, it's possible to make sure all angles are right. The process then continues as on the glass fibre: a textile glue was applied, and the sample was cut [Figure 3.13 - Figure 3.14].

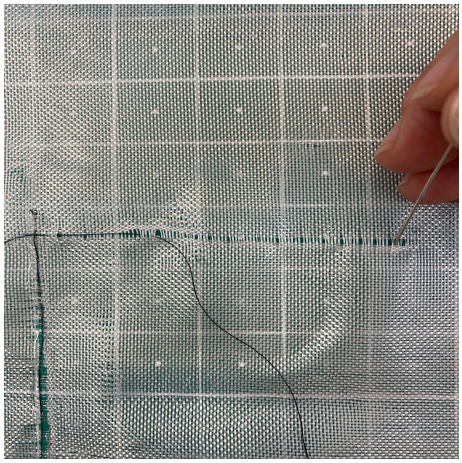

Figure 3.9: Sewing the geometry in the glass fiber fabric

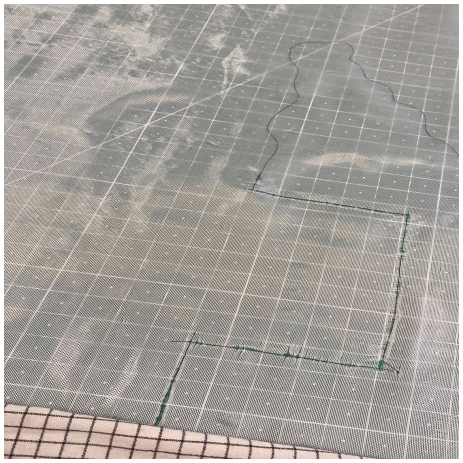

Figure 3.10: The geometry follows the yarn pattern making perpendicular angles

Figure 3.11: Two picture frame specimens in the glass fibre fabric

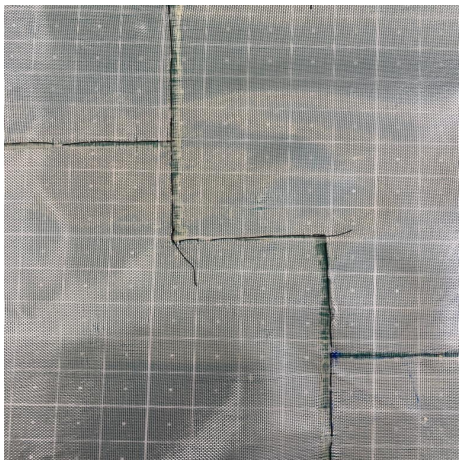

Figure 3.12: Textile glue is applied to the boarders so the cutting process can begin

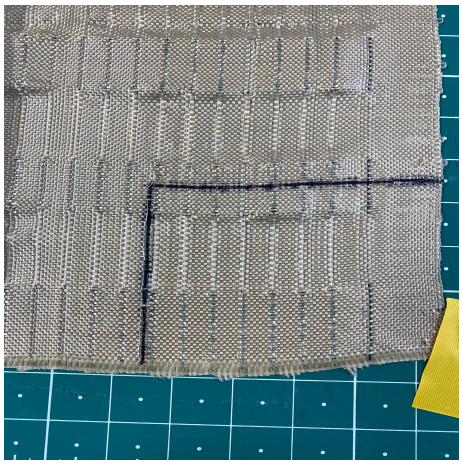

Figure 3.13: Drawing the geometry on the handwoven fabric

Figure 3.14: The geometry follows the yarn pattern making perpendicular angles

As the process on the previous samples proved to be successful, the mechanically woven sample could be finally cut following the procedure of the hand-woven textile [Figure 3.15 - Figure 3.18].

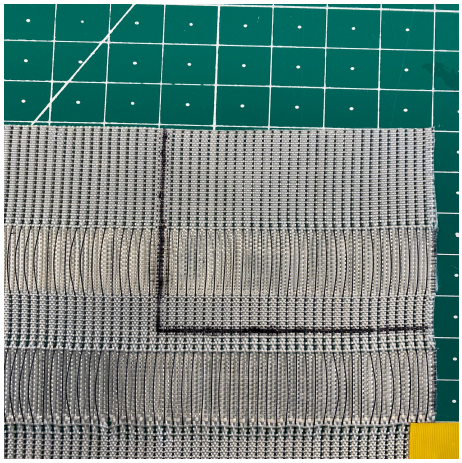

Figure 3.15: Drawing the geometry on the studied textile

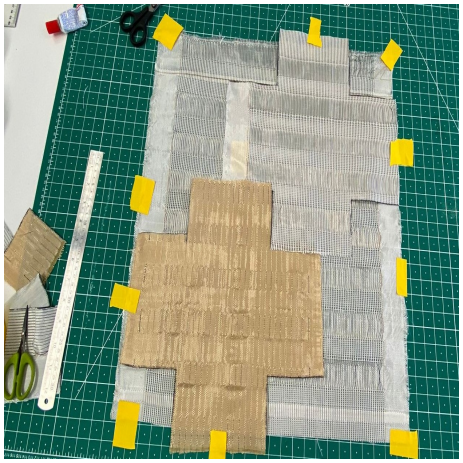

Figure 3.16: Making sure that two picture frame specimens fit on sample C

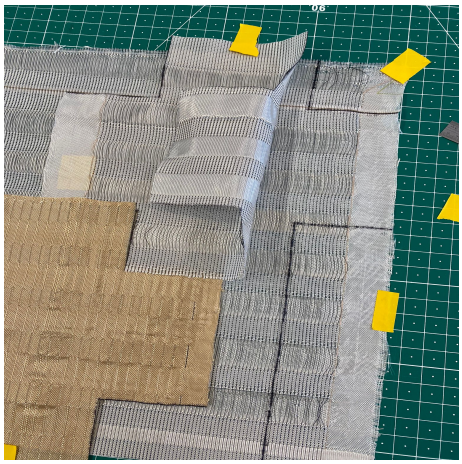

Figure 3.17: The geometry follows the yarn pattern making perpendicular angles

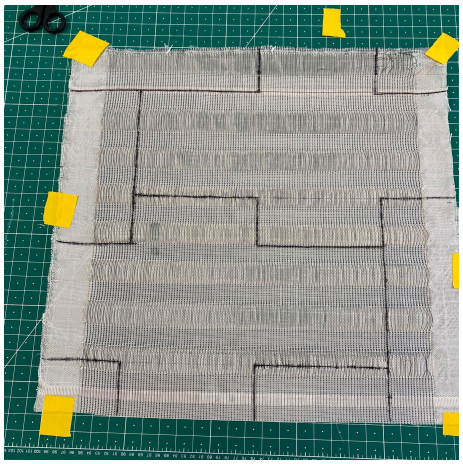

Figure 3.18: Textile glue is applied to the boarders so the cutting process can begin

At this point warp and weft specimens were ready (Figure 3.19 - Figure 3.20) but the picture frame ones needed further preparations.

Once the picture frame specimens were cut, it was possible to proceed with fixating them to a surface and applying the resin to the ”flanges”. This process is done in order to avoid yarn damage or misalignment when the bolts of the picture frame go through the specimen and to avoid slippage of the clamps. The used resin is a two-component epoxy resin that can be applied with a brush [Figure 3.7]. As the resin is quite liquid, to avoid bleeding on unwanted parts, a glue barrier was created and the resin was applied on the inside of this boundary. This method turned out to be insufficient [Figure 3.22]. A solution to this problem was found with an iterative process which consisted of trying a different number of barrier lines and different glue types [Figure 3.21 - Figure 3.28].

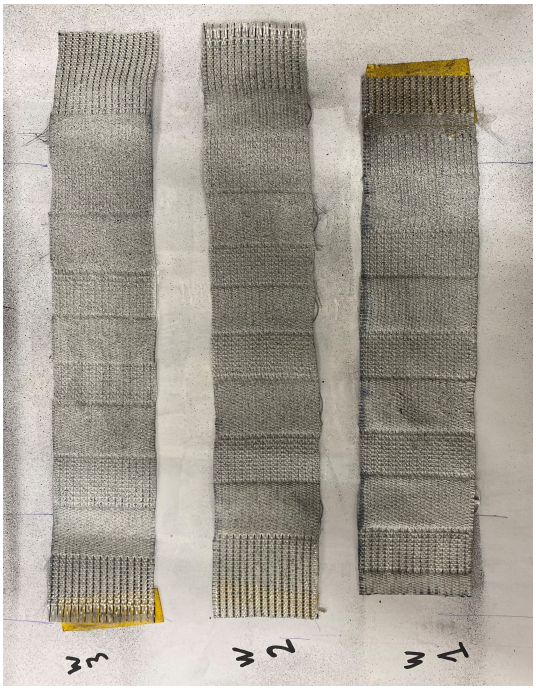

Figure 3.19: Warp specimens after the application of a speckle patterned necessary for Digital Image Correlation (DIC) system

Figure 3.20: Weft (or *fill*) specimens after the application of a speckle patterned necessary for DIC system

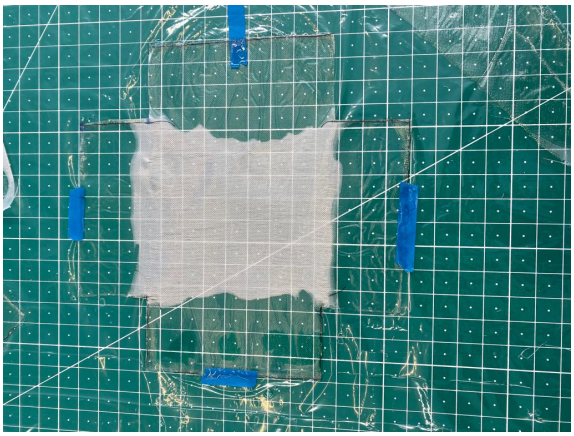

Figure 3.21: First attempt on applying resin to glass fibre: the resin did not stay in place

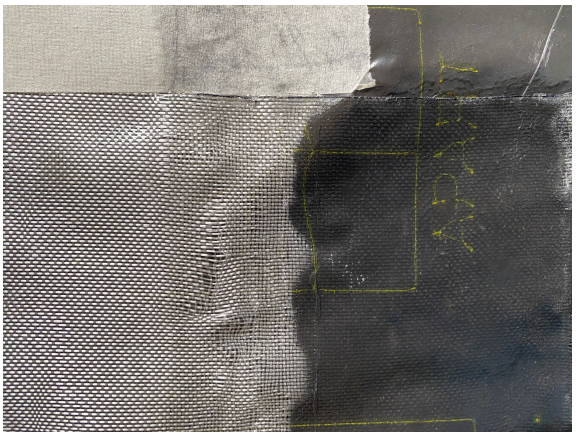

Figure 3.22: Second attempt with glass fibre: the glue acts like a barrier but is still not sufficient

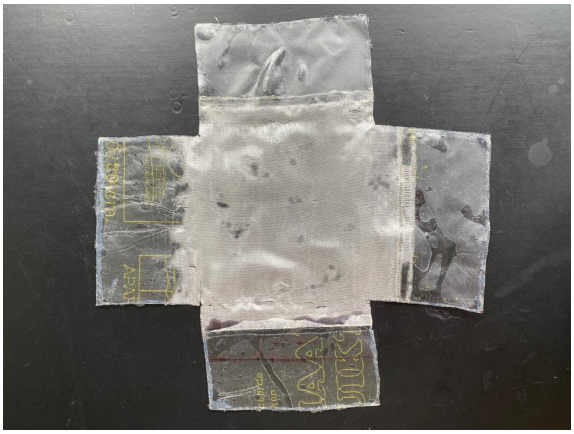

Figure 3.23: When using a different textile glue the barrier method becomes sufficient. The bottom and left wings were made with textile adhesive HT2 which didn't stop leakage. The top and right wings were made with latex-based glue which stopped leakage.

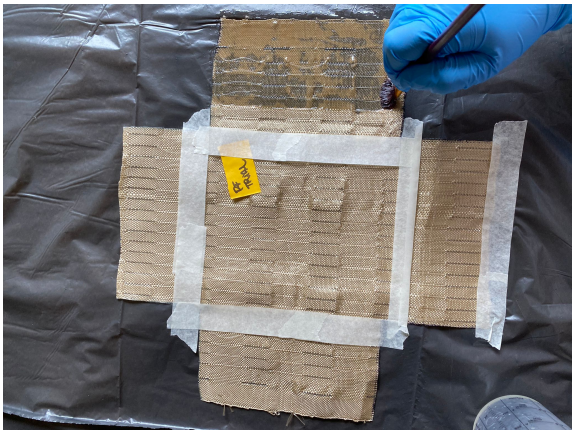

Figure 3.24: The same comparison of two different types of glue has been done on the picture frame trial specimen (hand woven)

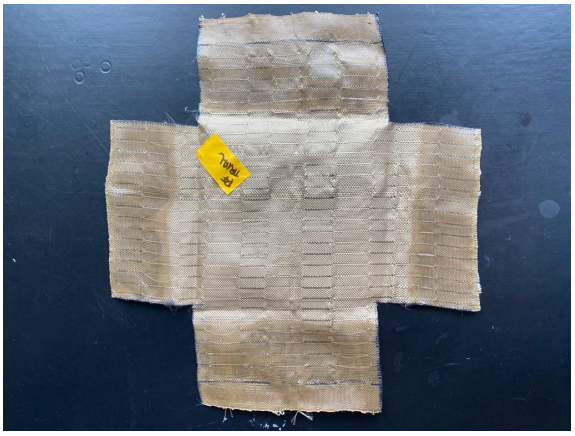

Figure 3.25: We can notice resin leakage on the bottom and left wings while the top and right wings have perfectly straight borders.

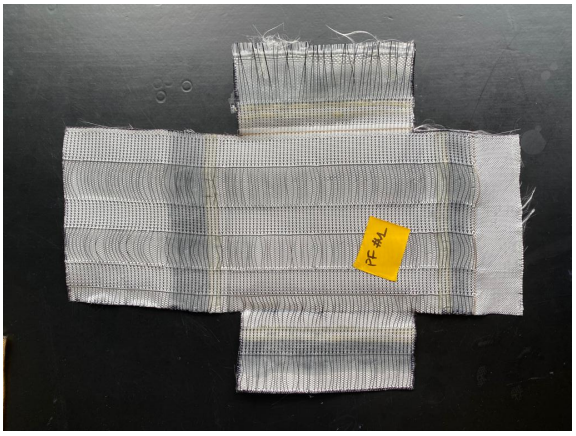

Figure 3.26: On the Suntex specimens only the latex-based glue was used. Specimen $PF1$ before punching the holes.

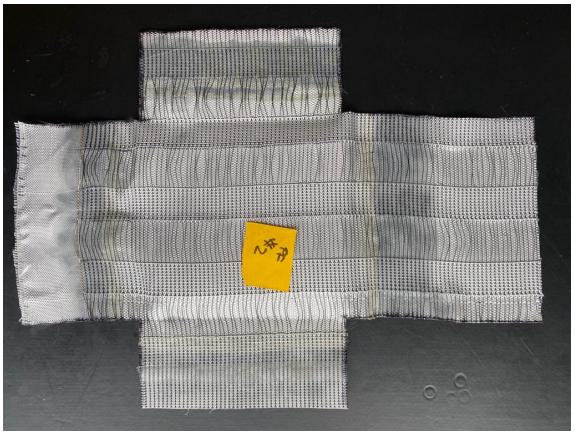

Figure 3.27: Specimen $PF2$ before punching the holes.

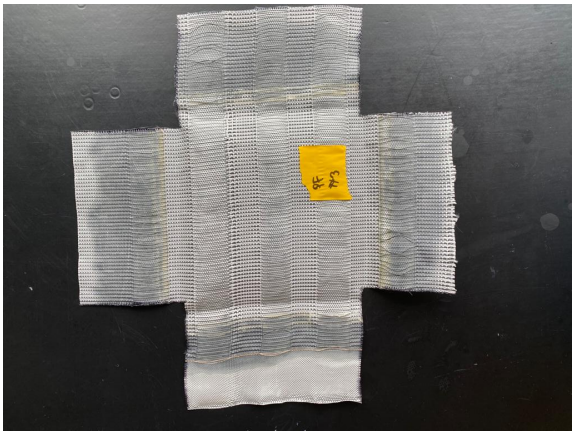

Figure 3.28: Specimen $PF3$ before punching the holes.

3.3. Strength Evaluation

The tests regard three specimens on warp and tree specimens on the weft direction [Figure 3.19 - Figure 3.20]. Those were pulled on a monoaxial tensile machine until rupture. The average warp strength results in 280 daN/5cm, while the weft strength results in 340 daN/5cm. The elongation in both directions is less than 17% therefore the material is within the norm for architectural textiles. The warp strength of the studied textile results are not sufficient for a type I textile ($\geq 300daN/5cm$). The complete test report can be found on Appendix B.

The monoaxial tensile machine used was Instron 1122 and Digital Image Correlation (DIC) system was used to measure the elongation and strain field along the specimens. The chosen testing rate was 1 mm/s (displacement-controlled test). Tests were performed on 9/08/2022 at TU Delft Stevin Lab II. Dimensions of the specimens are specified on Table 3.1. *W* refers to warp specimens, while *F* refers to weft specimens, which is also called fill direction in order to distinguish when using abbreviations.

Table 3.1: Specimens dimensions

	Width (mm)	Gauge Lenght (mm)
W01	50	200
W02	50	201
W03	50	200
F01	50	198
F02	50	200
F03	50	200

The load cell is connected to both measuring systems. A small difference in force values can be observed in all tests due to the manual start of both systems. A difference in displacement can also be observed due to the nature of the two systems:

- DIC system measures displacement and strain field in a set surface in 3 dimensions
- Tensile test measures the distance between the two clamps

It is known from previous tests performed by Tentech that the photovoltaic strips will not undergo any stresses during elongation, hence their absence in the experiments.

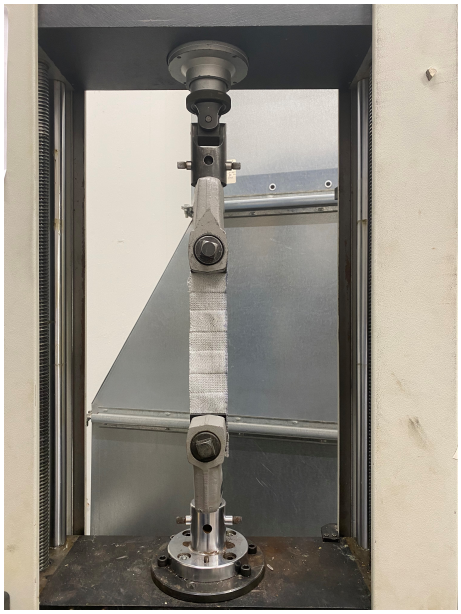

Figure 3.29: Tensile machine test set up (W01: Warp is aligned with tensile extension)

3.3.1. Warp Strength Results

Three warp specimens were tested: W01, W02 and W03. As mentioned, they were pulled on a monoaxial tensile machine until rupture.The damage evolution for specimen W01 is reported in Figure 3.30 - Figure 3.33; pictures of all specimens can be found in Appendix B.

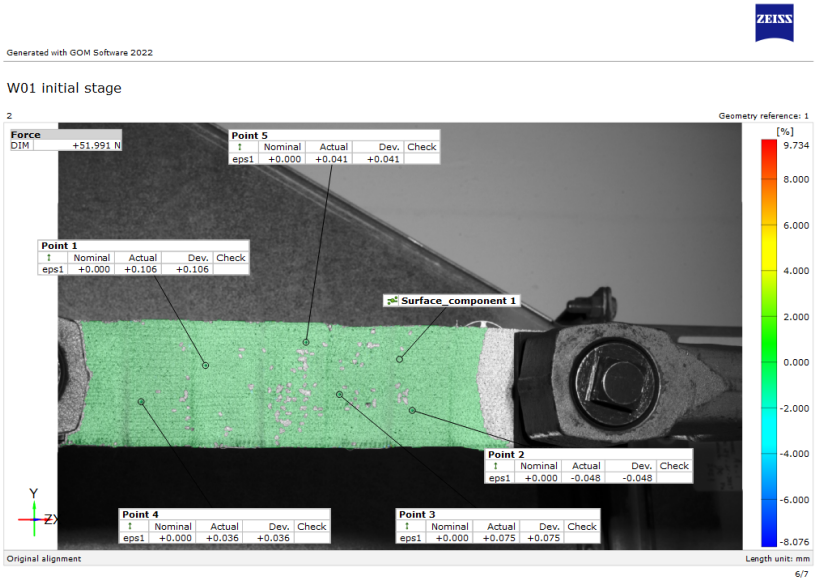

Figure 3.30: W01 unloaded. F_0= 52N

F_0 is the force needed to keep the specimen in place and at the correct gauge length.

Figure 3.31: W01 before rPET failure. Rupture force = 2700 - F_0 = 2648 N

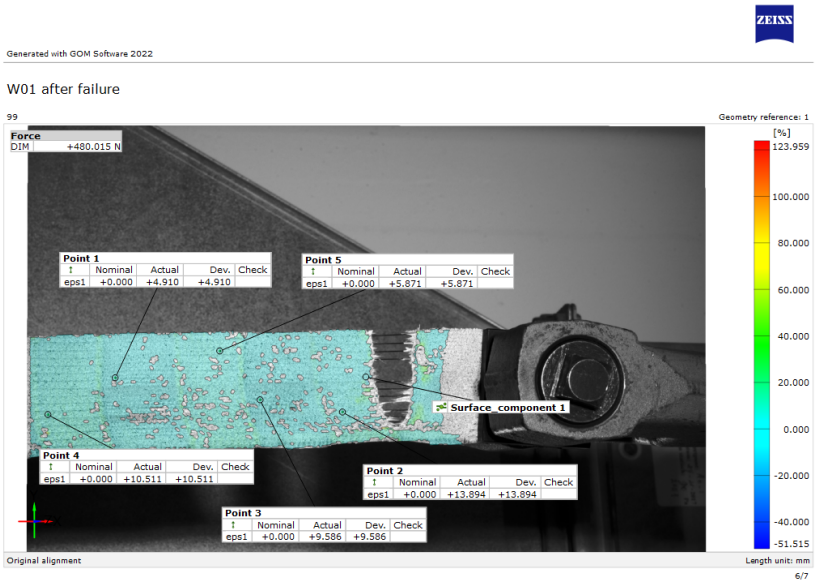

Figure 3.32: W01 after rPET failure. F=400N

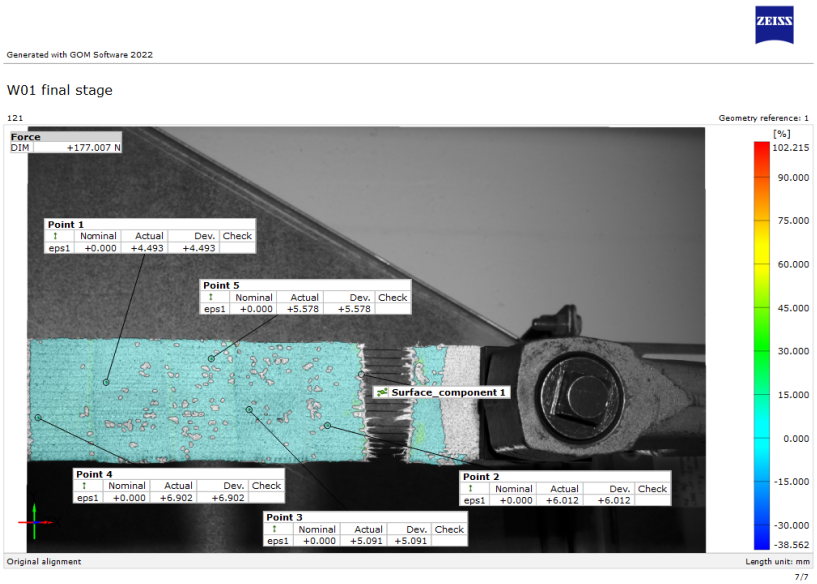

Figure 3.33: W01 final stage: mono-filament has not failed. Test has been stopped. F=177N

As noticeable from Figure 3.30 - Figure 3.33, when the specimen is pulled in the warp direction no slippage can be observed. Moreover, the presence of two different yarn materials with different stiffnesses resulted in the two materials failing separately rather than having a coherent “clear-cut” fabric failure. The remaining force after rPET rupture is taken by the mono-filament yarns. Failure of the latter was not within the scope of the test as the fabric is considered to have failed when at least one of the yarns breaks.

The force-elongation graph in Figure 3.34 represents the response measured with the DIC system of the W01 specimen. P_i are points randomly placed along the specimen and *average* is the curve that averages the response of all points (P1:P5), with its corresponding standard deviation. The graph

increases gradually, until rPET yarn ruptures. The reason why some of the curves have blank spots is that the data couldn't be measured with the DIC system, because of rapid changes or clusters of the speckle patterns. The maximum registered force is 2647.6 N which corresponds with an elongation of 11.6 %. In the graph one can observe the behaviour of the specimen, from unloaded stage (origin) to specimen failure.

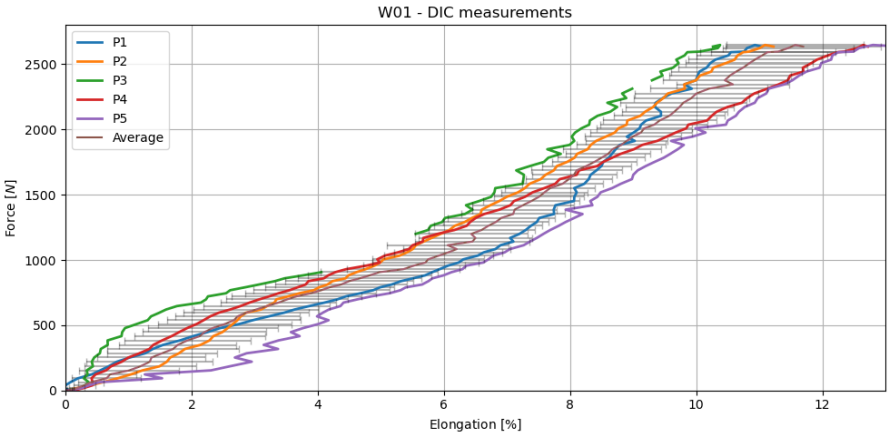

Figure 3.34: W01 DIC response: P_i are different points along the specimen as seen on Figure 3.30

Each specimen has been measured with DIC system and with the tensile machine *Istron 1122*. As mentioned, the tests are force driven, therefore the displacement has been measured. The percentage of elongation has been calculated as such:

$$\epsilon = \frac{l - l_0}{l_0} * 100 \tag{3.1}$$

Where:
l = measured displacement
l_0 = initial length of the specimen, gauge length as specified in Table 3.1

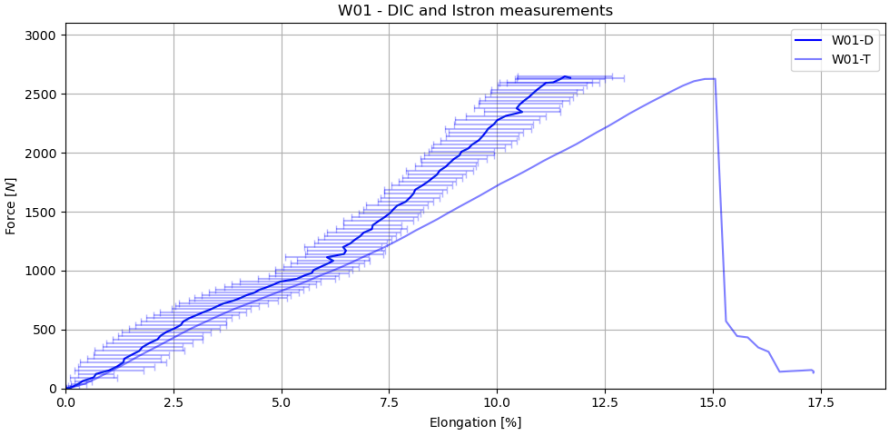

Figure 3.35: W01 measured with DIC (-D) and Istron (-T)

A similar representation of all other specimens can be found in Appendix B. An overview of all warp experiments follows.

Figure 3.36 represents the response of all specimens measured with the tensile machine (-*T*) and with the DIC system (-*D*). For -*D* the average of all measured points of each specimen (W01:W03) has been considered.

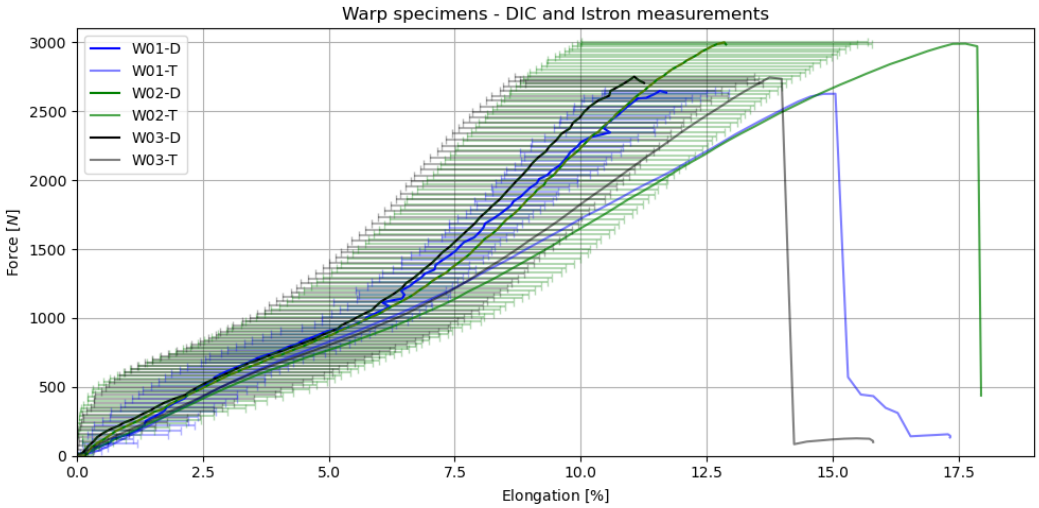

Figure 3.36: Warp response of all specimens: -T are data measured via Istron tensile machine, while -D are measured DIC

The graph in Figure 3.36 increases gradually, almost linearly, until failure. The drop in force for *-T* curves corresponds to the failure of rPET warp yarns, while for *-D* curves such event is represented by the end of collected data. For all curves, the remaining force after rPET rupture is taken by the mono-filament yarns. Failure of the latter was not within the scope of the test. All standard deviations corresponding to each -DIC curve have been represented in the graph. It is noticeable how the standard deviation increases with larger deformations. It is also larger for specimens W02 and W03 compared to W01.

A comparison between DIC and tensile machine measurements is summarised on Table 3.2. All $-_T$ refers to measurements recorded by the tensile machine, the elongation has been analytically calculated, while all $-_D$ refers to measurements recorded by the DIC system.

Table 3.2: Warp strength evaluation: comparison between tensile test data and DIC

	F_T (N)	dL_T (mm)	ε_T%	F_D (N)	ε_D%
W01	2625.6	30.1	15.1	2647.6	11.6
W02	2998.5	35.5	17.6	2999.4	12.9
W03	2739.1	27.5	13.8	2750.7	11.0
Average	2784.4	31.0	15.5	2799.2	11.8
σ	185	4	2	181	1
CV %	7	13	13	7	8

As seen on Table 3.2, the analytical calculations from tensile machine measurements differ from DIC in regards to elongation. As mentioned in section 3.3, the reason behind the difference is due to the intrinsic characteristics of each system. While the difference in force value depends on the manual start of both systems, even though they are both connected to the same load cell. It's recommended to use the data from the DIC system, as considered more accurate. Standard deviation and coefficient of variation (CV) are also reported.

From testing three specimens on warp direction, we can conclude the warp strength of the studied material is equal to 280 daN/5cm and the elongation is 12%. Both strength and elongation have been rounded according to ISO 13934-1 [17].

3.3.2. Weft Strength Results

Three weft specimens were tested: F01, F02 and F03. They were pulled on a monoaxial tensile machine until rupture. One of the specimens is reported *F02* (Figure 3.37 - Figure 3.40), pictures of all specimens can be found in Appendix B.

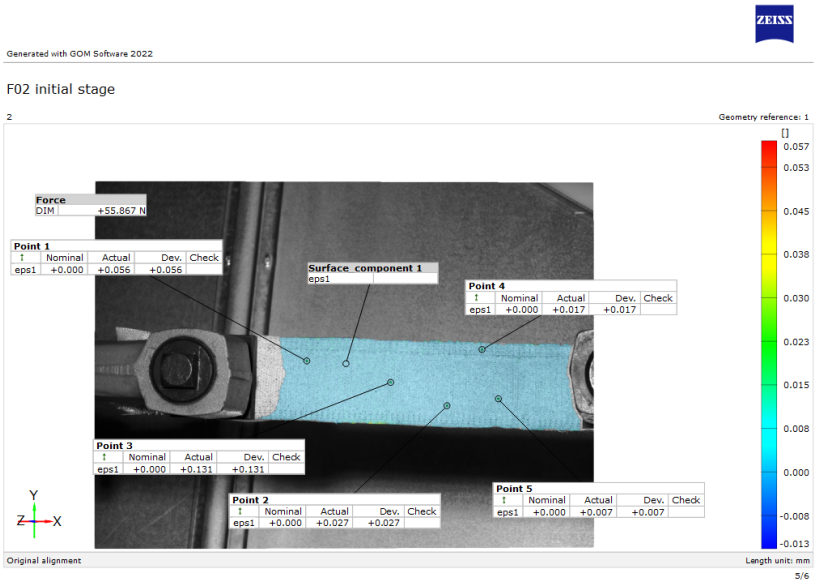

Figure 3.37: F02 unloaded. F_0= 56N

F_0 is the force needed to keep the specimen in place and at the correct gauge length.

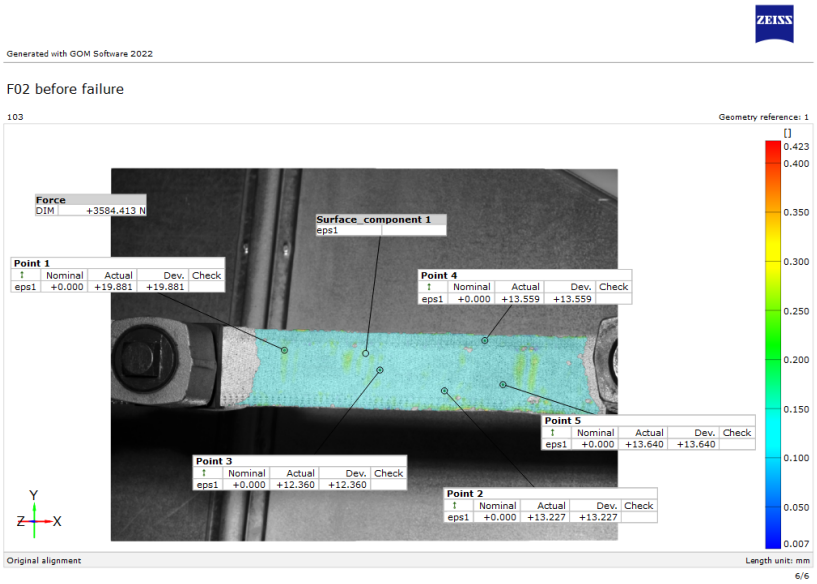

Figure 3.38: F02 before rPET failure. Rupture force = 3580 - F_0 N

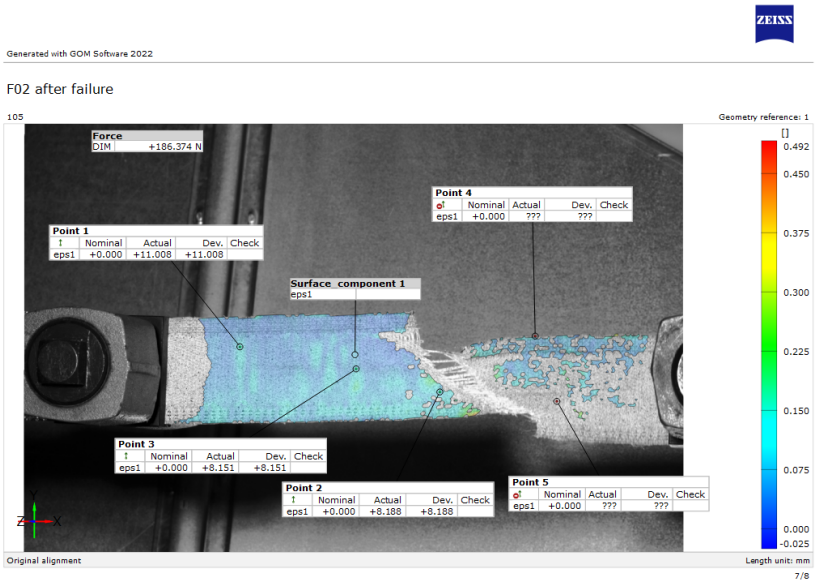

Figure 3.39: F02 after failure

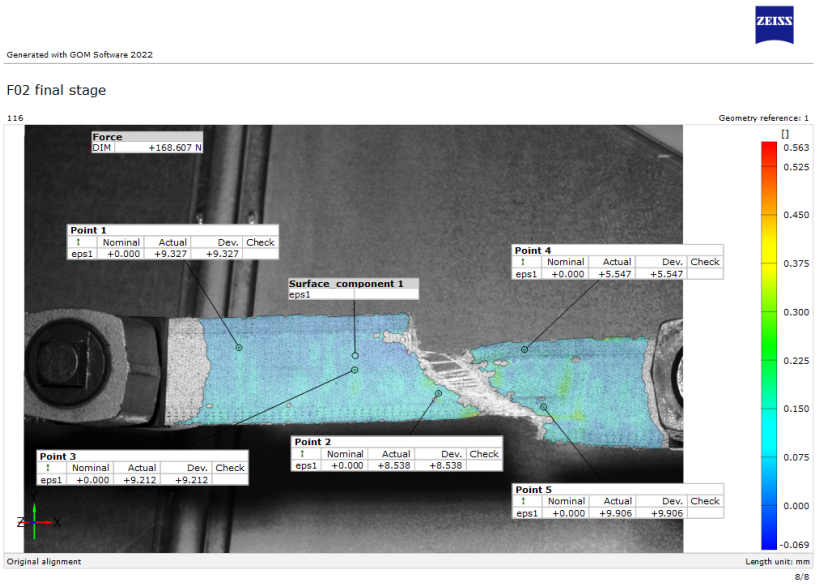

Figure 3.40: F02 final stage. Test has been stopped.

As noticeable from Figure 3.37 - Figure 3.40, when the specimen is pulled in the weft direction no slippage can be observed. Moreover, the absence of two different yarn materials resulted in a coherent "clear-cut" fabric failure. The only type of yarn on weft specimens is rPET yarn, as seen from weaving notes in Appendix A.

The force-elongation graph in Figure 3.41 represents the response measured with the DIC system of the F02 specimen. P_i are points randomly placed along the specimen and *average* is the curve that averages the response of all points (P1:P5), with its corresponding standard deviation. The graph increases gradually, until rPET yarn ruptures. The reason why some of the curves have blank spots is that the data couldn't be measured with the DIC system, because of rapid changes or clusters of

speckle patterns. The maximum registered force is 3529.2 N which corresponds with an elongation of 14.5 %. In the graph one can observe the behaviour of the specimen, from unloaded stage (origin) to specimen failure.

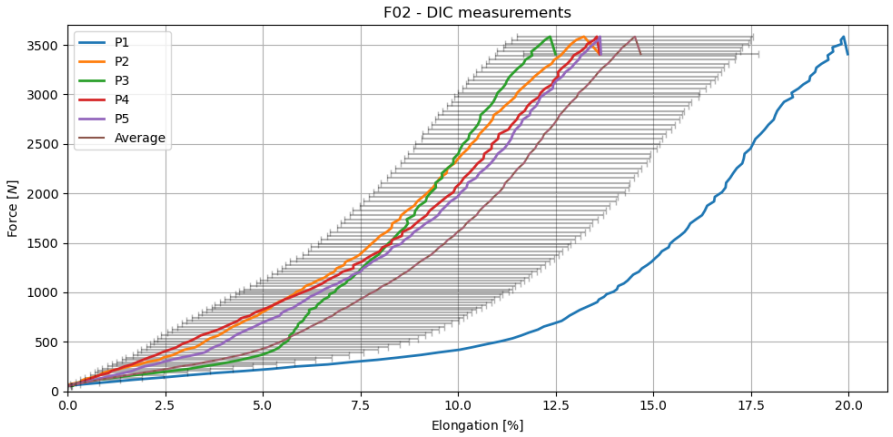

Figure 3.41: F02 DIC response: P_i are different points along the specimen as seen in Figure 3.37

Each specimen has been measured with DIC system and with the tensile machine *Istron 1122*. As mentioned, the tests are force driven, therefore the displacement has been measured. The percentage of elongation has been calculated as such:

$$\epsilon = \frac{l - l_0}{l_0} * 100 \tag{3.2}$$

Where:
l = measured displacement
l_0 = initial length of the specimen as specified in Table 3.1

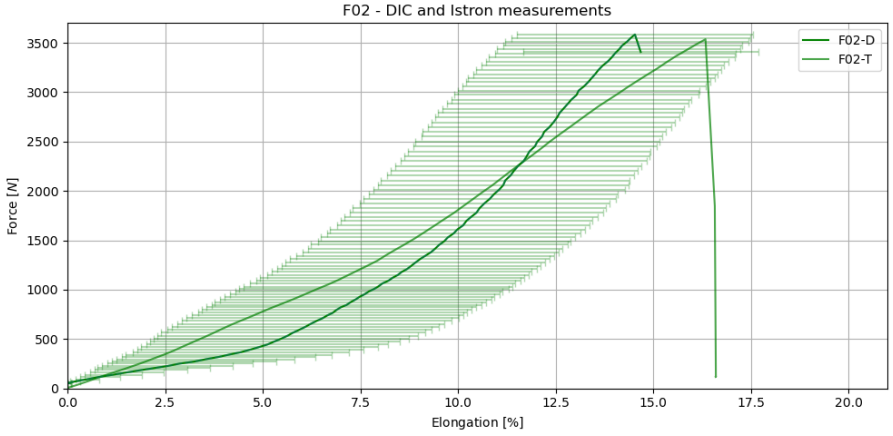

Figure 3.42: F02 measured with DIC (-D) and Istron (-T)

A similar representation of all other specimens can be found in Appendix B. An overview of all warp experiments follows.

Figure 3.43 represents the response of all specimens measured with the tensile machine (*-T*) and with the DIC system (*-D*). For *-D* the average of all measured points P_i of each specimen (F01:F03) has been considered.

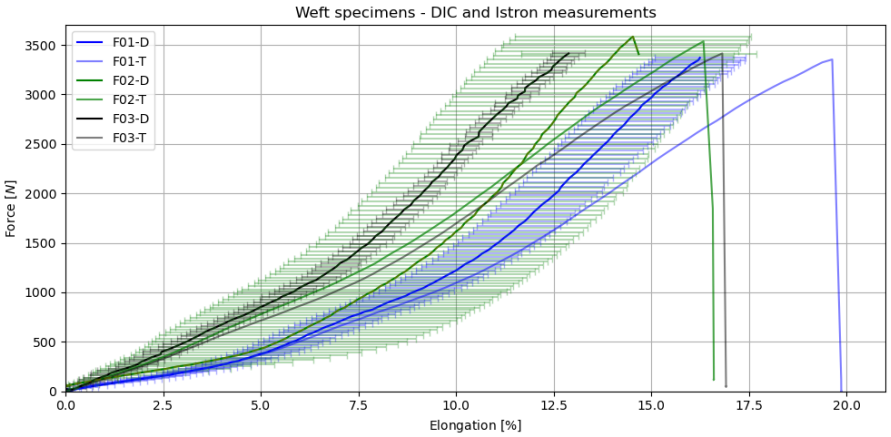

Figure 3.43: Weft response of all specimens: -T are data measured via Istron tensile machine, while -D are measured DIC

The graph in Figure 3.43 increases gradually until failure. The drop in force for *-T* curves corresponds to the failure of rPET warp yarns therefore failure of the specimen. For *-D* curves failure corresponds to the end of testing data.

A comparison between DIC and tensile machine measurements is summarised in Table 3.3. All $-_T$ refers to measurements recorded by the tensile machine, the elongation has been analytically calculated, while all $-_D$ refers to measurements recorded by the DIC system. Standard deviation and coefficient of variation (CV) are also reported.

Table 3.3: Weft strength evaluation: comparison between tensile test data and DIC

	F_T (N)	dL_T (mm)	ε_T%	F_D (N)	ε_D%
F01	3350.8	39.3	19.6	3370.3	16.3
F02	3530.9	32.7	16.3	3529.2	14.5
F03	3412.2	33.7	16.8	3413.5	12.9
Average	3431.3	35.2	15.5	3437.7	14.6
σ	92	2	2	82	2
CV %	3	8	10	2	12

As seen in Table 3.3, the analytical calculations from tensile machine measurements differ from DIC in regards to elongation. As mentioned in section 3.3, the reason behind the difference is due to the intrinsic characteristics of each system. While the difference in force value depends on the manual start of both systems, even though they are both connected to the same load cell. It's recommended to use the data from the DIC system, as it is considered more accurate. All standard deviations corresponding to each -DIC curve have been represented in the graph. It is noticeable how the standard deviation increases with larger deformations. It is also larger for specimens F02 and F03 compared to F01.

From testing three specimens in the weft direction, we can conclude the weft strength of the studied material is equal to 340 daN/5cm and the elongation is 15%. Both strength and elongation have been rounded according to ISO 13934-1 [17].

3.3.3. Discussion

In this chapter results and observations of strength tests will be discussed.

As noticeable from the pictures below, for all three warp specimens, the failure happens around the transition between the float area and the plain weave area. The floating part is the part of the textile where the OPV (Organic Photovoltaic) strips are inserted. The floating part of the weave is composed of a plain weave made of rPet yarns only. In the other parts of the material, the monofilament is part of the weave in warp direction as described in section 3.1.

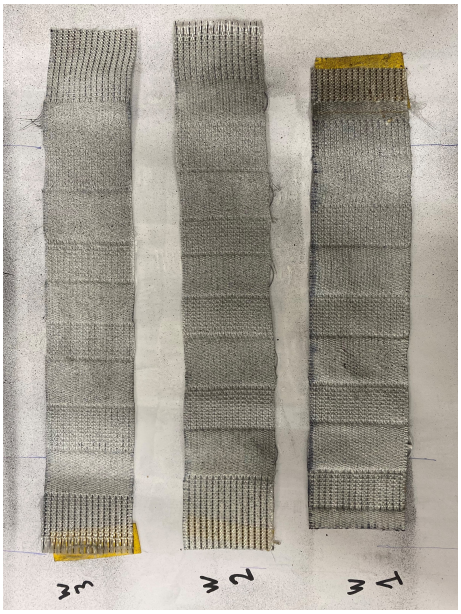

Figure 3.44: Warp specimens before testing. From left W03, W02, W01.

Figure 3.45: Warp specimens after testing. From left W03, W02, W01.

The weft specimens have different failure mechanisms: the ones including the floating area failed in a diagonal direction while the one composed by plain weave only has a straight clear cut.

Figure 3.46: Weft specimens before testing. From left F03, F02, F01.

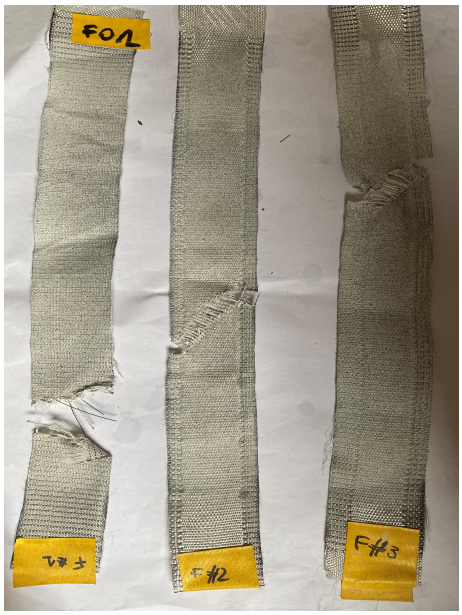

Figure 3.47: Weft specimens after testing. From left F01, F02, F03.

Therefore the transition area between the floating and plain weave area seems to be a sensitive area, making it an area of interest for future tests.

Moreover, as noticeable from Figure 3.46, specimen F01 does not have any float area. This resulted in a different behaviour when compared to the other specimens: it seems to have a more elastic behaviour, especially when focusing on -*T* measurements (see Figure 3.43). As the material is made by both parts (floats and plain weave) it is reasonable to include both parts of the weave when testing

and making conclusions, hence the inclusion of F01 in strength conclusions (Table 3.3).

As seen from the test results (Figure 3.36 and Figure 3.43) the presence of floats and the amount of monofilaments influences the strength of the material. It is recommended to study the optimum amount of monofilaments in order to have a more consistent failure mechanism and higher strength.

The absence of monofilaments in the weave in the weft direction is related to its higher strength. By weaving a lower amount of monofilaments in the warp direction, the strength can therefore also be higher and the requirement of type I architecture textile can be reached for the strength in both directions.

3.3.4. Conclusive Remarks

By knowing the tensile strength of a textile, it is possible to calculate the maximum membrane stress. This corresponds to:

$$\sigma_{max} = \frac{F_T}{\gamma} \tag{3.3}$$

Where:
σ_{max} is the maximum membrane strength
F_T is the tensile strength of the textile
γ is the safety factor: 5

The maximum membrane stress corresponds to the maximum allowable stress in the membrane after load application. For the studied textile this corresponds to:

Table 3.4: Maxim membrane stress

	F_T (daN/5cm)	F_T (kN/m)	σ_{max} (kN/m)
Warp	280	56	11.2
Weft	340	68	13.6

3.4. Shear Angle Evaluation

It is well known that the determination of shear characteristics of advanced composites is one of the most difficult types of mechanical static tests. One of the principal difficulties of the development of a shear test method for these materials is to induce a stress state of pure shear in a gauge section of the specimen which has to be only subjected to a shear stress of a constant magnitude [35]. Out of all available tests illustrated in section 2.2, in order to evaluate shear stresses and angles, three picture frame tests were executed. The choice of the number of tested specimens is limited due to the sample availability.

Usually, on a picture frame test, all the corners of each frame are pinned. When the fabric is loaded into the frame, it is clamped on all edges to prevent slippage. The corners of a sample are cut out to allow the tows to rotate without wrinkling the fabric. Thus, it appears that each sample has four flanges. With the fabric properly aligned and tightly clamped in the frame, the distance between two opposing corners is increased with the aid of the tensile testing machine, and therefore the tows begin to reorient themselves as they shear.

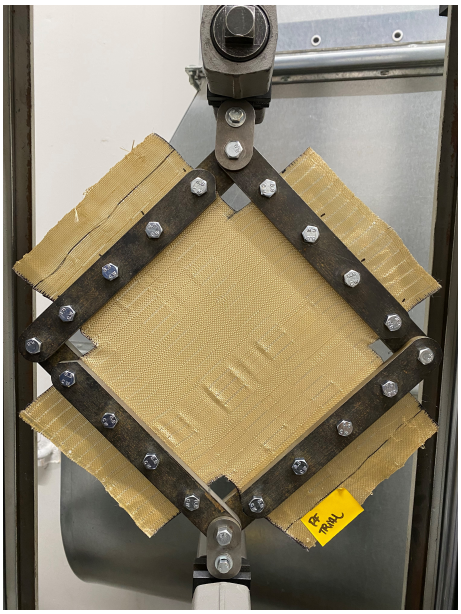

Figure 3.48: PF set up. Trial specimen initial position

Figure 3.49: Trial specimen after deformation

As seen in the literature review the angle can be calculated from a picture frame test based on the measured tensile machine displacement. It is often assumed that the shear strains are uniform in the gauge area such that a global shear force and shear strain can be obtained from kinematic and static analysis of the frame. It is, however, common practice to use either Digital Image Correlation (DIC) measurements or to manually check the fibre angles from pictures of the test as a validation [24]. In this case, a 3D DIC was used, therefore the strain field was measured by two cameras positioned under different angles with respect to the measured object.

As mentioned, the testing procedure has been done following EN 17117 [18], which is the standard for coated fabrics as shear standards for uncoated fabrics do not exist yet. The picture frame was mounted in the monoaxial tensile machine Instron 1122 and DIC (Digital Image Correlation) system was used to measure the elongation and strain field along the specimens. The chosen testing rate was 0.5 mm/s (displacement-controlled test). Tests were performed on 11/08/2022 at TU Delft Stevin Lab II. Dimensions of the specimens are specified on Table 3.5. It was assumed that all clamping mechanisms held the fabric rigidly in the frame and there was no slippage.

Table 3.5: Specimens dimensions in mm

	Warp Flange	Weft Flange	Float Width
PF01	160	162	30 - 35
PF02	160	160	32 - 33
PF03	160	164	28 - 28

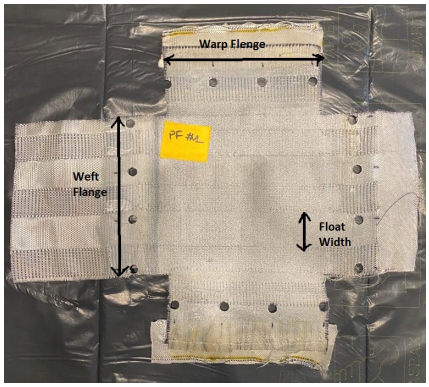

Figure 3.50: PF Specimen dimensions

The fabric conforms to its final geometry mostly by yarn rotation, thus shearing between weft and wrap yarns, denoted as the shear angle γ. As seen in subsection 2.1.1, the shear angle is commonly assigned as zero at the initial stage when weft and warp yarns are perpendicular to each other. γ is an average shear value over the entire specimen, the actual shear angle at any point on the fabric may vary. Optical methods like DIC can aid in the determination of the shear angle at any particular point on the fabric specimen.

To avoid damaging the photovoltaic strips they have been removed from the specimens. The deformation on the float parts has been measured in order to evaluate the limit of the textile deformation. The float width is measured as the distance between two parallel lines placed at the extremity of the float area as seen in Figure 3.50.

3.4.1. Test Preparation

Once the choice of which test to perform has been made, the next step that needs to be taken for an experiment is to design the appropriate clamps or choose from the commercially available ones and prepare the specimens.

Frame

An appropriate clamp holds the textile in place and does not allow slippage while testing. In this case, the chosen frame was designed by Tentech.

Previous to performing the experiments at TU Delft laboratory, the frame was tested in order to assess the correct movement and slippage of the specimen (Table 3.48 - Table 3.49). It could be concluded that connections placed on the corners of the frame did not act as pinned but clamped when the bolts were completely tightened. To avoid this issue it has been decided to tighten the bolts until the two sides of the frame touch and not go further until the bolt limit is reached. Bolts along the flanges are helpful to avoid slippage and keep the specimen pre-tensioned, for this reason, they have been tightened to their limit and therefore acted as a clamped connection. On the contrary, the bolts placed in the corner of the frame hold the frame in place and if tighten to their limit they would block the frame movement or require higher forces to deform it.

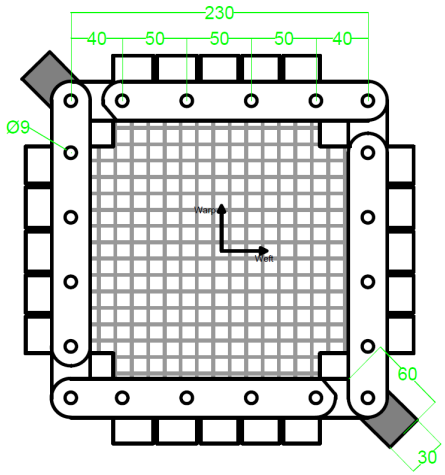

Figure 3.51: Picture frame design

Pre-tension

In general, all tensile structures are subjected to pre-tension. In the design process, the prestress level is defined by the structural engineer so the structure meets aesthetic and structural requirements. Aesthetics requirements are defined in cooperation with the architect and the building owner. Structural requirements are in avoidance of fluttering, ponds and high deformations under the design loads [32]. Moreover, architectural fabrics must be biaxially prestressed before being deformed under shear to ensure that the fabric will remain under tension for all load conditions, and to reduce excessive deflections [21].

Recommendations for minimum values propose as a “rule of thumb” prestress levels not less than 1.3 of the short-term tensile strength for PVC-coated polyester fabrics and 2.5 for PTFE-coated glass fibre fabrics, but not less than 2.0 kN/m for the least [32]. Concrete minimum values are given for PVC-coated polyester fabrics depending on the material type:

- Type I: p > 0.70 kN/m,
- Type II: p > 0.90 kN/m,
- Type III: p > 1.30 kN/m,
- Type IV: p > 1.60 kN/m,
- Type V: p > 2.00 kN/m.

In literature, many attempts have been made to measure the shear force versus shear angle behaviour of engineering fabrics, usually without paying much attention to in-plane fibre tension, though only a few attempts to characterise a shear–tension coupling experimentally have been reported; early investigations involved pre-tensioning the fabric prior to placement in a picture frame using biaxial pre-tensioning devices. These studies indicated a significant increase in shear stiffness with increasing pre-tension, typical values of a *coupling factor.* These mesoscale simulations showed that as the tensile strain increased, the shear resistance also increased [21]. During the picture frame test, if fibre tension across the sample is too low, the sample might not shear to the same extent as the frame. On the other hand, if the tension is too high, then the results might be compromised, especially if the sample is misaligned in the frame [24] .

As the scope of this research does not focus on the coupling effect between pre-tension and shear, the chosen pre-tension for all the specimens is within the same range. In this case, the main reason for pre-tensioning is so the fabric belongs to the same plane as much as possible and initial wrinkles are avoided. In order to achieve pre-tension and ensure that it will remain during testing, the fabric has been stretched and the picture frame was mounted to the fabric while tensed. As mentioned, the M8 bolts along the steel frame are used to apply pressure and avoid slippage.

Additionally, to be able to place the specimens in the steel frame, it's necessary to add holes to the fabric, so the bolts can pass through. With the help of a 1:1 scale drawing, a textile punch set and a hammer, the holes were punched through the fabric. The frame was later placed on the fabric and the bolts were tightened in order to ensure pressure and no slippage [Figure 3.52 - Figure 3.57]. This process has been implemented on all specimens. The achieved pre-tension was registered from the bi-axial machine. All fabrics were stretched bi-axially up to around 200 N in the warp direction and 180 N in the weft direction. Detailed force values on Table 3.6.

Table 3.6: Pre-tension values of picture frame specimens

	PF01	PF02	PF03	Average
F_{weft} (N)	175.8	190.3	169.7	178.6
$Flange_{weft}$ (mm)	162	160	164	162
P_{weft} (kN/m)	1.09	1.19	1.04	1.11
F_{warp} (N)	193.9	228.0	200.8	207.6
$Flange_{warp}$ (mm)	160	160	160	160
P_{warp} (kN/m)	1.21	1.43	1.26	1.30

Where:
F is the applied force from the bi-axial ring
$Flange$ is the width of the flange as shown in Figure 3.50
P is the pre-tension applied to the fabric before the picture frame is added and shear testing begins and it is the result of the applied force divided by the width of the flange

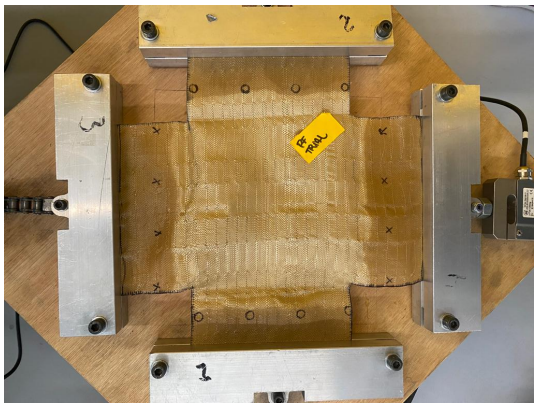

Figure 3.52: Specimen before pre-tension on bi-axial ring

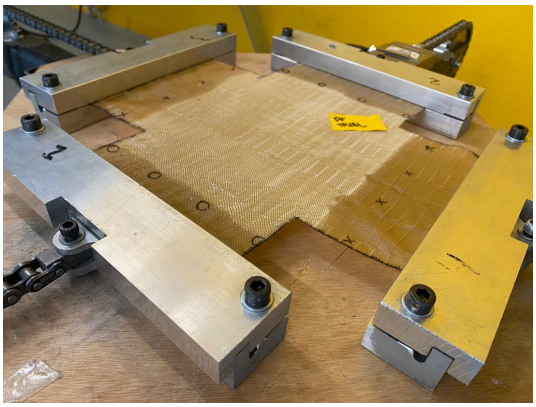

Figure 3.53: Specimen after pre-tension on bi-axial ring

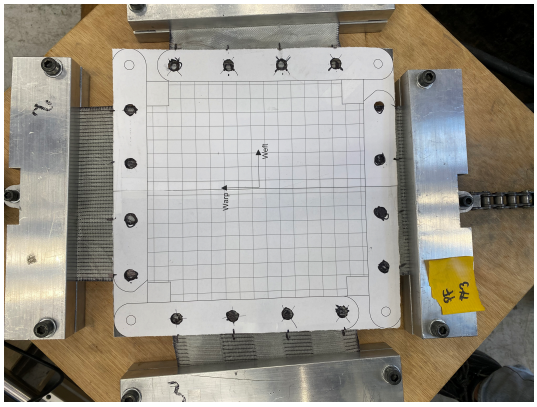

Figure 3.54: Marking of holes with help of a 1:1 scale drawing

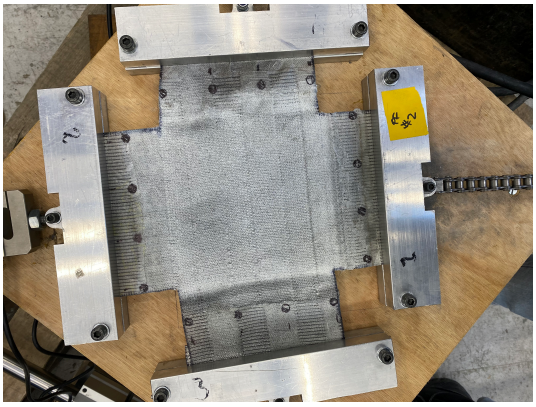

Figure 3.55: Holes have been marked

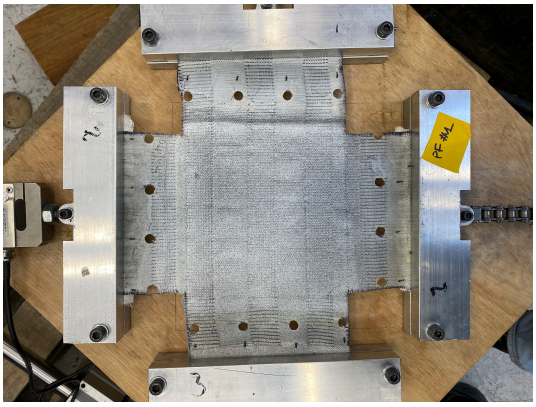

Figure 3.56: Holes have been punched through the fabric using a punching set and a hammer

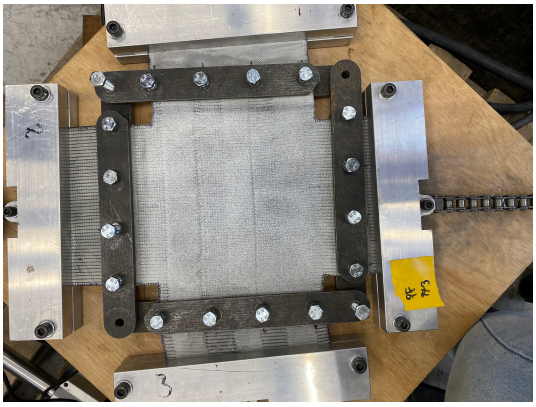

Figure 3.57: The frame is added to the fabric while is being pre-tensioned

Calibration

In order to proceed with the test execution it is necessary to know the force range to be used for the specimens. In the literature, there are a few examples where the load cell and the crosshead speed are explicitly mentioned.

On [29] the picture frame was mounted onto a Lloyd Instruments T30K tensile testing machine, with a 5 kN load cell. The fabric was placed on the pins of the frame arms, where each arm had 20 homogeneously distributed thin pins. The fabric was held on the frame in such a way as to allow rotation of the fibre bundles around the pins. The testing machine was then set in tensile mode at a constant crosshead speed. Various crosshead speeds were tried in the range of 0.08–1.6 mm/s. On [21], a universal test machine (ZwickZ2) with a 2kN load-cell was used to measure the vertical axial force in all tests and all experiments were conducted at a speed of 3.3 mm/s. The mentioned data has been used as a starting point to understand the optimal test speed.

Based on literature examples, firstly a test was performed with a trial specimen, a hand-woven Suntex fabric. During the calibration test, it was noticeable that the deformation of the frame depends not only on the speed of the test but also on how much the bolts were tightened. Unfortunately, the used frame was wrongly designed and the corners of the frame are not pinned connections. It has been decided to tighten the bolts until contact between the plates was reached as mentioned in chapter *Frame*. The test speed was selected as 0.5 mm/s. All the tests were performed maintaining the same speed of 0.5 mm/s. Initially, a stereo correlation and calibration of the camera set-up is performed from which the relative camera position and any possible distortions are identified.

3.4.2. Test Results

For tensile structure applications, the aim is for the material to be under tension only. In the case of shear stress presence, it will anyways be small and limited. In addition, the presence of OPV cells (Organic Photovoltaic) limits the deformation range of the fabric. The test results regard three specimens. Specimens were deformed on a picture frame up to around 30 degrees as it is considered the limit of linearity for shear deformation (section 2.2). The conservative maximum angle within the limit of no damage to solar cells results in 27 degrees. For angles below 27 degrees, no damage to the OPV strips occurred.

Figure 3.58: PF01 specimen

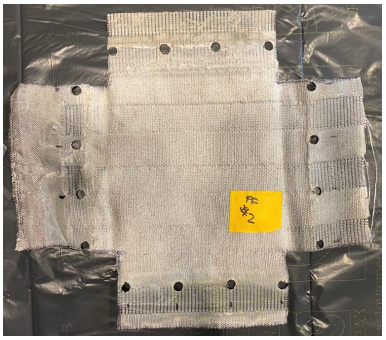

Figure 3.59: PF02 specimen

Figure 3.60: PF03 specimen

GOM is the software that allows the inspection of a specimen measured with DIC. In this software, it is possible to add inspection points, lines, angles and more. The scope is to focus on the specific part of the specimen and be able to retrieve data regarding different properties.

One of the specimens is reported *PF01* (Figure 3.61 - Figure 3.64), pictures of all specimens can be found on Appendix C. Eight angles have been randomly measured along each of the specimens in order to have a better understanding of the behaviour at different points. In this case, a *3-point angle* has been used on GOM software. The measured angle is then compared to a right angle to obtain the shear angle change. Regarding the floats where the OPV strips should be placed, the shortening in the warp direction has been measured in order to ensure the OPV strips do not undergo any stress. In this case, the shortening has been measured on GOM as *distance 1 and 2*, which is the distance between two lines as shown in Figure 3.61. At a later stage, it has been possible to associate the limit of the shortening of floats with a limited angle.

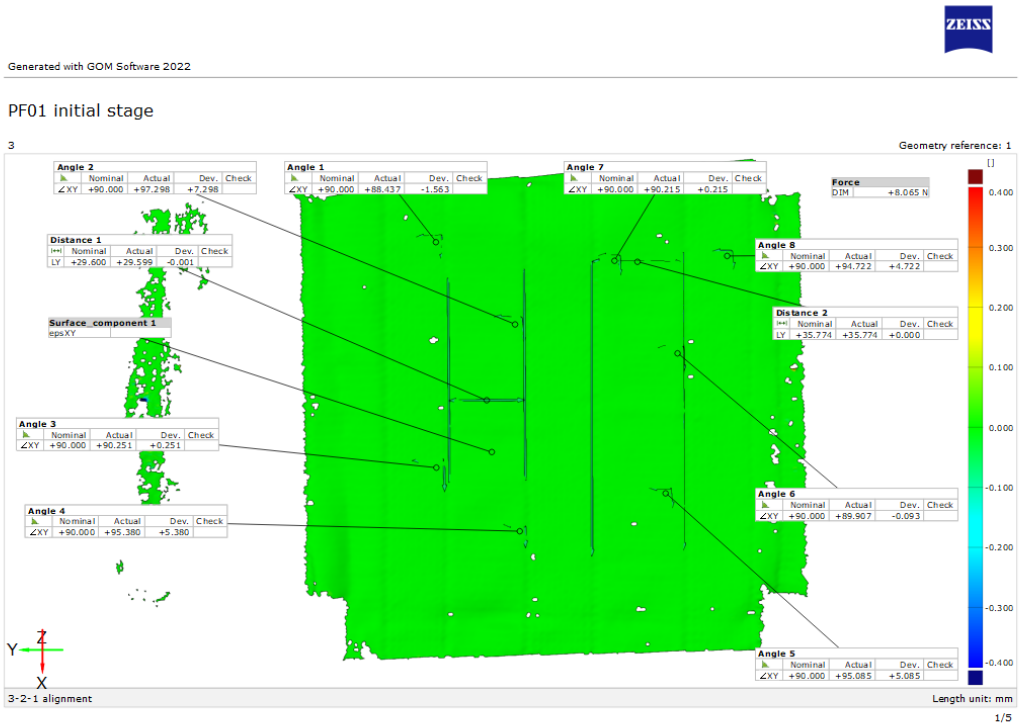

Figure 3.61: PF01 initial stage: unloaded F0=8 N

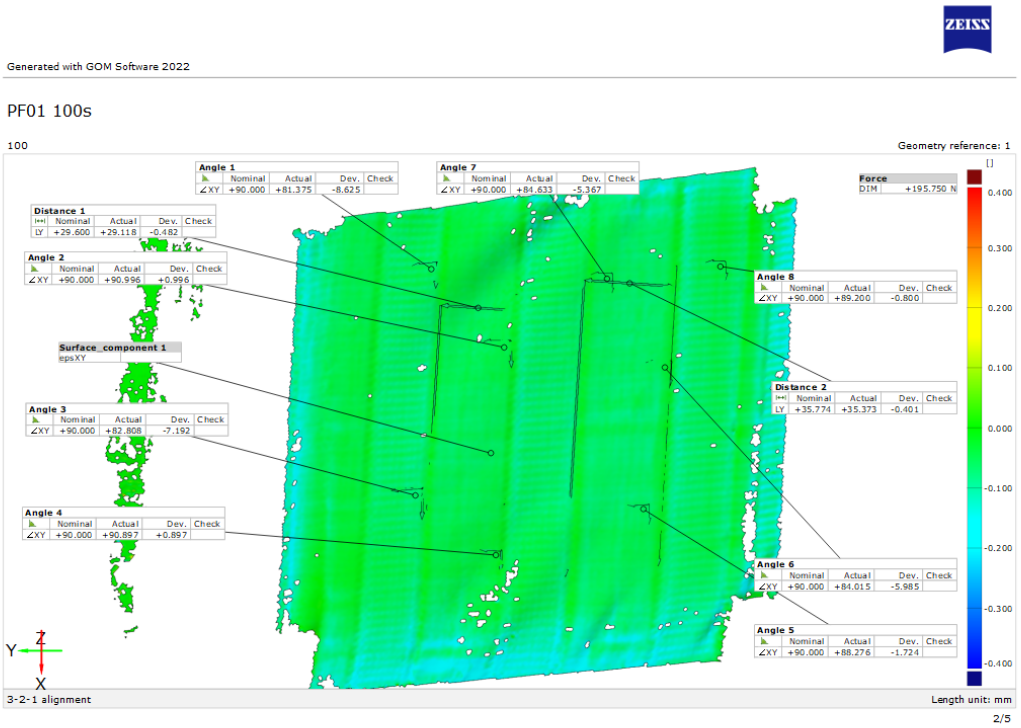

Figure 3.62: PF01 after 100s: shear force 196 N

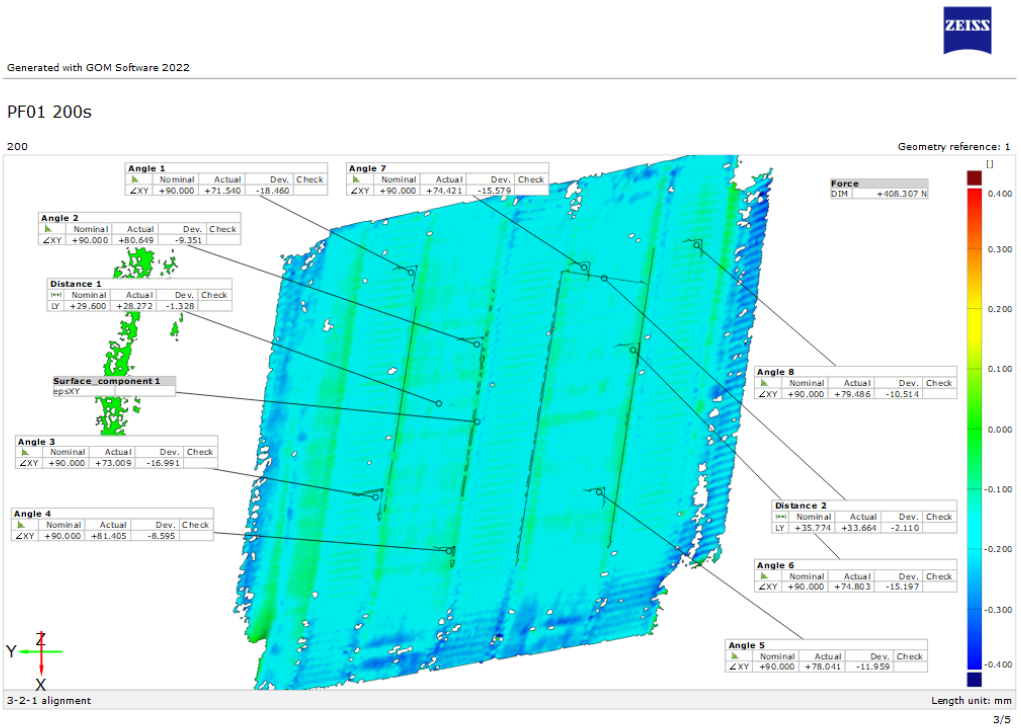

Figure 3.63: PF01 after 200s: shear force 408 N

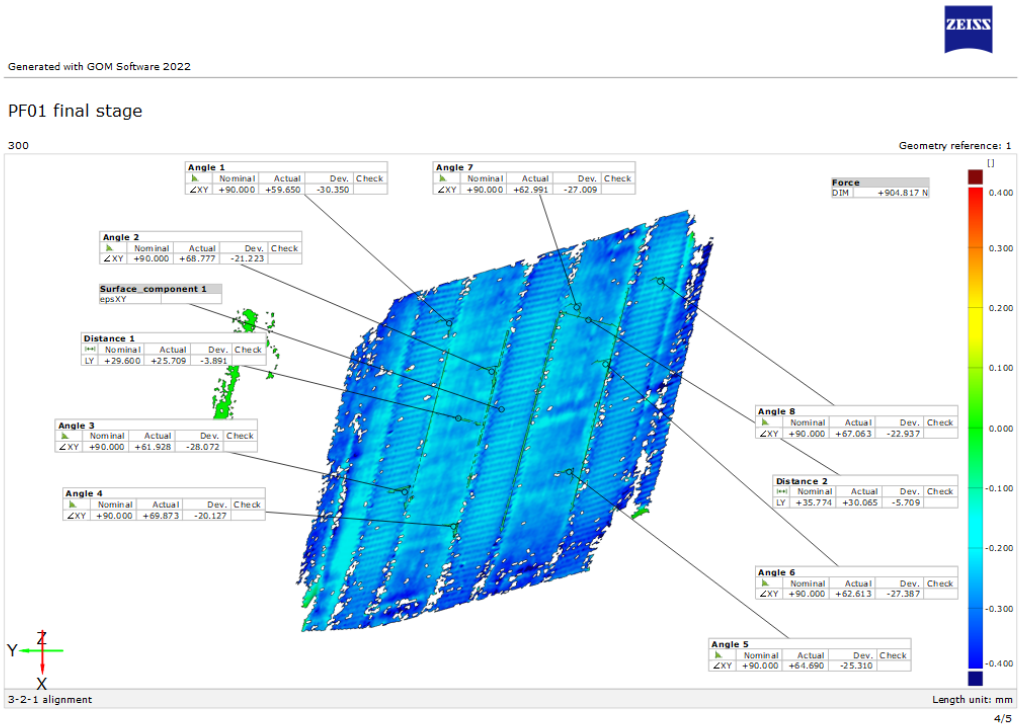

Figure 3.64: PF01 after 300s: shear force 905 N - end of test

In Figure 3.61 - Figure 3.64 warp direction corresponds to the y-axis, while weft corresponds to the x-axis. The colour scale refers to the major strain along the specimen. F0 is the force needed to keep the frame at starting position, with warp and weft at a right angle.

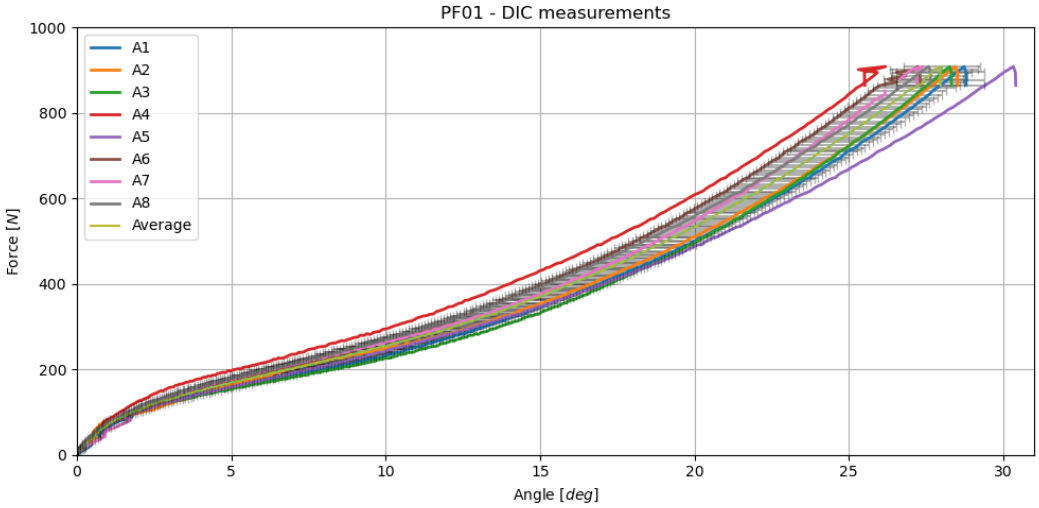

Figure 3.65: PF01 DIC response: all A_i are different points along the specimen where the angle change has been measured (Figure 3.61)

The graph in Figure 3.65 illustrates the force-angle behaviour of specimen PF01 measured with the DIC system. The origin corresponds to the beginning of testing, while the end corresponds to the where testing has been manually stopped. The average and standard deviation have also been reported in the graph. A_i reported in the graph, are different points along the specimen where the angle

change has been measured (Figure 3.61). The reference angle is 90 degrees as warp and weft have this orientation when no shear stresses are being applied, the difference between a right angle and the deformed angle is the shear angle which is represented in Figure 3.65. The graph increases gradually, starting with a downward curvature until around 7.5 degrees followed by an upwards curvature. The possible reasons for the curvature change will be discussed later in this chapter.

Usually, the interesting limit angle for textiles is where wrinkles start to appear, as mentioned in subsection 2.1.1. In the case of the studied material, the limit angle is limited by the space needed for the OPV strips in order to avoid their damage. Hence the measure of the shortening of the floating part of the weave.

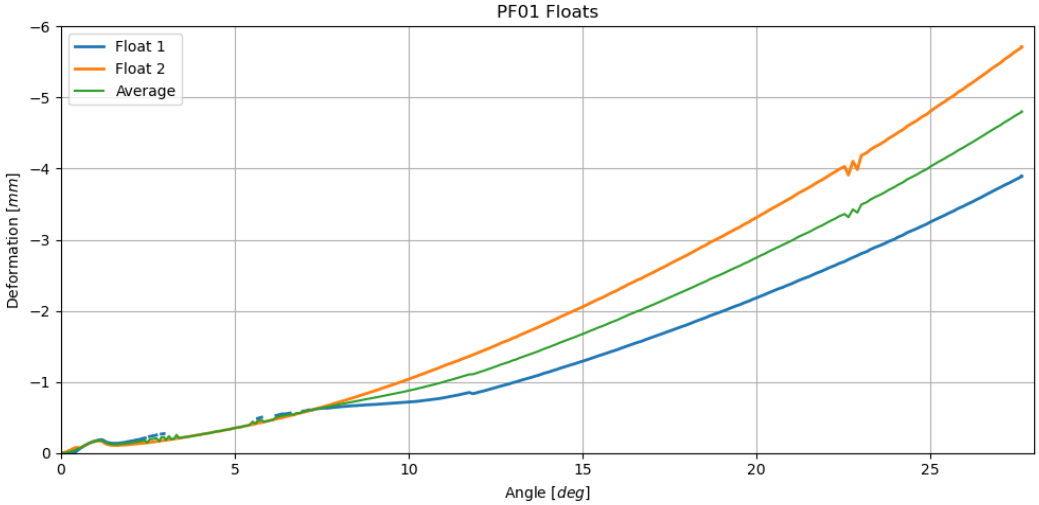

Figure 3.66: PF01 DIC response: $Float_i$ is the distance between two lines, representing the float width, as seen in Figure 3.61

The deformation-angle graph in Figure 3.66 represents the shortening in of the weave floats. In this case, at 7.5 degrees the curves start to diverge. The reason behind this is that *float 1* data couldn't be measured by the DIC system, therefore both average and float 2 have the same data.

The initial width of PF01 float is 30 and 35 mm (starting from the left float in Figure 3.61), as the width of OPV strips is 25mm the maximum feasible shortening width is 5mm. The average float deformation (*Float AVG*), of 5mm corresponds to an angle of 27.5 degrees which is considered the limit angle for PF01. This is considered a conservative limit as, from observing Figure 3.66, one can notice that at 27.5 degrees float 2 which has a starting length of 35 mm did not yet reach 10mm of shortening, while float 1 reaches 4mm at 27 degrees.

A similar representation of all other specimens can be found in Appendix C. An overview of all specimens follows. Figure 3.67 represents the response of all specimens measured in the DIC system. The angle change has been measured in eight different points for each specimen. The average of all specimens and standard deviation have also been reported in the graph.

As seen for PF01, the force-angle graph in Figure 3.67 increases gradually, starting with a downward curvature until around 7.5 degrees followed by an upwards curvature.

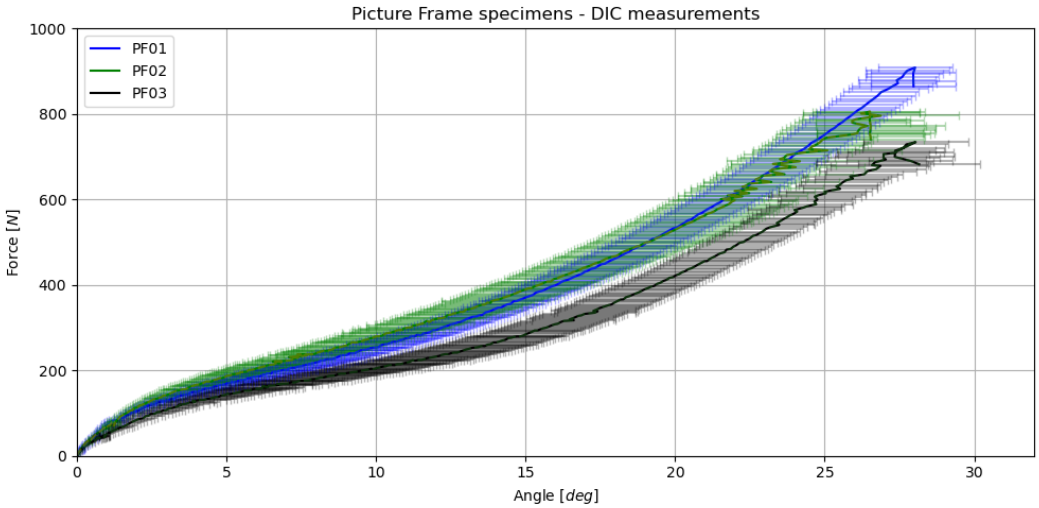

Figure 3.67: Angle response of all specimens measured with DIC system

The limit angle is defined by the space needed for the OPV strips in order to avoid damaging the system. In case of large shear deformations, the OPV can undergo compression stresses due to the shortening of the float length. An overview of the float deformation is given in Figure 3.68. The shown data regard the average of each specimen and the average of specimens PF01 and PF02 (AVG12) and its corresponding standard deviation. PF03 has been disregarded for conclusive data as it contained initial wrinkles due to an inappropriate pre-tension at the starting phase (more details on subsection 3.4.3).

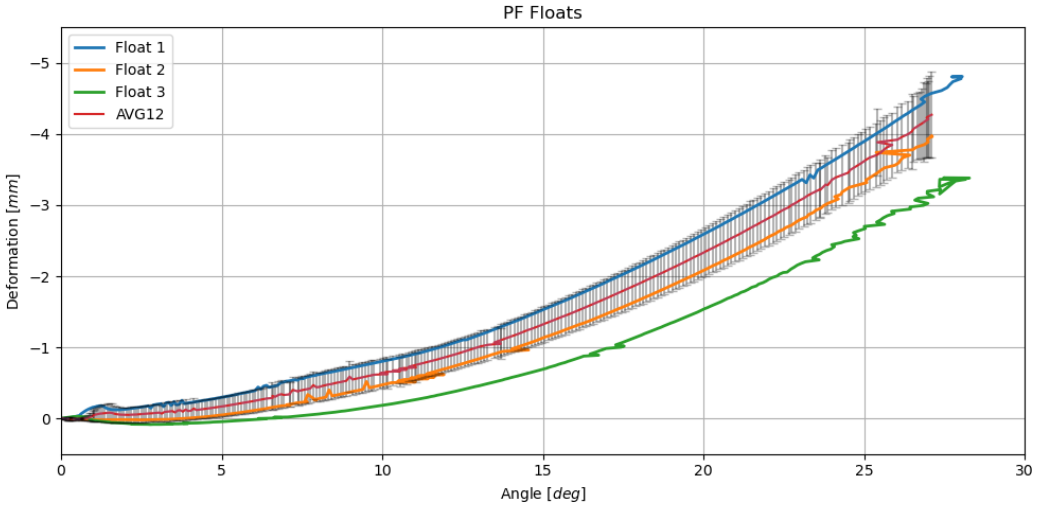

Figure 3.68: Average float shortening of all specimens

The deformation-angle graph in Figure 3.68 represents the shortening of the weave floats. The initial average width of all floats is 30 mm, as the width of OPV strips is 25mm the maximum feasible shortening width is 5mm. The average float deformation of specimens PF01 and PF02 (*AVG12*) is considered representative of all specimens. The limit of 5mm has not been reached during testing, meaning up to 27 degrees of shearing angle the OPV strips will not undergo any compressive stress.

3.4.3. Discussion

In this chapter results and observations of picture frame tests will be discussed.

All performed tests were measured using the DIC system in order to obtain more detailed information about the specimen deformation such as the shortening of the floating part of the weave, but displacement and force can also be retrieved from the tensile machine. The global angle change can be calculated from the vertical displacement.

By measuring the displacement of the tensile machine, d, where the frame is attached and through trigonometric relations, the angle of the frame θ is calculated:

$$cos\theta = \frac{\sqrt{2}L_{frame} + d}{2L_{frame}} \tag{3.4}$$

The shear angle γ is calculated from the geometry of the picture frame as $\gamma = 90° - 2\theta$. γ is also called the global shear angle. Note that this value is taken to be an average shear value over the entire specimen, the actual shear angle at any point varies as noticeable from DIC results in subsection 3.4.2.

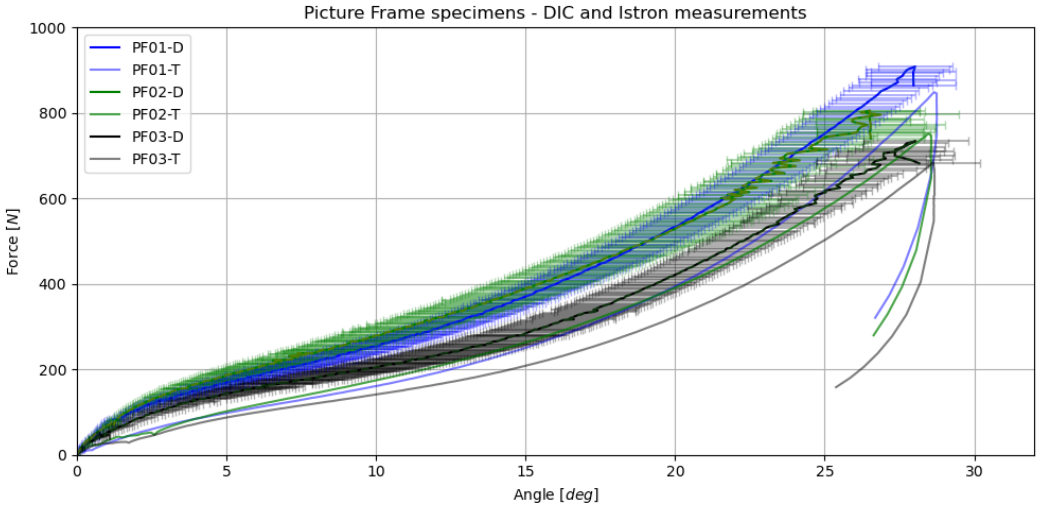

Figure 3.69: Angle response of all specimens: comparison between measurements with DIC and tensile machine

As noticeable from the graph above, all curves are subjected to a change in curvature between 5 and 10 degrees. This phenomenon is less enhanced on the tensile machine retrieved data (*-T curves*).

The reasons behind the change of curvature observed in the graph can differ. The initial higher resistance to shearing can be due to the following reasons:

- From the frame assessment it could be concluded that the bolts placed on the corners of the frame did not act as a pinned connection, but clamped when those were completely tightened. This might have influenced the initial deformation as the applied force had to be higher than the frictional resistance of the frame before starting to deform the textile itself. It is recommended to repeat the tests with a pinned frame in order to exclude this, most obvious, argumentation.
- In order to measure the shear angle at any particular point on the fabric specimen, digital image correlation (DIC) was used. The specimens were painted prior to testing so the DIC cameras could capture all the deformations along their surface. Seven layers of DIC-specific paint were used, the paint is considered elastic and works perfectly on many materials but it could have altered the stiffness of the textile. As usually this type of test is done on coated fabrics, only one or a few layers of paint are necessary - depending on the weave openness.
  There are different methods to obtain information at specific points of a specimen like using extensometers or strain gauges. In such cases, information will be available for one or more specific points and still not for the whole specimen. DIC is the only currently available method able to measure angle deformations along any point of a surface. Consequently, this argumentation can not be proven wrong with the current state of technology.

- The graph can represent the actual behaviour of the material. The force-elongation graph of warp specimens is also characterised by a change in curvature, yet the initial slope is lower. It is possible for a material, especially a textile, to have an initial higher resistance to shear which decreases once the yarns start to elongate and the crimp becomes consecutively lower. Friction between fibres should be the primary mechanism for shear resistance.

Moreover, specimen PF03 has been disregarded for conclusive data regarding shear angle evaluation as the initial pre-tension was not achieved properly. The DIC videos show initial wrinkles. This phenomenon is also visible from the graph below as the floating part of the weave starts by elongating, meaning wrinkles get flattened when increasing the applied load. The average refers o the average of specimens PF01 and PF02.

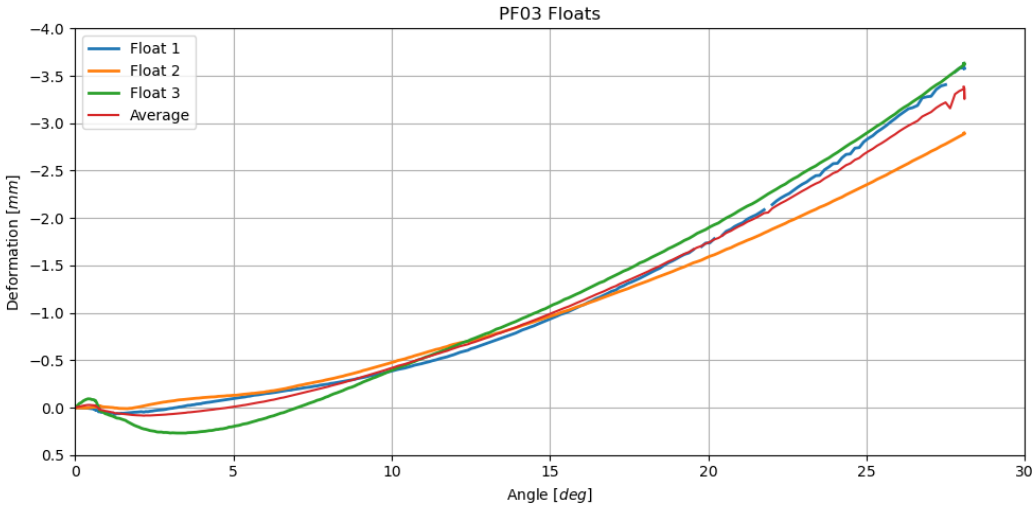

Figure 3.70: PF03 Float deformation

3.4.4. Conclusive Remarks

When investigating the damage to the OPV strips, the limit angle is defined by the space needed in order to avoid stresses caused by the weave in the strips. In case of large shear deformations, the OPV can undergo compression stresses due to the shortening of the float length.

The initial average width of all floats is 30 mm, as the width of OPV strips is 25mm the maximum shortening width is 5mm. The limit of 5mm has not been reached during testing, meaning up to 27 degrees of shearing angle the OPV strips will not undergo any compressive stress. The 27 degrees limit is imposed by the end of available data as tests have been stopped after small angle deformations, which are the most critical deformations for tensile structures and the ones investigated in this research.

For angles between 0 and 30 degrees a relation between angle and shear force has been found. This result will later be used to evaluate the shear stiffness of the studied material.

3.5. Elastic Modulus Evaluation

The determination of tensile stiffness properties and elastic moduli for coated fabrics is detailed on EN 17117-1 [18]. A similar procedure has been followed, guided by common engineering practice, to determine the elastic modulus of the uncoated studied material.

Three specimens (EL01:EL03) have been tested using a bi-axial ring machine available at Tentech on 5/12/2022. Specimens of cruciform shape are bi-axially loaded in the plane of the fabric. The loads are applied cyclically in the warp and weft directions simultaneously. The test execution procedure is similar to the pre-tensioning of the fabric previous to mounting the specimens in the picture frame as seen in subsection 3.4.1. In this case, the loading ratio conditions were:

- P:P pretension on warp and weft direction;
- P:1 pretension on warp direction and a higher force on weft direction (at least double the value of P);
- 1:1 both warp and weft directions were pulled with the same force (at least double the value of P);
- 1:P warp is kept to force value 1 while weft decreases again to P.

The exact load applied at each step can be found in subsection 3.5.1. Measurements of length are taken with a digital caliper of 0.01mm resolution. Those were later used to derive the biaxial properties of the fabric. To avoid damaging of the photovoltaic strips they have been removed from the specimens.

Figure 3.71: Caliper used to measure deformation

The specimens used were the same specimens used for angle evaluation. They are therefore coated with DIC elastic paint. Dimensions can be found in Table 3.5. The specimens, in this case, have been modified by applying resin and glass fibre which acted as a bond to the fabric used to extend to the flanges (not visible in the below pictures).

Figure 3.72: EL01 specimen

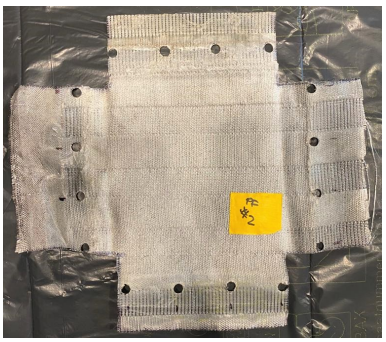

Figure 3.73: EL02 specimen

Figure 3.74: EL03 specimen

The distance between the silver plates applied to the specimen has been measured at each load adjustment. Specimen EL02 has failed as the flange extension ruptured while testing. EL01 and EL03 tests were concluded successfully.

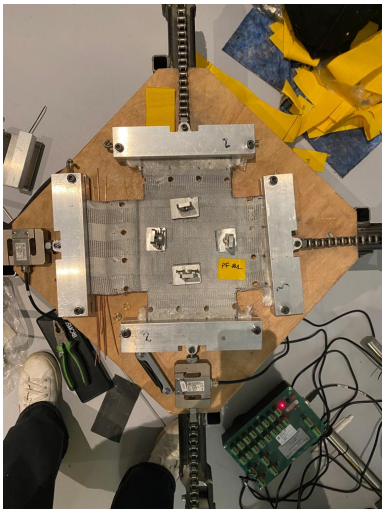

Figure 3.75: unloaded specimen

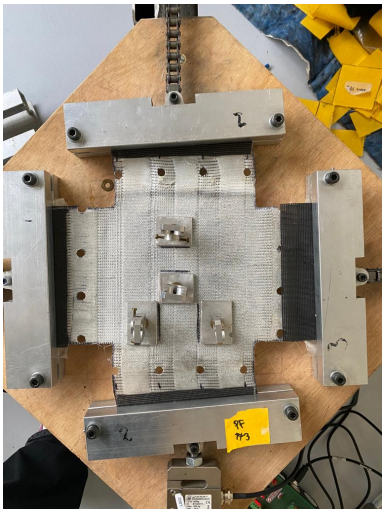

Figure 3.76: loaded specimen

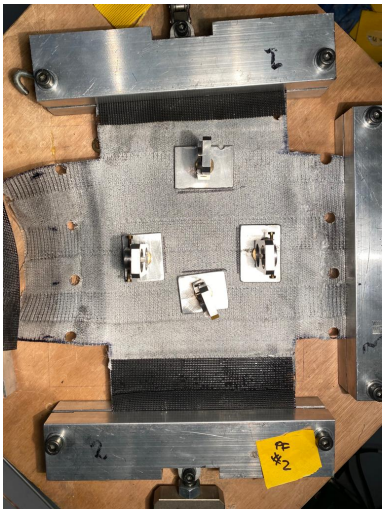

Figure 3.77: extension of flange failure on EL02 specimen

3.5.1. Test Results

In order to calculate the elastic modulus, it is necessary to find the load applied at each step. The used instrument is a bi-axial ring, it is an instrument able to apply loads to a textile in both directions. This is a force-driven test, but in this case, the force is applied through a pneumatic mechanism. Therefore, once the force is applied, the instrument is not able to maintain it to the same value as noticeable in Figure 3.78 and in Figure 3.79. The average force applied at each step has been considered and is reported in Table 3.7 and Table 3.8.

To calculate the elastic modulus the following equation has to be applied:

$$E = \frac{\sigma}{\epsilon} = \frac{\frac{F}{l_f}}{\frac{l - l_0}{l_0}} \tag{3.5}$$

Where:
F is the applied force
l_f is the length of the flange, where the force is applied = 160 mm
l_0 initial length - at load ratio P
l length after loading - at load ratio 1

Both valid tests are reported below, starting from EL01. As mentioned the specimen has been cyclically loaded. An overview of the cycles can be found in Table 3.7.

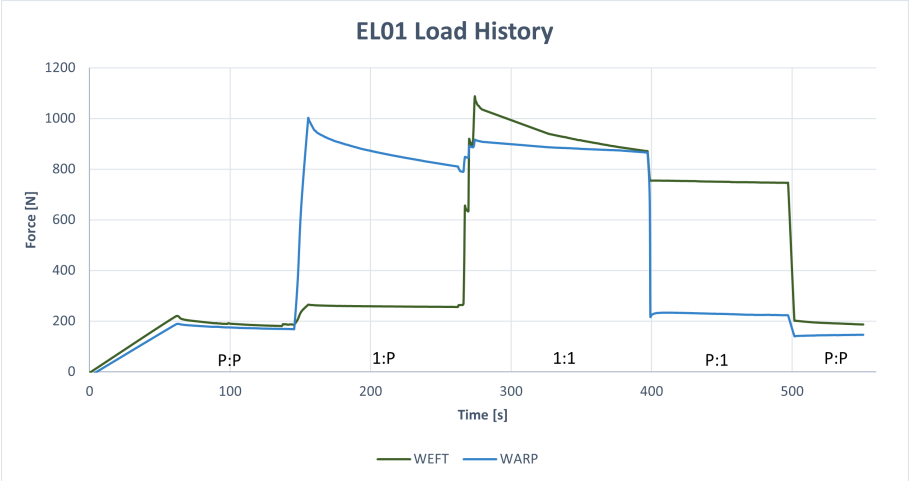

Figure 3.78: EL01 Load history

Table 3.7: EL01: elastic modulus evaluation

		Warp	Weft	Load ratio
F_0	(N)	172.8	186.2	P:P
l_0	(mm)	83.9	90.5	
F	(N)	866.2	258.4	1:P
l	(mm)	85.4	90.6	
E	(kN/m)	233.0	291.5	
F	(N)	880.6	932.5	1:1
l	(mm)	85.2	91.8	
E	(kN/m)	287.6	308.0	
F	(N)	232.6	750.4	P:1
l	(mm)	83.7	91.7	
E	(kN/m)	231.5	263.6	
F	(N)	143.6	192.3	P:P
l	(mm)	84.0	90.3	
E	(kN/m)	322.3	230.0	
E_{AVG}	(kN/m)	270	270	
σ		44	34	
CV	(%)	17	13	

As noticeable from Figure 3.78, the applied load does not remain constant. As mentioned, this is due to the pneumatic mechanism of loading. The average of all evaluated elastic moduli for this test is reported as E_{AVG}, its standard deviation as σ and the coefficient of variation CV. Both warp and weft elastic moduli resulted in 270 (kN/m) with a coefficient of variation below 20%.

EL03 has been cyclically loaded. An overview of the cycles can be found on Table 3.8.

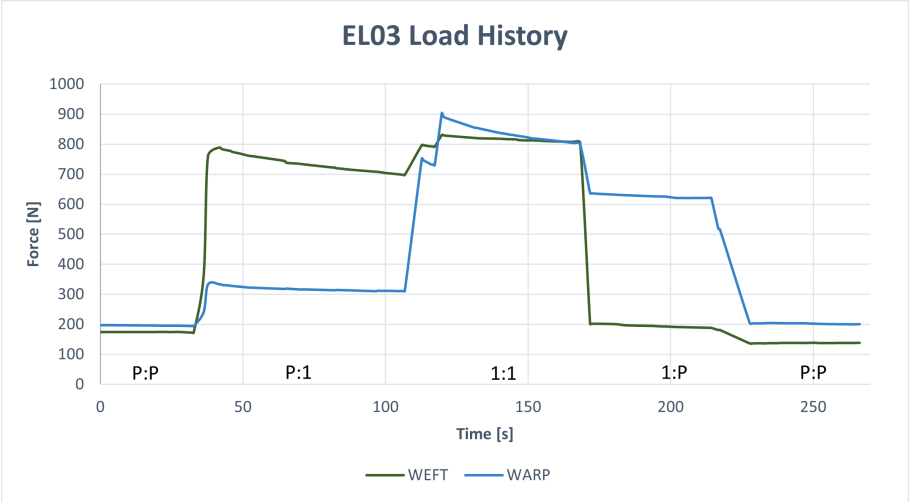

Figure 3.79: EL03 Load history

Table 3.8: EL03: elastic modulus evaluation

		Warp	Weft	Load ratio
F	(N)	196.4	174.1	P:P
Length	(mm)	64.2	89.1	
F	(N)	624.9	193.2	1:P
Length	(mm)	64.0	89.0	
E	(kN/m)		265.6	
F	(N)	827.0	814.2	1:1
Length	(mm)	64.8	90.3	
E	(kN/m)	383.1	315.5	
F	(N)	317.4	733.7	P:1
Length	(mm)	63.9	90.0	
E	(kN/m)	211	375.5	
F (N)		202.8	137.8	P:P
Length	(mm)	64.3	88.9	
E	(kN/m)	447.7	278.4	
E_{AVG}	(kN/m)	347	309	
σ		122	49	
CV	(%)	35	15	

The warp elastic modulus of the second load step (1:P) has been excluded from the final average, yet the coefficient of variation E_{warp} is 35%. The reliability of these results is not satisfactory.

In this case, the results differ slightly between warp and weft elastic moduli. The values are also not close to the ones from EL01.

3.5.2. Discussion

By performing two successful tests it can be concluded that an indication of the elastic moduli of Suntex has been found by averaging the results of the two tests. The warp elastic modulus is $E_w = 310kN/m$ and the weft elastic modulus is $E_f = 290kN/m$.

The results are not as expected. As the textile has a higher tensile strength in the weft direction, it was expected that the elastic modulus in the weft direction would be higher than the one in the warp direction. The low number of valid tests makes the results not reliable. Moreover, as the specimens used were the same specimens used for angle evaluation, they are coated with paint. This could have influenced the results. It is therefore recommended to perform new tests.

3.5.3. Conclusive Remarks

The found values are comparable with type I architecture textiles in literature, making it a promising achievement for the developing material. The obtained result can be adopted only in preliminary designs. It is recommended to test the material with project-specific bi-axial cycling loads as the parameter is related directly to the load history.

4

Shear Stiffness Evaluation

This chapter illustrates the characterisation of shear properties via a regression analysis performed to relate the studied material's shear angle to its shear stiffness. Regression is a powerful tool that can be used to understand the relationships between variables, make predictions, and test hypotheses.

The process follows literature examples as seen on section 2.3 where shear stress curves were fitted with polynomial functions. Firstly the shear stress τ_s is plotted against the measured angle, and then the obtained curves are assigned polynomial regressions equations. The derivative of those regression equations provides the shear rigidity modulus G_{12} as a function of the global shear angle γ. The shear rigidity modulus is one of the parameters we are looking for to design a tensile using the studied material.

Regression is a type of predictive modelling. It models a dependent variable *y* as a function of one or more independent variables *x*. The dependent variable is the response variable, and the independent variables are the predictor variables.

4.1. Data Collection

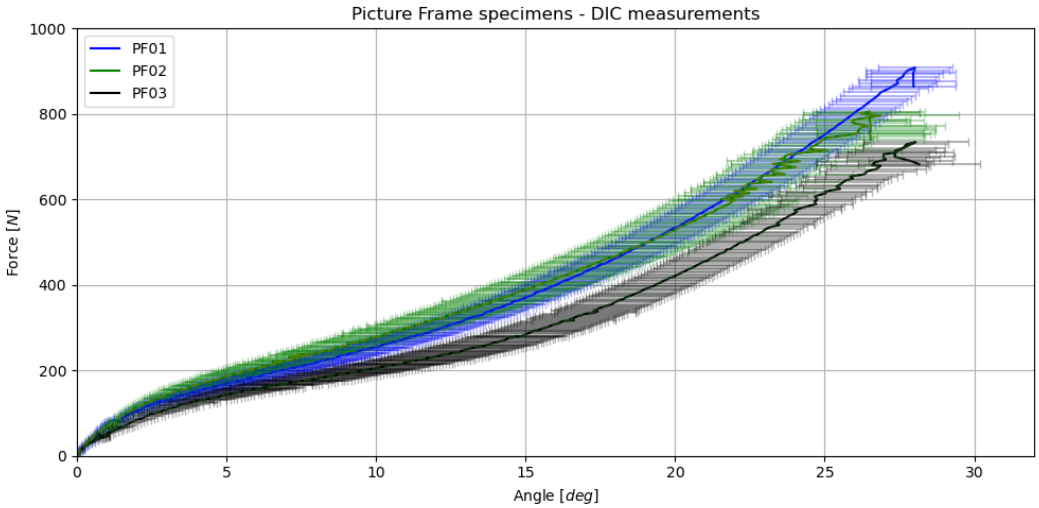

Figure 4.1: DIC response of picture frame tests: Shear Force - Average Angle relation of all tested specimens

Starting with the data from Figure 4.1, to follow the literature example the shear stress must be calculated as follows:

$$\tau_s = \frac{F_s}{HL_{frame}} \tag{4.1}$$

Where:
τ_s shear stress $[N/mm^2]$
F_s shear force needed to deform the frame $[N]$
H thickness of the material, $0.6mm$
L_{frame} length of one side of the picture frame, $230mm$

The regression analysis starts by observing the curve one wants to predict and deciding what type of model is the most suited. The model can be linear, polynomial, non-linear, logistic, etc. In this case, the curve we want to predict is one of the curves in Figure 4.2, which is the DIC response of angle-stress relation of all tested specimens, an average of all three (PF AVG123) and an average of PF01 and PF02 (PF AVG12).

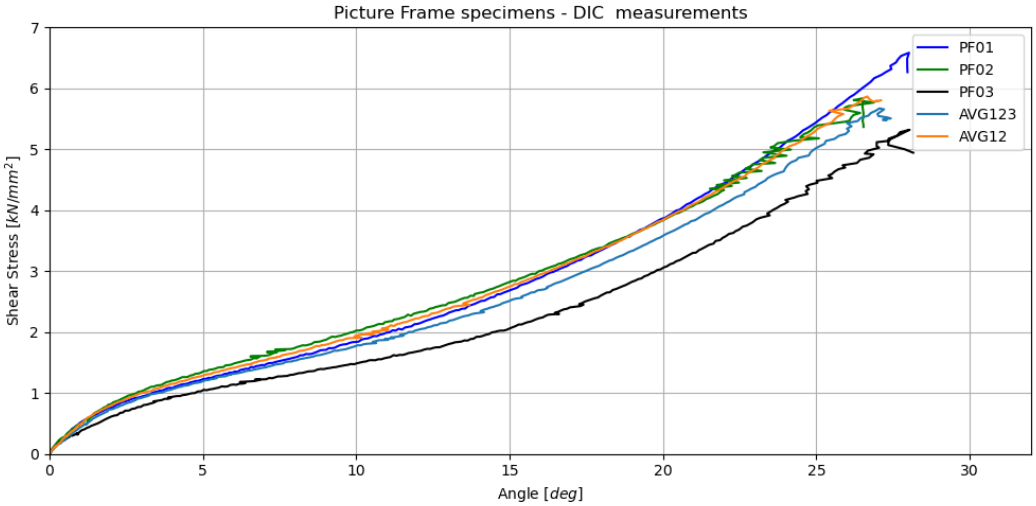

Figure 4.2: DIC response of picture frame tests: Shear Stress - Angle relation of all tested specimens, an average of all three (PF AVG123) and an average of PF01 and PF02 (PF AVG12)

From Figure 4.2, it is observed:

- The curvature of all sets begins negative and around 7.5 degrees it changes direction and becomes positive.
- The response of specimen PF01 and PF02 is very similar. PF03 follows the same trend but has lower stress values. This is because PF03 had an initial uneven surface and wrinkles, as mentioned in subsection 3.4.3.
- When averaging the response of all specimens (PF AVG123) the curve is below both PF01 and PF02.

Considering the above observations it has been decided to proceed with a regression analysis of the PF AVG12 curve as the most representative of all tests.

The chosen regression model is linear. Linear regression can not model nonlinear relationships between the predictor and outcome variables [2], consequently it is not possible to model the change of curvature that is visible in Figure 4.2. In the interest of having a realistic model, the different behaviour must be somehow considered therefore a bi-linear model prediction will be studied. The expected curve will consequently change its slope, starting with a higher value and subsequently decreasing it.

4.2. Regression Analysis

The basic goal of regression analysis is to model the expected value of a dependent variable *y* in terms of the value of an independent variable *x*. In this case, the dependent variable *y* can be considered the shear stress, while the independent variable *x* is the shear angle.

A linear regression starts by stating the following equation:

$$y = a_0 + a_1 x \tag{4.2}$$

The regression analysis intends to estimate a set of coefficients ($a_0 - a_1$) that minimises the difference between predicted and actual values. Root mean square error and coefficient of determination are commonly used to verify results. Both have been used for comparing the performance of the different models presented in this thesis.

Root Mean Square Error

It is extremely helpful to have a single number to judge a model's performance, root mean square error is one of the most widely used measures. Root Mean Square Error *RMSE* is the standard deviation of the residuals (prediction errors). Residuals measure how far from the regression line data points are: RMSE is a measure of how spread out these residuals are. In other words, it tells how concentrated the data is around the line of best fit. Based on a rule of thumb, it can be said that RMSE values between 0.2 and 0.5 show that the model can relatively predict the data accurately. The formula is:

$$RMSE = \sqrt{\frac{\sum_{i=1}^{N}(e_i - o_i)^2}{N}} \tag{4.3}$$

Where:
e = expected values (unknown results)
o = observed values (known results)
N = number or data points

Coefficient of Determination

The coefficient of determination also referred to as R^2 can be thought of as a percentage. It gives an idea of how many data points fall within the results of the line formed by the linear regression equation. The higher the coefficient, the higher percentage of points the line passes through when the data points and line are plotted. If the coefficient is 0.80, then 80% of the points should fall within the regression line.
R is called the correlation coefficient. Correlation coefficients are used to measure how strong a relationship is between two variables. Pearson's R is a correlation coefficient commonly used in linear regression. The formula is:

$$R^2 = 1 - \frac{SSR}{SST} \tag{4.4}$$

With SSR (sum of squared residuals)

$$SSR = \sum_{i=1}^{N}(e_i - o_i)^2 \tag{4.5}$$

and SST (total sum of squares)

$$SST = \sum_{i=1}^{N}(e_i - \frac{\sum_{i=1}^{N} e_i}{N})^2 \tag{4.6}$$

Where:
e = expected values (unknown results)
o = observed values (known results)
N = number or data points

Analysis Results

In an attempt to find the optimal point for the slope change in the analysis, three attempts have been made. Root mean square error and coefficient of determination have been used for comparing the performance of the different presented models. Full analysis code is shown on Appendix D.

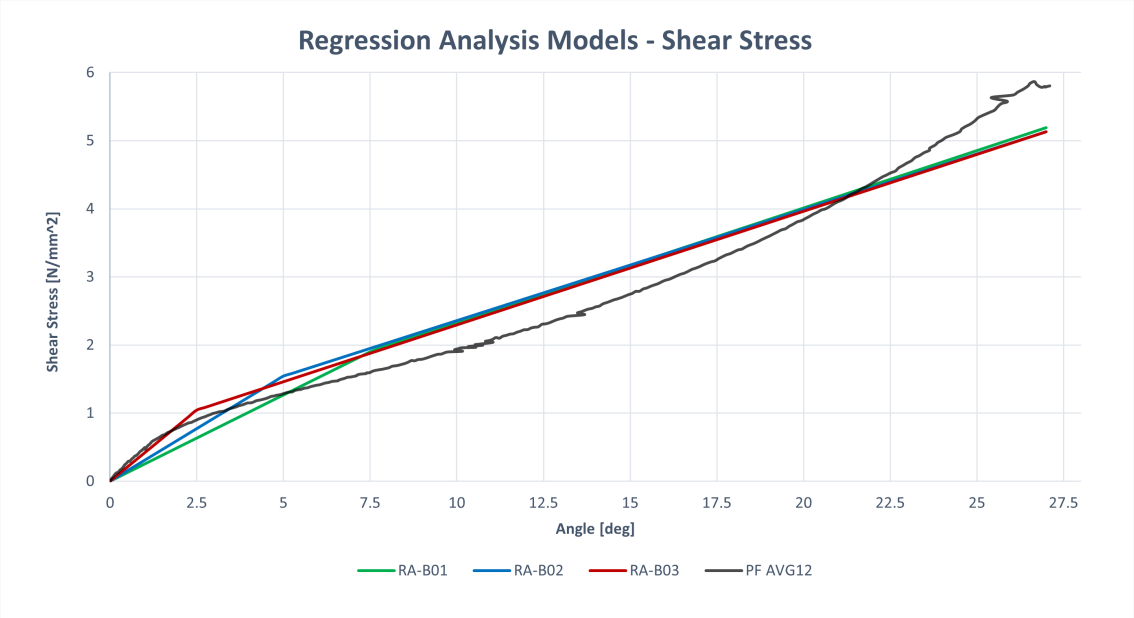

Figure 4.3: Models obtained with bi-linear regression analysis with an attempt to fit PF AVG12 curve

As seen in Figure 4.3, three different bi-linear curves have been presented in an attempt to fit curve PF AVG12 (black curve). On Table 4.1 all results are compared. The angle of slope change is called *kink point*. Every variable with *-1* refers to the initial part of the graph (from zero to kink point), and every *-2* refers to the last part of the graph (from kink to end).

Table 4.1: Comparison of results

Model	Kink Point [deg]	Slope 1	Slope 2	RMSE 1	RMSE 2	R^2 1	R^2 2
RA-B01	7.5	0.25	0.17	0.034	0.149	0.85	0.91
RA-B02	5	0.31	0.16	0.019	0.157	0.88	0.91
RA-B03	2.5	0.42	0.17	0.004	0.119	0.95	0.94

As noticeable from Table 4.1, RA-B03 seems to be the most accurate model as 95% of predicted values fit the expected values on the first part of the model, while 94% fit in the second part. Moreover, this model has the lowest RMSE for both parts of the equation. We can consider model RA-B03 the best-fitting model to represent the shear force-angle response.

The equation of this model is:

$$y = 0.42x \text{ for } 0 \leq x \leq 2.5 \tag{4.7}$$

$$y = 0.17x + 0.63 \text{ for } 2.5 < x \leq 27 \tag{4.8}$$

x being the angle in degrees and *y* being the shear stress in kN/mm.

4.3. Shear Stiffness

As highlighted in the literature, on section 2.3, shear stress curves were fitted with polynomial functions and the derivative of those regressions equations provide the shear rigidity modulus G as a function of the global shear angle γ. The same procedure has been followed to determine the shear modulus G of the studied material.

By derivating the RA-B03 equation and converting the results to the proper units, we obtain:

$$G = 42 \text{ for } 0 \leq x \leq 2.5 \tag{4.9}$$

$$G = 17 \text{ for } 2.5 < x \leq 27 \tag{4.10}$$

Those results are reasonable when observing shear stress-angle response graphs (Figure 4.3). We can notice a higher stiffness for small angles compared to larger angles. The obtained result positions the studied material into low shear stiffness for small angles and medium shear stiffness for angles higher than 2.5 degrees by comparison with other textiles. Meaning for angles higher than 2.5 degrees the textile has some shear carrying capacity. Typically type I textiles have shear rigidity equal to 30.

5

Conclusions and Recommendations

This study provides a methodology to characterise a novel uncoated woven solar cell integrated textile for tensile structure application. One should be aware that, typically in the early phases of a project, the final used membrane material is not yet known, as it happens in the case of this novel material called *Suntex*, which is currently under development.

Membrane structures are a relatively new type of construction, therefore, technical guidance and recommendations on matters of design, specification and testing information tend to be available for more specific rather than general purposes [19]. Especially for tensile structures, the common practice is to use coated textiles because of their high strength and weather-resistant properties. The desire to use an innovative and uncoated material such as Suntex for tensile structures applications comes with difficulties in terms of characterisation. With this research, it is now possible to start a preliminary design of a tensile structure with the newly developed material. It is the first step in the introduction of a new building technique.

Membrane properties determined in preliminary tests are helpful to be used in the early stages of the design. However, in a later stage, when the design is fixed, it is better to determine certain parameters based on the project and its specific load levels. This is especially important for a biaxial test intended to determine elastic and shear stiffness values and crimp interchange as those parameters are related to load level.

5.1. Conclusions

The main findings of chapter 3 and chapter 4 have already been presented at the end of their respective chapters. This section will provide the specific answers to the research questions presented in the introduction and problem statement (chapter 1).

How can the shear behaviour of an uncoated woven solar cell integrated textile be characterised for its application in tensile structures?

A method for the characterisation of shear properties has been developed in order to answer this question. It consists of investigating the limit angle that avoids damage to the inserted solar strips and the determination of the shear stiffness of the material. Finally, to evaluate the applicability of the material different mechanical properties have been assessed.

As the studied material is an innovative material that has solar strips integrated into the weave, more steps are needed to evaluate its applicability and characterise its shear behaviour. As prevously mentioned, the process of answering the main research question has been divided into sub-questions. Sub-question 1 regards the angle change due to shear stresses and to which range it would not damage the solar strips. The parameters needed for design are membrane maximum stresses, crimp interchange and elastic and shear modulus. Those are addressed in sub-question 2.

1. Can an uncoated woven solar cell integrated textile undergo shear deformation without damaging the solar cells?

When investigating the damage to the Organic Photo Voltaic (OPV) strips due to shear deformation, the limit angle is defined by the space needed to avoid stresses caused by the weave in the strips. In case of large shear deformations, the OPV can undergo compression stresses due to the shortening of the float length.

It has been found that the initial average width of the floating part of the weave, containing the solar strips, is 30 mm. As the width of OPV strips is 25mm, the maximum feasible shortening is 5mm.

The limit of 5mm has not been reached during testing, meaning up to 27 degrees of shearing angle the OPV strips will not undergo any compressive stress. The 27 degrees limit is imposed by the end of available data as tests have been stopped after small angle deformations, which are the most critical deformations for tensile structures and the ones investigated in this research. For angles below 27 degrees, there will be no damage to the solar strips.

2. What are the parameters needed for the design of a tensile structure?

Different steps will be necessary depending on which type of form-finding program will be used to design each tensile structure. Once the boundary conditions are set and the preliminary form of the structure has been chosen, it is time to apply a material to the structure and check its strength and deflections considering different load cases. The design is then modified in an iterative manner in order to achieve the desired form compatible with the chosen material.

This thesis focuses on the characterisation of the parameters needed to define a novel material and be able to apply it to a defined structure. Those parameters are:

- Membrane Maximum Stress: is a parameter related to the textile tensile strength. It gives information about the maximum allowed stresses of the loaded membrane. The tensile strength of the textile is the force at which the material fails.
- Elastic Modulus: is the material resistance of being elastically deformed. Warp and weft values differ due to the anisotropic nature of textiles.
- Shear Modulus: is the material resistance to shear deformation.
- Crimp Interchange: crimp in a textile is a measurement of its waviness. When a fabric is subjected to uniaxial stress, the crimp in the direction of loading is gradually reduced and the crimp in the transverse threads increases, this is called crimp interchange. This parameter plays an important role in yarn extensibility, compressibility, and fabric extensibility and improves fabric quality. Because of the testing complexity of this parameter, its characterisation is not included in this thesis.

The applicability and design possibilities for a tensile structure with this material are dependent on the mentioned parameters.

2.1 What is the warp and weft strength of the studied textile?

Specimens were pulled on a monoaxial tensile machine until rupture. The average warp strength resulted in $Ft_w = 280daN/5cm$, while the weft strength resulted in $Ft_f = 340daN/5cm$. The warp strength of the studied textile is not sufficient for a type I (≥ 300daN/5cm) which is the lower boundary for textiles for application in tensile structures. The elongation in both directions resulted in less than 17% therefore the material is within the norm in regards to elongation.

By knowing the tensile strength of a textile, it is possible to calculate the maximum membrane stress. The maximum membrane stress corresponds to the maximum allowable stress in the membrane after load application. For the studied textile this corresponds to $\sigma_w = 11.2kN/m$ and $\sigma_f = 13.6kN/m$.

2.2 What is the elastic modulus of the studied material?

Specimens of cruciform shape are bi-axially loaded in the plane of the fabric. The loads are applied cyclically in the warp and weft directions simultaneously. By performing two successful tests it could be concluded that an indication of the elastic moduli of Suntex has been found by averaging the results of the two tests. The warp elastic modulus is $E_w = 310kN/m$ and the weft elastic modulus is $E_f = 290kN/m$.

The results are not as expected. As the textile has a higher tensile strength in the weft direction, it was expected that the elastic modulus in the weft direction would be higher than the one in the warp direction. The low number of tests makes the results not reliable. Moreover, as the specimens used were the same specimens used for angle evaluation, they are coated with paint. This could have influenced the results.

However, the obtained results can be adopted in preliminary designs as they are in the expected range for a type I textile, which E = 250-350, making it a promising achievement for the developing material. But it is recommended to test the material with project-specific bi-axial cycling loads as the parameter is related directly to the load history.

2.3 What is the relation of the shear angle of a textile to its shear stiffness and what is the shear stiffness of the studied textile?

From the literature, it has been found that the slope of a shear stress-angle curve represents the textile shear stiffness.

For angles between 0 and 30 degrees a relation between angle and shear force has been found through experiments. The shear stress-angle curve found during testing has been subjected to regression analysis to find a fitting curve.

After a few iterations, the most accurate model has been found. The coefficient of determination is 95% on the first part of the model and 94% in the second part. Moreover, this model has the lowest mean root square error (RMSE) for both parts of the equation.
The equation of this model is:

$$y = 0.42x \text{ for } 0 \leq x \leq 2.5 \tag{5.1}$$

$$y = 0.17x + 0.63 \text{ for } 2.5 < x \leq 27 \tag{5.2}$$

x being the angle in degrees and *y* being the shear stress in kN/mm.

The derivative of the regression equations provides the shear rigidity modulus G as a function of the global shear angle γ. The shear stress curve was fitted with linear functions and the derivative of those regression equations provides the shear rigidity modulus G as a function of the global shear angle γ.

the shear rigidity modulus of the studied material has been found and results in:

$$G = 42kN/m \text{ for } 0 \leq \gamma \leq 2.5 \tag{5.3}$$

$$G = 17kN/m \text{ for } 2.5 < \gamma \leq 27 \tag{5.4}$$

Where γ is the shear angle of the textile.

Shear stiffness, curvature and maximum deflection are related. For example, in a hypar structure, when the corner height and fabric curvature increase, the structure must span between diagonally opposite corners and the effect of fabric orientation and shear stiffness on deflections becomes pronounced. The stress that occurs under the load of the fabric is inversely proportional to the curvature of the shape. Therefore large curvature radius will compensate under load by curving more until equilibrium

is reached. Textiles with higher shear stiffness are capable of larger deflections without damage and failure.

The obtained result positions the studied material into low shear stiffness for small angles and medium shear stiffness for angles higher than 2.5 degrees by comparison with other textiles. Meaning for angles higher than 2.5 degrees the textile has some shear carrying capacity. Typically type I textiles have shear rigidity equal to 30 kN/m.

An overview of the parameters found is given on Table 5.1 and Table 5.2. Those answer sub-question 2.

Table 5.1: Overview assessed parameters

Parameter	Unit	Warp	CV %	Weft	CV %	Nr specimens
Ft	daN/5cm	28	7	34	2	3
ϵ	%	12	8	15	12	3
σ_{max}	kN/m	11.2	7	13.6	2	3
E	kN/m	310	26	290	15	2

Table 5.2: Overview shear modulus

Parameter	Unit	Value	Boundary	Nr specimens
G	kN/m	42	$0 \leq \gamma \leq 2.5$	3
G	kN/m	17	$2.5 < \gamma \leq 27$	3

Where:
CV coefficient of variation
Ft tensile strength
ϵ strain
σ_{max} maximum membrane stress
E Elastic modulus
G Shear modulus, γ shear angle

5.2. Recommendations for Future Research

This section provides recommendations for future research that can help expand the current knowledge on the characterisation of novel uncoated textiles and prepare for the final design stage of the studied material.

Warp and Weft Tensile Strength

As noticeable from the pictures below, for all three warp specimens, the failure happens around the transition between the float area and the plain weave area. The floating part is the part of the textile where the OPV (Organic Photovoltaic) strips are inserted. Therefore the transition area between the floating and plain weave area seems to be a sensitive area, making it an area of interest for future tests. The weft specimens have different failure mechanisms: the ones including the floating area failed in a diagonal direction while the one composed by plain weave only has a straight clear cut.

Figure 5.1: Warp specimens after testing. From left W03, W02, W01.

Figure 5.2: Weft specimens after testing. From left F01, F02, F03.

It is interesting to investigate further the failure mechanisms and understand their relationship with the weave pattern and the different types of yarns.

As seen from the test results the presence of floats and the amount of monofilaments influences the strength of the material. It is recommended to study the optimum amount of monofilaments to have a more consistent failure mechanism and higher strength. The absence of monofilaments in the weave in the weft direction is related to its higher strength. By weaving a lower amount of monofilaments in the warp direction, the strength can therefore also be higher and the requirement of type I architecture textile can be reached for the strength in both directions.

Elastic Modulus

The found values are comparable with type I architecture textiles in literature, making it a promising achievement for the developing material. The low amount of successful test makes the found results not reliable. It is recommended to test the material with project-specific bi-axial cycling loads as the parameter is related directly to the load history.

Damage of OPV strips

It is interesting to investigate further on this matter to understand what happens when the float space becomes too small: the OPV strips could be subjected to compressive forces or the mono-filaments could get damaged because of the contact with the OPV strips. It is suggested to test the material at higher angles and include the solar strips. It is also interesting to know if, by increasing the float dimensions, the strength of the material will be influenced.

Picure Frame Test and Shear Angle Evaluation

The investigation of the shear behaviour of an uncoated material is not yet normalised and its presence in literature is scarce. Hence the difficulties faced during this research. One of the difficulties was understanding the shear angle behaviour of the textile after performing the tests. A change of curvature was observed in all specimens for an angle between 5 and 10 degrees. Possible reasons for this behaviour have been established. However, further investigations are recommended to conclude.

Additionally, from the frame assessment it could be concluded that the corners should have been pinned connections instead of clamped. This might have influenced the initial deformation as the ap-

plied force had to be higher than the frictional resistance of the frame before starting to deform the textile itself. It is recommended to repeat the tests with a pinned frame to exclude this, most obvious, argumentation.

Shear Stiffness

In literature, we can find a few attempts to characterise a shear–tension coupling of textiles. These studies indicated significant increases in shear stiffness with increasing pre-tension, typical values of a coupling factor. Hence, the shear stiffness found in this report is related to the pre-stress state of the specimens. It is therefore recommended to evaluate the stiffness related to different pre-stress states for a greater understanding of the shear characteristics of this material.

References

[1] Tensinet Symposium 2013. *[RE]thinking lightweight structures*. Tensinet, 2013.

[2] Data 36. *Polynomial Regression in Python - visited on 02/11/22*. URL: https://data36.com/polynomial-regression-python-scikit-learn/.

[3] B. El Abed et al. “On the shear behavior of woven fabrics”. In: *International Conference of Applied Research in Textile* (2008).

[4] Barlow. *The History and Principles of Weaving by Hand and by Power*. Low, Marston, Searle, & Rivington, 1878.

[5] Paolo Beccarelli. *Biaxial testing for fabrics and foils*. Springer, 2015.

[6] B. Bridgens and M. Birchall. “Form & function: the significance of material properties in the design of tensile fabric structures”. In: *Engineering Structures* (2012).

[7] J. Cao et al. “Characterization of mechanical behavior of woven fabrics: Experimental methods and benchmark results”. In: *Composites: Part A* (2008).

[8] A.G. Colman et al. “Shear behaviour of architectural fabrics subjected to biaxial tensile loads”. In: *Composites: Part A* (2014).

[9] European Commission. *Buildings and constructions - visited on 30/6/22*. URL: https://ec.europa.eu/growth/industry/sustainability/buildings-and-construction_en.

[10] European Commission. *EU Solar Energy Strategy - visited on 26/04/22*. URL: https://eur-lex.europa.eu/legal-content/EN/TXT/HTML/?uri=COM:2022:221:FIN.

[11] D.Samir and H. Satha. “Experimental approach for determining the shear rigidity modulus of commingled glass/ propylene woven fabrics”. In: *Conference: Cinquièmes Journées de Chimie ENITA* (2013).

[12] Arch Daily. *visited on 03/04/2022*. URL: https://www.archdaily.com/.

[13] Apurba Das. “Tactile aspects of clothing comfort”. In: *Science in Clothing Comfort* (2010).

[14] Pauline van Dongen et al. “Suntex: weaving solar energy into building skin”. In: *Journal of Facade Design and Engineering - Special Issue Power Skin 2022* (2022).

[15] P. Drew and A.L. Drew. *Frei Otto Form & Structu/h*. Avalon Publishing, 1976.

[16] *EN 1421-1*. Rubber- or plastics-coated fabrics - Determination of tensile strength and elongation at break, 1998.

[17] *EN ISO 13934-1*. Textiles — Tensile properties of fabrics - Part 1: Determination of maximum force and elongation at maximum force using the strip method, 2013.

[18] *EN ISO 17117-1*. Rubber or plastics-coated fabrics - Mechanical test methods under biaxial stress states - Part 1: Tensile stiffness properties, 2018.

[19] Brian Foster and Marijke Mollaert. *European design guide for tensile surface structures*. Tensinet, 2004.

[20] Iaso Global. *Structural Fabrics - visited on 15/06/22*. URL: https://www.iasoglobal.com.

[21] P. Harrison et al. “Characterising the shear–tension coupling and wrinkling behaviour of woven engineering fabrics”. In: *Composites: Part A* (2012).

[22] Virpi Heybroek. “Textile in Architecture”. In: *TU Delft thesis repository, Faculty of Architecture* (2013).

[23] L. Jackson, N. Bridgens, and D. Gosling. “A new biaxial and shear protocol for architectural fabrics”. In: *International Association for Shell and Spatial Structures (IASS) Symposium* (2009).

[24] Christian Krogh, Kari D. White, and Alessandro Sabato andJames A. Sherwood. “Picture-frame testing of woven prepreg fabric: An investigation of sample geometry and shear angle acquisition”. In: *International Journal of Material Forming* (2020).

[25] Sylvie Kruger. *Textile Architecture*. Jovis, 2009.

[26] C. Mack and H. M. Taylor. “The Fitting of Woven Cloth to Surfaces”. In: *Journal of the Textile Institute Transactions* (1956).

[27] Van Mele et al. “Shaping tension structures by actively bent linear elements”. In: *International Journal of Space Structures* (2013).

[28] Y. E. El Mogahzy. *Engineering textiles - integrating the design and manufacture of textile products*. Woodhead Publishing Limited, 2009.

[29] U. Mohammed et al. “Shear deformation and micromechanics of woven fabrics”. In: *Composites: Part A* (2000).

[30] Kevin L. Peil, Ever J. Barbero, and Eduardo M. Sosa. “Experimental evaluation of shear strength of woven webbings”. In: *SAMPE conference and exhibition* (2012).

[31] Iaso Global Projects. *visited on 03/04/2022*. URL: `https://www.iasoglobal.com/en/projects`.

[32] Joint Research Center: Science and Policy Report. *Prospect for European Guidance for the Structural Design of Tensile Membrane Structures*. European Commission Publications Office, 2016.

[33] Mohsen Shanbeh et al. “Analysis of shear characteristics of woven fabrics and their interaction with fabric integrated structural factors”. In: *Journal of engineered fibers and fabrics* (2019).

[34] Miriam Euni Son. “The Design and Analysis of Tension Fabric Structures”. In: *MIT thesis repository, Faculty of Civil Engineering* (2007).

[35] Yu. M. Tarnopol’skii, A.K. Arnautov, and V.L. Kulakov. “Methods of determination of shear properties of textile composites”. In: *Composites: Part A* (1998).

[36] Tentech. *visited on 03/04/2022*. URL: `https://tentech.nl/en/textile-architecture-projects`.

[37] *Textile composites and inflatable structures III - Barcelona 2007*. Cimne, 2007.

[38] Tootal. *Tootal Fabrics - visited on 15/06/22*. 2017. URL: `https://www.tootal.nl/en/news/show/22/the-history-of-woven-textiles`.

A

Weaving Trial 02

PAULINE VAN DONGEN

SUNTEX MIT-RD-20-00359838

Weaving Trial 02
Warping datasheet

Creator: Anna Wetzel
Date: 17-02-2022

Warp A (658 dents → only 638 warp yarns can be used because of reed deformation (658-20) →minus 12 for lenos either side (638-24) = 614 finally used)

Warp yarn 1	Warp yarn 2	Warp yarn 3	E.p.cm	Reed (661 dents)	Shafts	Heddles	Picks per cm (set on machine)	Shrinkage weft:	Weft yarn 1	Weft yarn 2
rPET 1100 dtex d=0,32 mm (MSP)	HTR-B, 1600dtex d=0,39 mm (Filva)	High-Flex 3981, 7x1, copper with silver coating d=0,42 mm (Karl Grimm)	11,8	118,07	10 + 2 leno	6 leno heddles on shaft A+B Shaft 1,2: 126 Shaft 3,4: 127 Shaft 5, 10: 2 Shaft 6,7,8,9: 26	plain weave: 10 twill weave: 13 double weave: 30	width expected: 50cm width result: 53cm	rPET 1100 dtex d=0,32 mm (MSP)	High-Flex 3981, 7x1, copper with silver coating d=0,42 mm (Karl Grimm)

PAULINE VAN DONGEN

SUNTEX MIT-RD-20-00359838

							Sample 1	
Company	**Product**	**diameter**	**dtex**	**Breaking Load (cN)**	**Elongation at break (%)**	**Tenacity cN/dTex**	**Warp**	**Weft**
Filva	HTR-B Monofilament	0,39 mm	1600	2745	97	1,72	TRUE	
Karl Grimm	High-Flex 3981, 7x1, copper with silver coating	0,42 mm	2325	2,8	-	1,18	TRUE	TRUE
MSP	rPET	0,32 mm	1100	8430	13,8	7,54	TRUE	TRUE

Figure A.1: Yarn specification

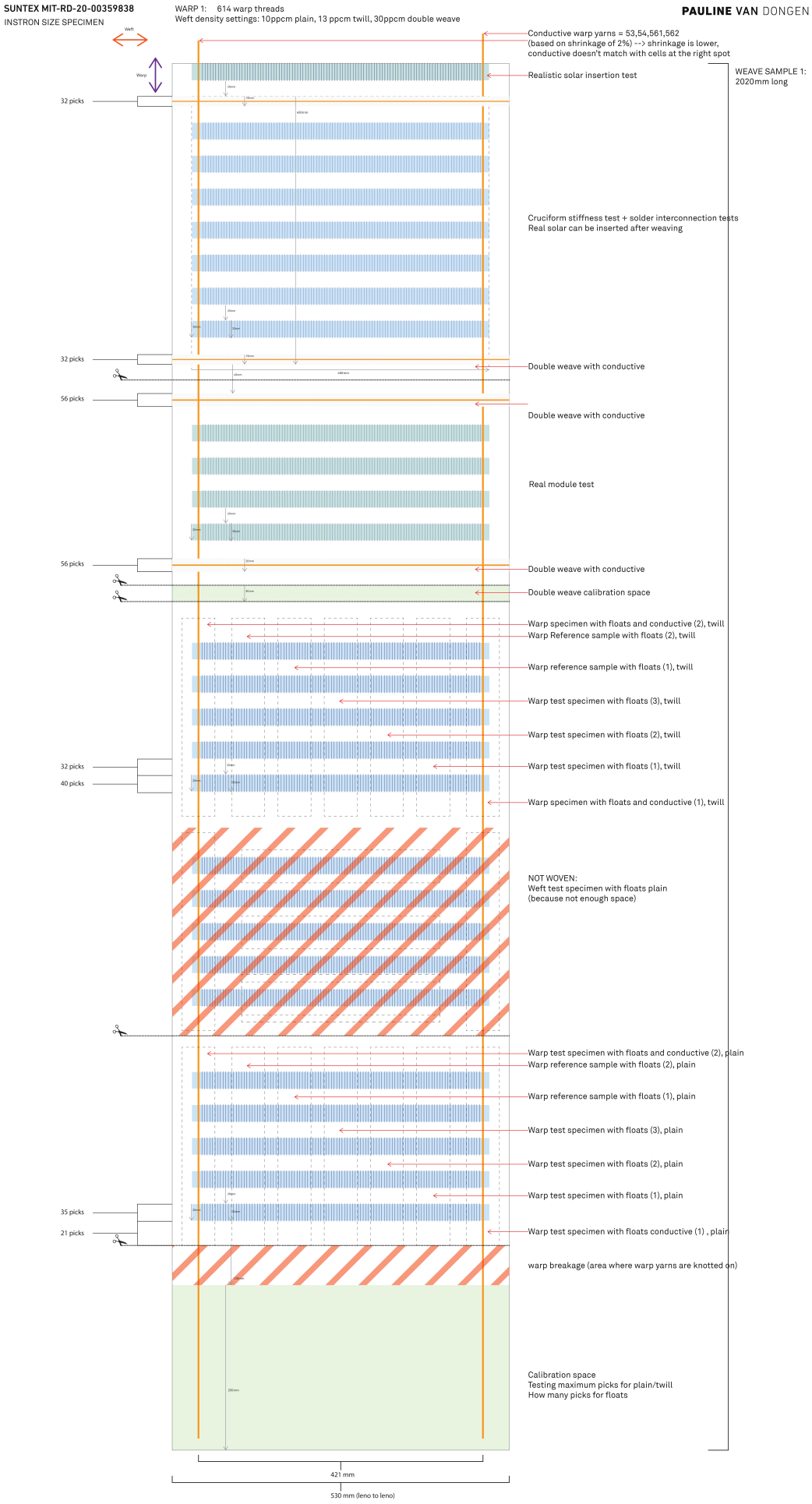

Figure A.2: Weave pattern plan

B

Warp and Weft Strength Evaluation

The tests regards three specimens on warp and tree specimens on weft direction [Fig. 3.19 - 3.20]. Those were pulled on a monoaxial tensile machine until rupture. The average warp strength results 280 daN/5cm, while the weft strength results 340 daN/5cm. The elongation on both directions results less than 17% therefore the material is within the norm for architecture textiles. The warp strength of the studied textile results not sufficient for a type I textile ($\geq 300daN/5cm$).

The monoaxial tensile machine used was Instron 1122 and DIC (Digital Image Correlation) system was used to measure the elongation and strain field along the specimens. The chosen testing rate was 1 mm/s (displacement controlled test). Tests were performed on 9/08/2022 at TU Delft Stevin Lab II in a temperature controlled room. Dimension of the specimens are specified on table B.1. *W* refers to warp specimens, while *F* refers to weft specimens, which is also called fill direction in order to distinguish when using abbreviations.

Table B.1: Specimens dimensions

	Width (mm)	Gauge Lenght (mm)
W01	50	200
W02	50	201
W03	50	200
F01	50	198
F02	50	200
F03	50	200

The load cell is connected to both measuring systems. A small difference in force values can be observed in all tests due to manual start of both systems. A difference in displacement can also be observed due to the nature of the two systems:

- DIC system measures displacement and strain field in a set surface in 3 dimensions
- Tensile test measures the distance between the two clamps

It is know from previous tests performed by Tentech that the photovoltaic strips will not undergo any stresses during elongation, hence their absence in the experiments.

Figure B.1: Tensile machine test set up (W01: Warp is aligned with tensile extension)

B.1. Warp Strength

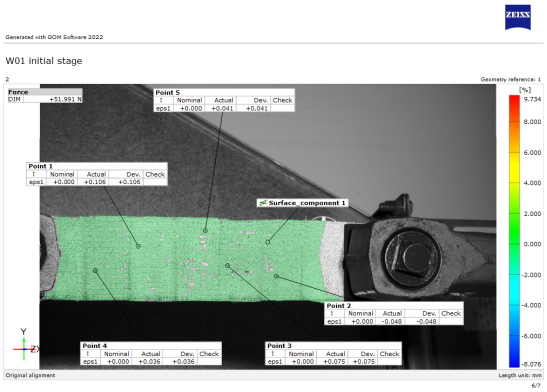

Figure B.2: W01 initial stage

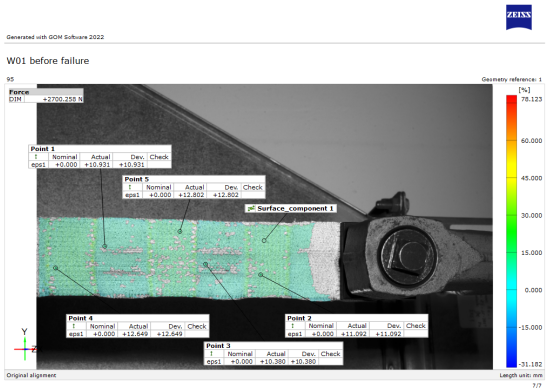

Figure B.3: W01 before rPET failure

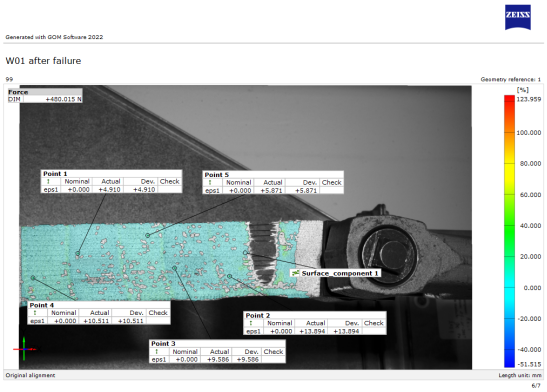

Figure B.4: W01 after rPET failure

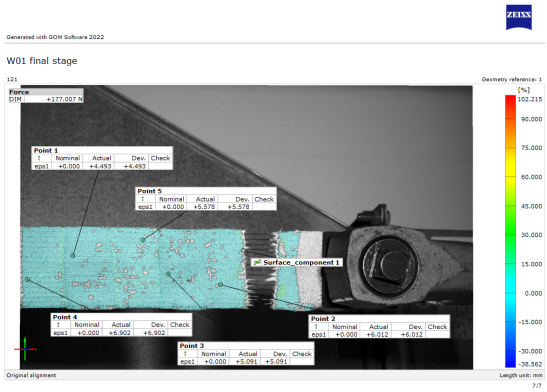

Figure B.5: W01 final stage - mono-filament has not failed

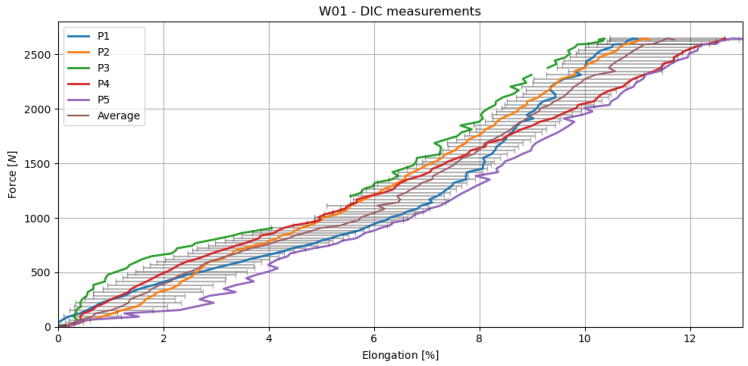

Figure B.6: W01 DIC response: P_i are different points along the specimen as seen on figure B.2

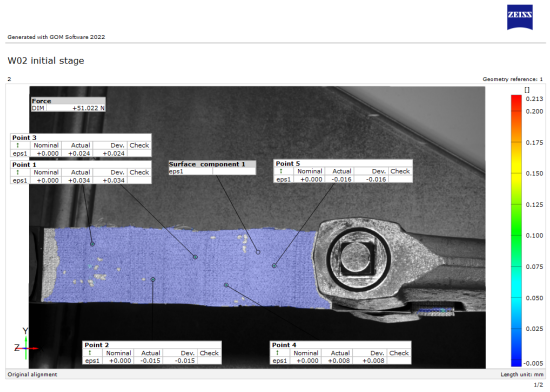

Figure B.7: W02 initial stage

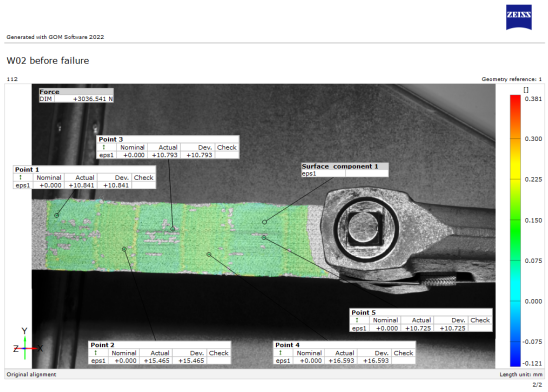

Figure B.8: W02 before rPET failure

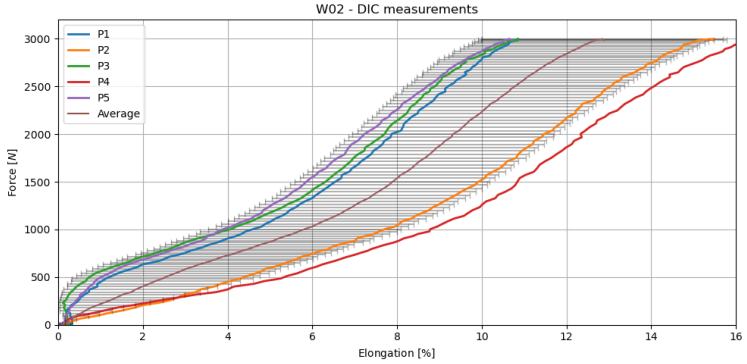

Figure B.9: W02 DIC response: P_i are different points along the specimen as seen on figure B.7

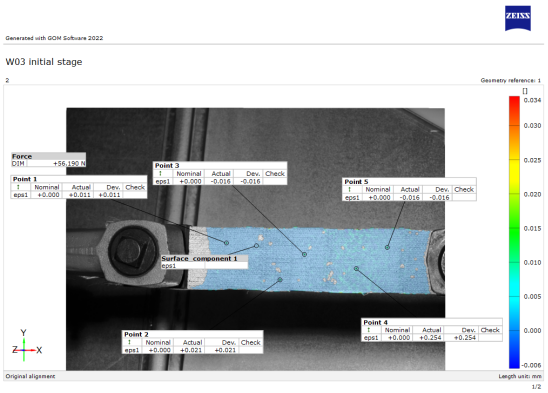

Figure B.10: W03 initial stage

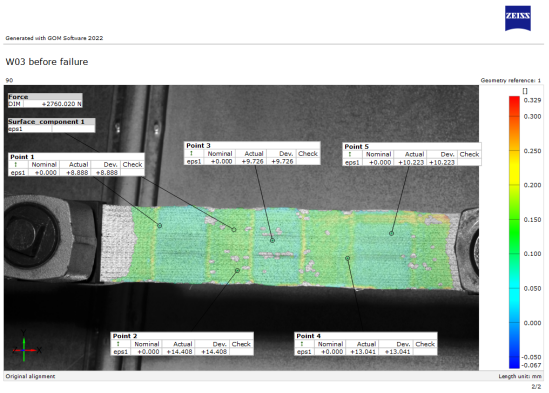

Figure B.11: W03 before rPET failure

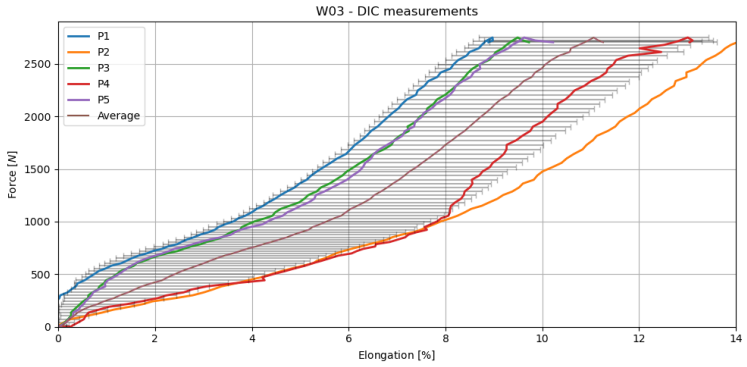

Figure B.12: W03 DIC response: P_i are different points along the specimen as seen on figure B.10

As noticeable from figure B.2 - B.11, when the specimen is pulled in the warp direction no slippage can be observed. Moreover, the presence of two different yarn materials with different stiffnesses resulted in the two materials failing separately rather than having a coherent “clear-cut” fabric failure. The remaining force after rPET rupture is taken by the mono-filament yarns. Failure of the later was not within the scope for the test as the fabric is considered failed when at least one of the yarns breaks.

Force vs. elongation graphs on figure B.6, B.9 and B.12 represent the response measured with the DIC system of W01 specimen. P_i are points randomly placed along the specimen and *average* is the curve that averages the response of all points (P1:P5). The graph increases gradually, until rPET yarn rupture. The reason why some of the curves have blank spots is because the data couldn’t be measured with DIC system, because of rapid changes or cluster of speckle pattern.

An overview of all warp experiments follows. Figure B.13 represents the response of all specimens measured with the tensile machine (-*T*) and with the DIC system (-*D*). For -*D* data the average of all measured points of each specimen (W01:W03) has been considered.

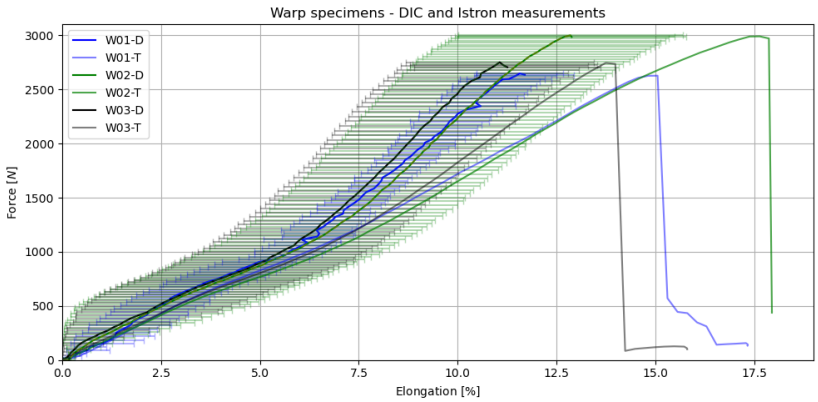

Figure B.13: Warp response of all specimens : -T are data measured via Istron tensile machine, while -D are measured DIC

The graph on figure B.13 increases gradually, almost linearly, until failure. The drop in force corresponds to failure of rPET warp yarns. In all cases the remaining force after rPET rupture is taken by the mono-filament yarns. Failure of the later was not within the scope for the test. As noticeable from the pictures below , for all three specimens the failure happens around the transition between float area and plain weave area, making it an area of interest for future tests as it seems to be a sensible area.

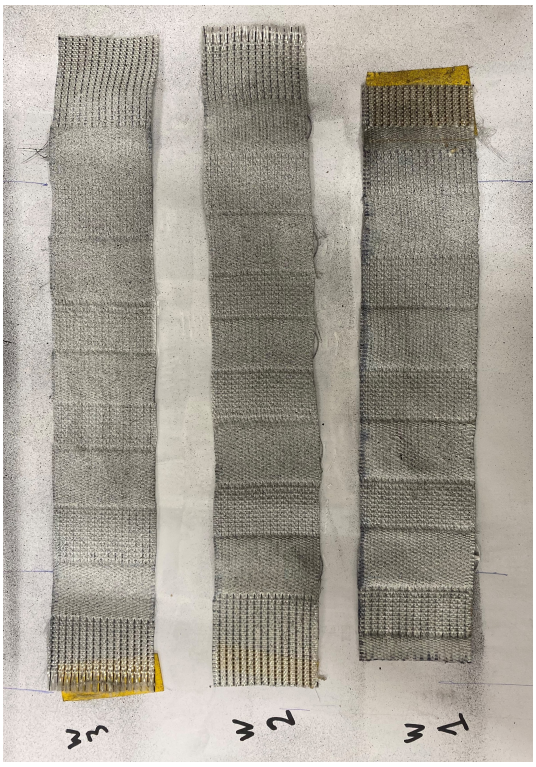

Figure B.14: Warp specimens before testing. From left W03, W02, W01.

Figure B.15: Warp specimens after testing. From left W03, W02, W01.

A comparison between DIC and tensile machine measurements is summarised on table B.2. All $-_{Ist}$ refers to measurements recorded by the tensile machine, the elongation has been analytically calculated, while all $-_{DIC}$ refers to measurements recorded by the DIC system.

Table B.2: Warp strength evaluation: comparison between tensile test data and DIC

	F_{Ist} (N)	dL_{Ist} (mm)	$\varepsilon_{Ist} = dL/L0\%$	F_{DIC}	$\varepsilon_{DIC}\%$
W01	2625.6	30.1	15.1	2647.6	11.6
W02	2998.5	35.5	17.6	2999.4	12.9
W03	2739.1	27.5	13.8	2750.7	11.0
Average	2787.7	31.0	15.5	2799.2	11.8

As seen on table B.2, the analytical calculations from tensile machine measurements differ from DIC in regards to elongation. As mentioned before, the reason behind the difference is due to the intrinsic characteristics of each system. While the difference in force value depends on the manual start of both systems, even though they are both connected to the same load cell. It's recommended to use the data from DIC system, as considered more accurate.

From testing three specimens on warp direction, we can conclude the warp strength of the studied material is equal to 280 daN/5cm and the elongation is 12%. Both strength and elongation have been rounded according to ISO 13934-1 [17].

B.2. Weft Strength

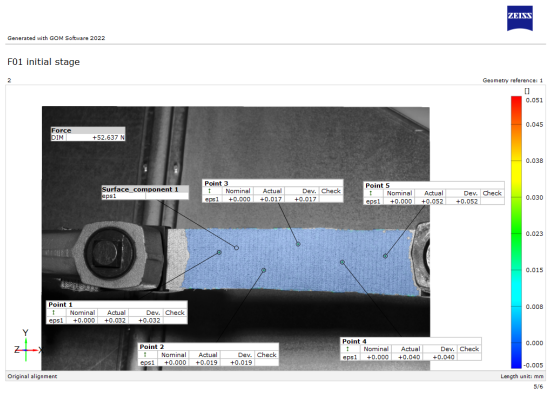

Figure B.16: F01 initial stage

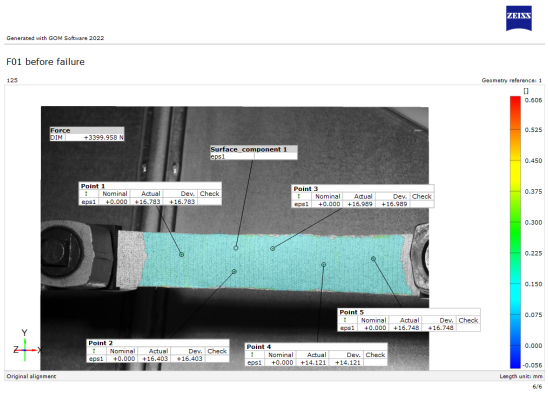

Figure B.17: F01 before rPET failure

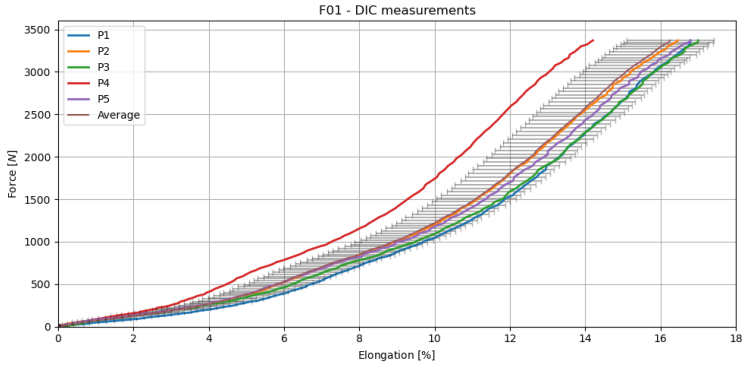

Figure B.18: F01 DIC response: P_i are different points along the specimen as seen on figure B.16

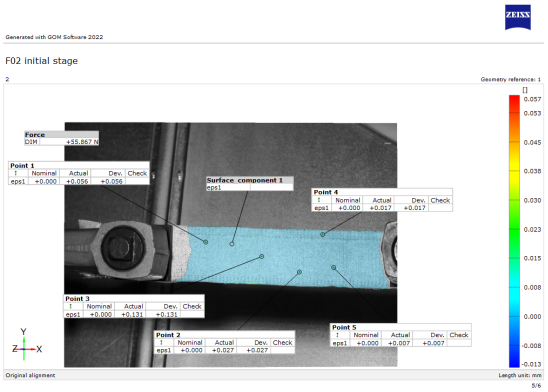

Figure B.19: F02 initial stage

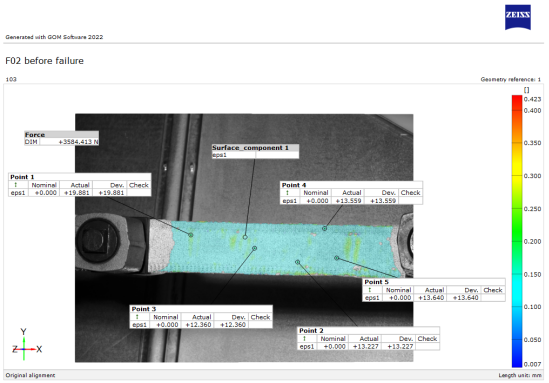

Figure B.20: F02 before rPET failure

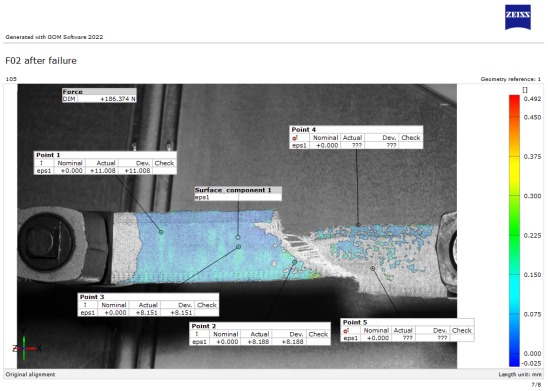

Figure B.21: F02 after failure

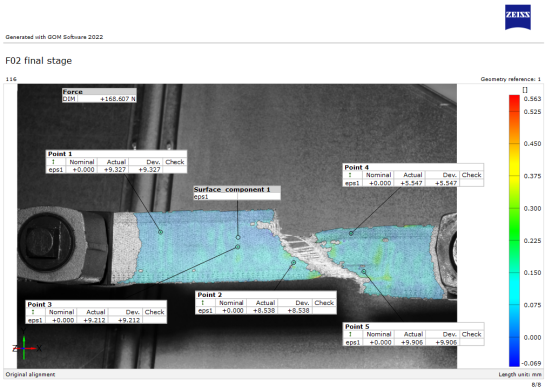

Figure B.22: F02 final stage

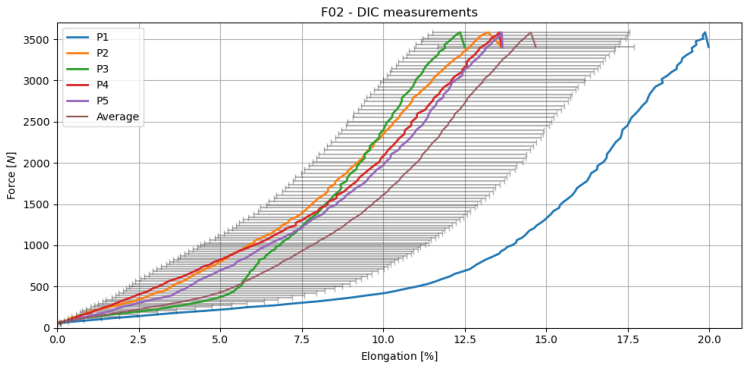

Figure B.23: F02 DIC response: P_i are different points along the specimen as seen on figure B.19

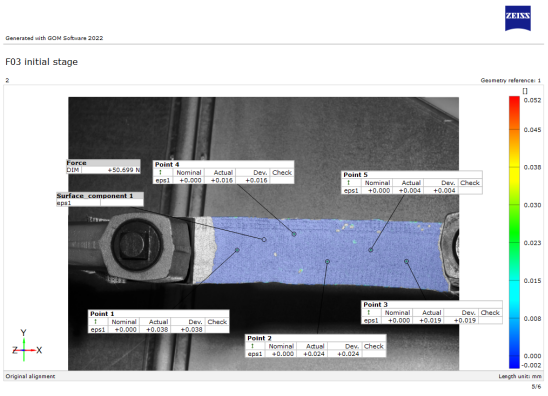

Figure B.24: F03 initial stage

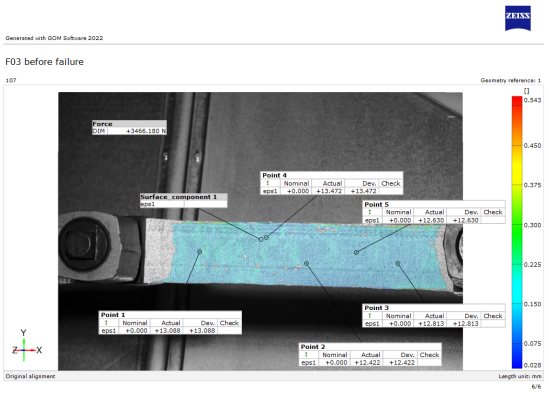

Figure B.25: F03 before rPET failure

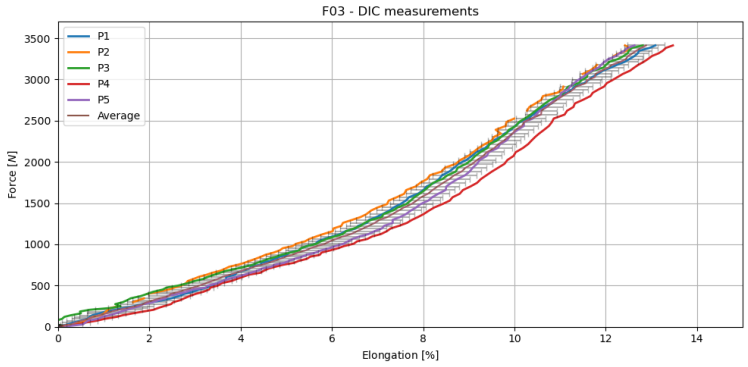

Figure B.26: F03 DIC response: P_i are different points along the specimen as seen on figure B.24

As noticeable from figure B.16 - B.25, when the specimen is pulled in the weft direction no slippage can be observed. Moreover, the absence of two different yarn materials resulted in a coherent “clear-cut” fabric failure. The only type of yarn on weft specimens is rPET yarn, as seen from weaving notes on appendix A.

Force vs. elongation graphs on figure B.18, B.23 and B.26 represent the response measured with the DIC system of F02 specimen. P_i are points randomly placed along the specimen and *average* is the curve that averages the response of all points (P1:P5). The graph increases gradually, until rPET yarn rupture. The reason why some of the curves have blank spots is because the data couldn’t be measured with DIC system, because of rapid changes or cluster of speckle pattern.

An overview of all weft experiments follows. Figure B.27 represents the response of all specimens measured with the tensile machine (-*T*) and with the DIC system (-*D*). For -*D* data the average of all measured points of each specimen (F01:F03) has been considered.

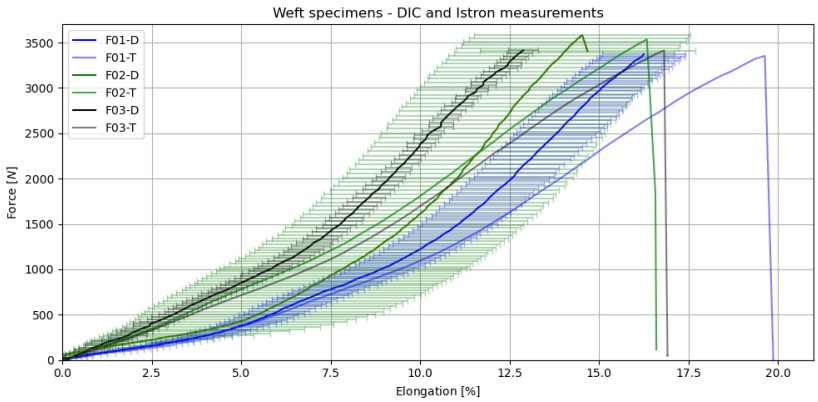

Figure B.27: Weft response of all specimens : -T are data measured via Istron tensile machine, while -D are measured DIC

The graph on figure B.27 increases gradually until failure. The drop in force corresponds to failure of rPET warp yarns therefore rupture of the specimen.

As noticeable from figure B.28, specimen F01 does not have any float part, which is the part of the textile where the OPV (Organic Photovoltaic) strips are inserted. The float part of the weave is composed by a plain weave made of rPet yarns only. In the other parts of the material the monofilament is part of the weave in warp direction. This results in a different behaviour when compared to the other specimens: yellow and light blue lines have a more elastic behaviour (see graph B.27). All data has been considered when averaging the elongation and force at break. The material is made by both parts therefore it is reasonable to include both parts of the weave when testing and drawing conclusions.

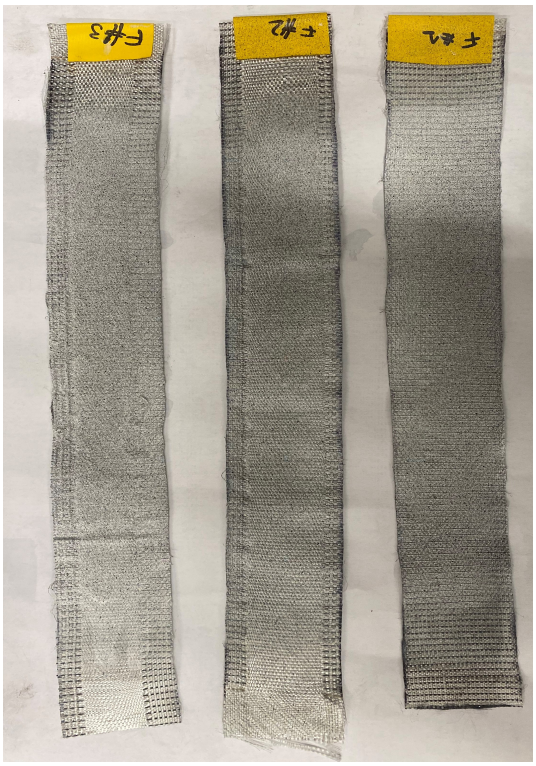

Figure B.28: Weft specimens before testing. From left F03, F02, F01.

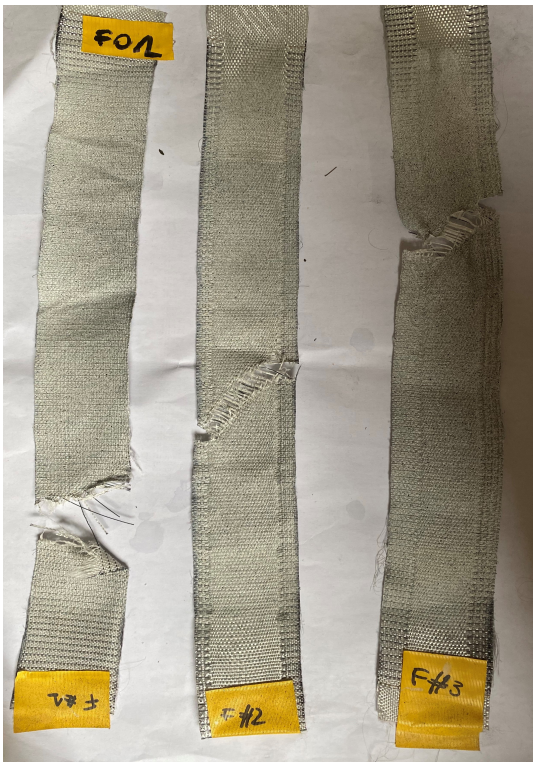

Figure B.29: Weft specimens after testing. From left F01, F02, F03.

A comparison between DIC and tensile machine measurements is summarised on table B.3. All

$-_{Ist}$ refers to measurements recorded by the tensile machine, the elongation has been analytically calculated, while all $-_{DIC}$ refers to measurements recorded by the DIC system.

Table B.3: Weft strength evaluation: comparison between tensile test data and DIC

	F_{Ist} (N)	dL_{Ist} (mm)	$\varepsilon_{Ist} = dL/L0\%$	F_{DIC}	$\varepsilon_{DIC}\%$
F01	3350.8	39.3	19.6	3370.3	16.3
F02	3530.9	32.7	16.3	3529.2	14.5
F03	3412.2	33.7	16.8	3413.5	12.9
Average	3431.3	35.2	15.5	3437.7	14.6

As seen on table B.3, the analytical calculations from tensile machine measurements differ from DIC in regards to elongation. The reason behind the difference is due to the intrinsic characteristics of each system. While the difference in force value depends on the manual start of both systems, even though they are both connected to the same load cell. It's recommended to use the data from DIC system, as considered more accurate.

From testing three specimens on weft direction, we can conclude the weft strength of the studied material is equal to 340 daN/5cm and the elongation is 15%. Both strength and elongation have been rounded according to ISO 13934-1 [17].

C

Shear Angle Evaluation

The following pages report shear angle evaluation on three specimens.

The test results regard three specimens. Specimens were deformed on a picture frame up to around 30 degrees as it is considered the limit of linearity for shear deformation (chapter 2.2). Furthermore, for tensile structure applications, the aim is for the material to be under tension only, in case of shear stress presence the later will anyways be small and limited. In addition, the presence of OPV cells (Organic Photovoltaic) limits the deformation range of the fabric. The (conservative) maximum angle within the limit of no damage to solar cells results in 27 degrees.

Figure C.1: PF01 specimen

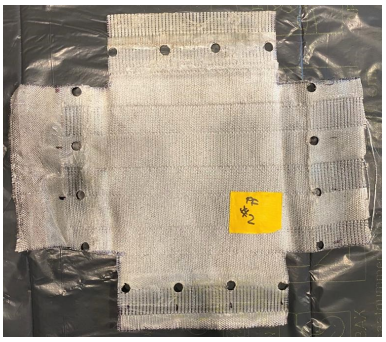

Figure C.2: PF02 specimen

Figure C.3: PF03 specimen

All specimens are reported. Eight angles have been randomly measured along each of the specimens in order to have a better understanding of the behaviour at different points. Regarding the floats where the OPV strips should be placed, the shortening in warp direction has been measured in order to ensure the OPV strips do not undergo any stress (for example distance 1 and 2 on picture C.4). At a later stage, it has been possible to associate the limit of the shortening of floats to a limited angle.

PF01

In figures, C.4 - C.7 warp direction corresponds to y-axis, while weft corresponds to x-axis. The colour scale refers to the major strain along the specimen.

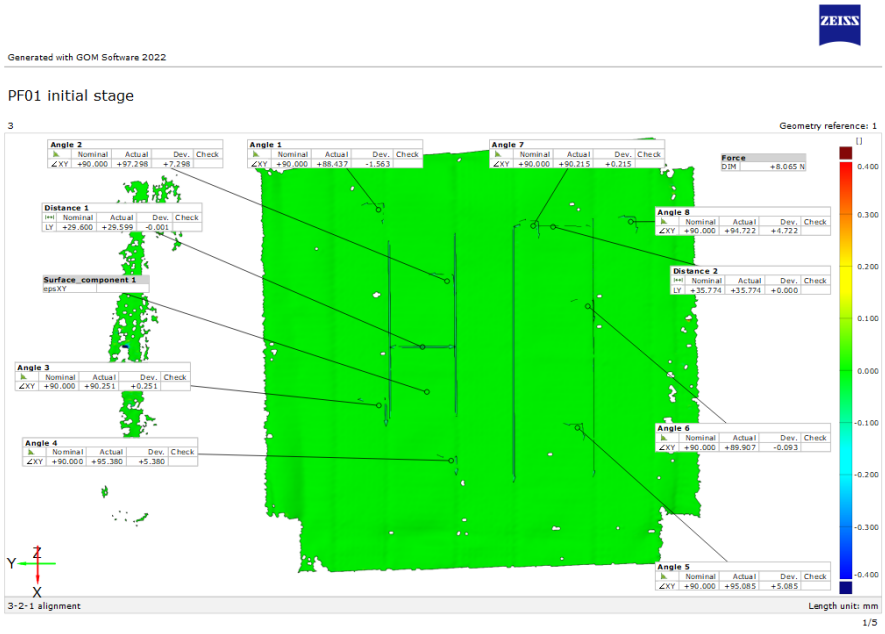

Figure C.4: PF01 initial stage

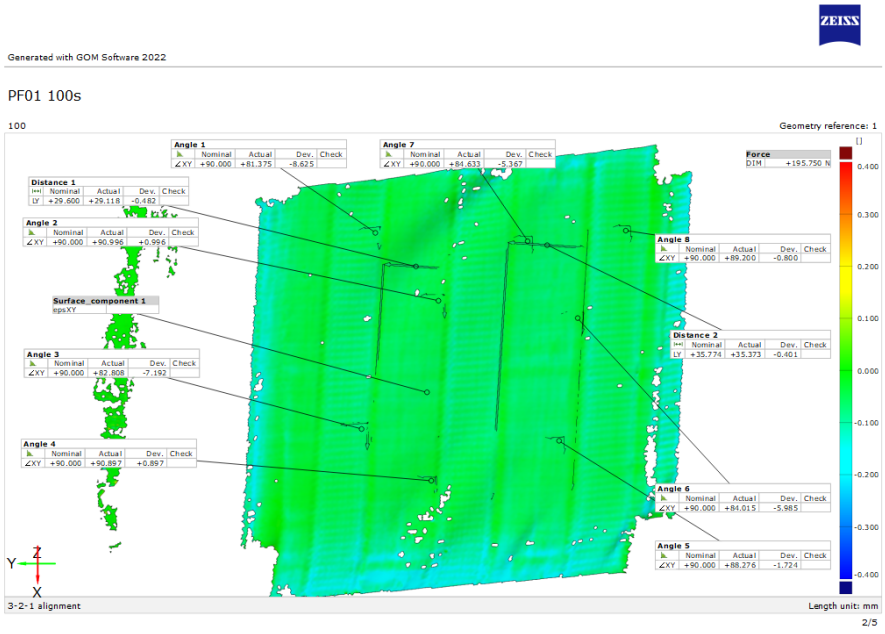

Figure C.5: PF01 after 100s

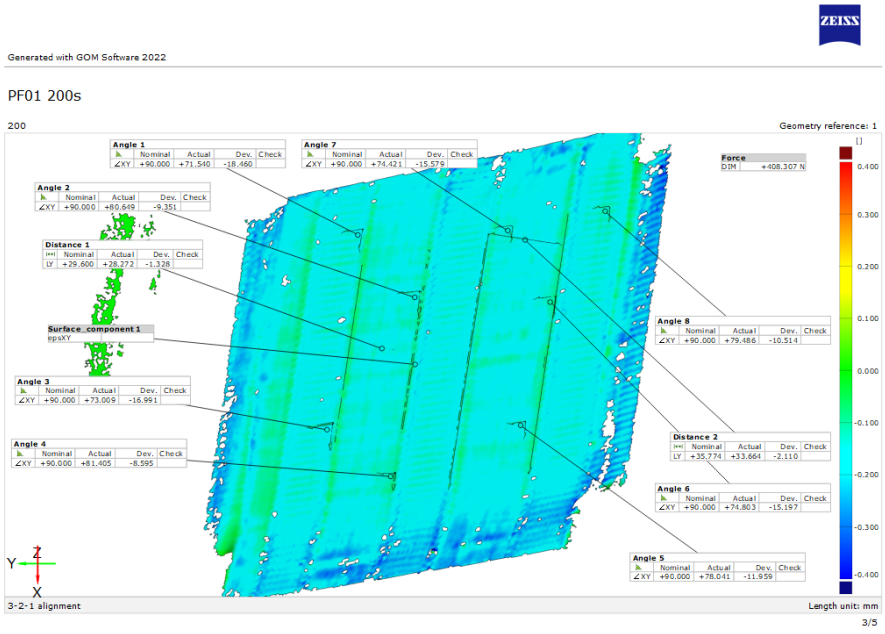

Figure C.6: PF01 after 200s

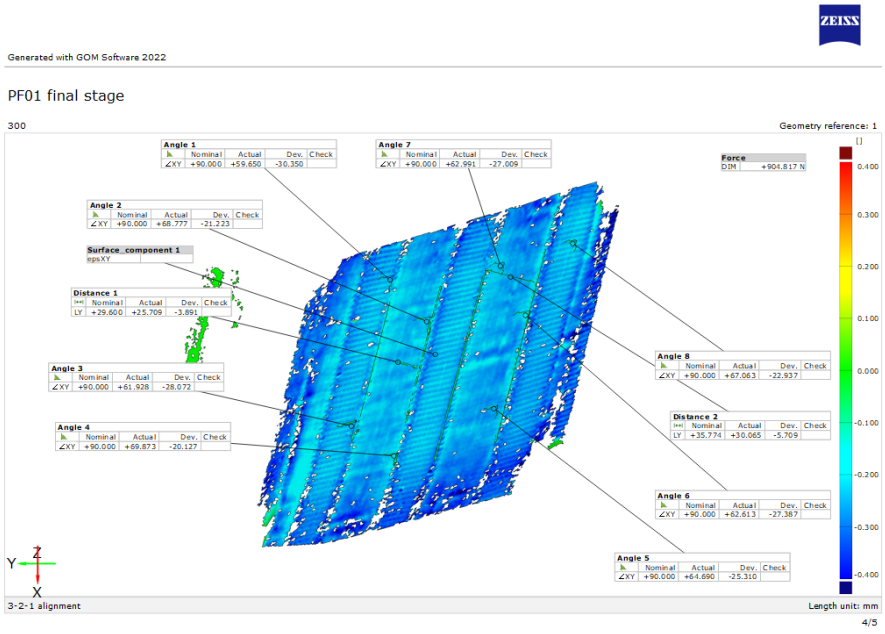

Figure C.7: PF01 after 300s - end of test

The graph in figure C.8 illustrates the force-angle behaviour of specimen PF01 measured with the DIC system. $Angle_i$ reported in the graph below, are different points along the specimen where the angle change has been measured (figure C.4). The reference angle is 90 degrees as warp and weft have this orientation when no shear stresses are being applied, the difference between 90 degrees and the deformed angle is the shear angle which is represented in the curve below.

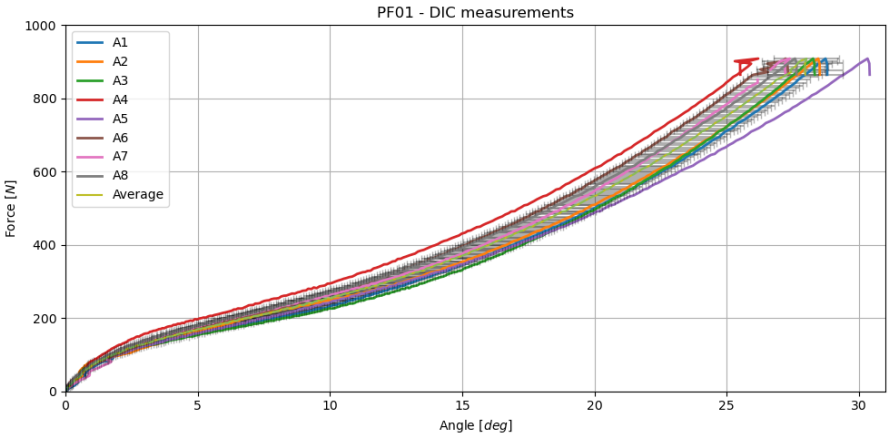

Figure C.8: PF01 DIC response: all $Angle_i$ are different points along the specimen where the angle change has been measured (figure C.4)

Usually, the interesting limit angle for textiles is where wrinkles start to appear. In the case of the studied material, the limit angle is limited by the space needed for the OPV strips in order to avoid their damage. Hence the measure of the shortening of the floating part of the weave.

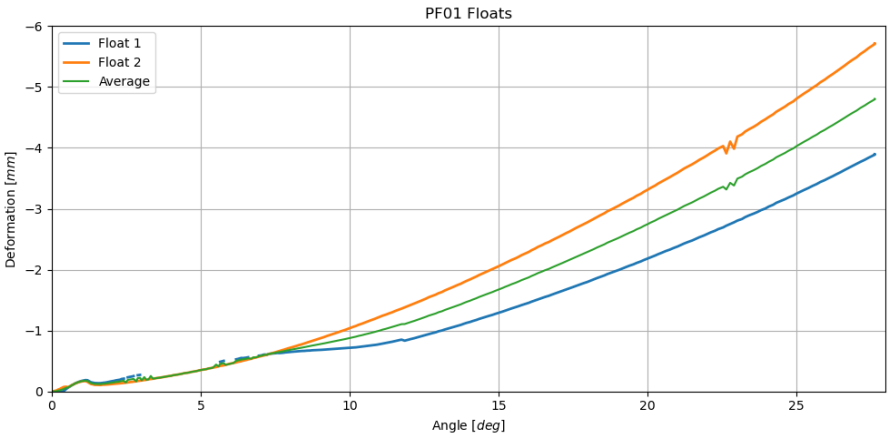

Figure C.9: PF01 DIC response: all $Float_i$ are different points along the upper and lower float of the specimen, where the length change has been measured (figure C.4)

The deformation-angle graph in figure C.9 represents the shortening in of the weave floats. It is noticeable in this case too how the curve starts with an upwards curvature up to around 7.5 degrees followed by a downward curvature, which is the opposite seen on graph C.8.

The initial width of PF01 float is 30 and 35 mm (starting from the left float on figure C.4), as the width of OPV strips is 25mm the maximum feasible shortening width is 5mm. The average float deformation (*Float AVG*), of 5mm corresponds to an angle of 27 degrees which is considered the limit angle for PF01. This is considered a conservative limit as from observing figure C.9 one can notice that at 27 degrees float 2 which has a starting length of 35 mm did not yet reach 10mm of shortening, while float 1 reaches 4mm at 27 degrees.

PF02

In figures, C.10 - C.13 warp direction corresponds to y-axis, while weft corresponds to the x-axis. The colour scale refers to the major strain along the specimen.

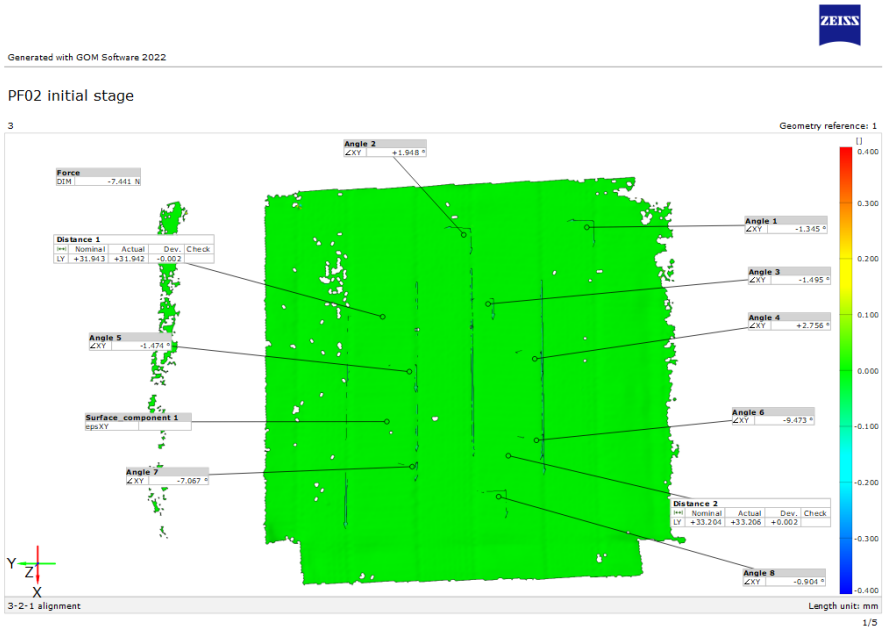

Figure C.10: PF02 initial stage

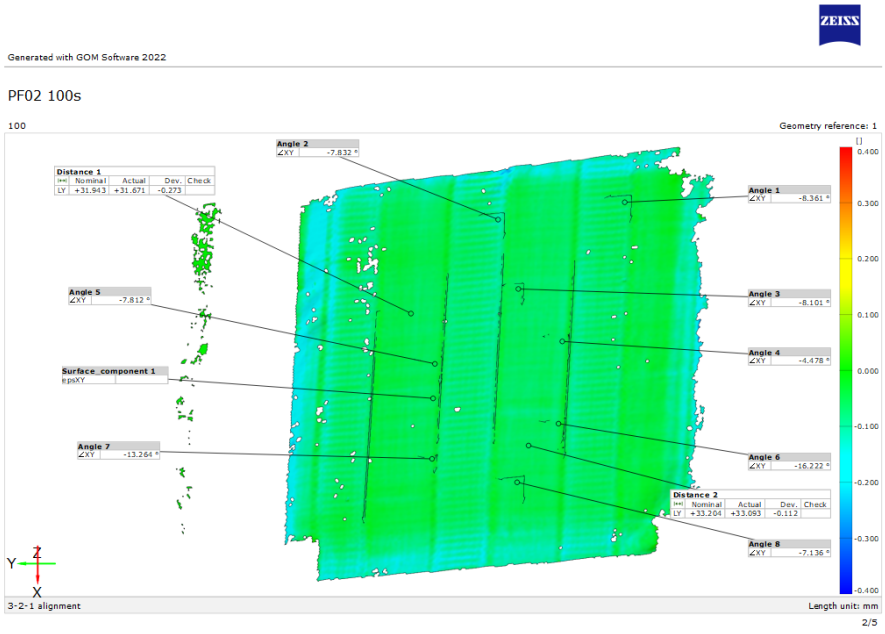

Figure C.11: PF02 after 100s

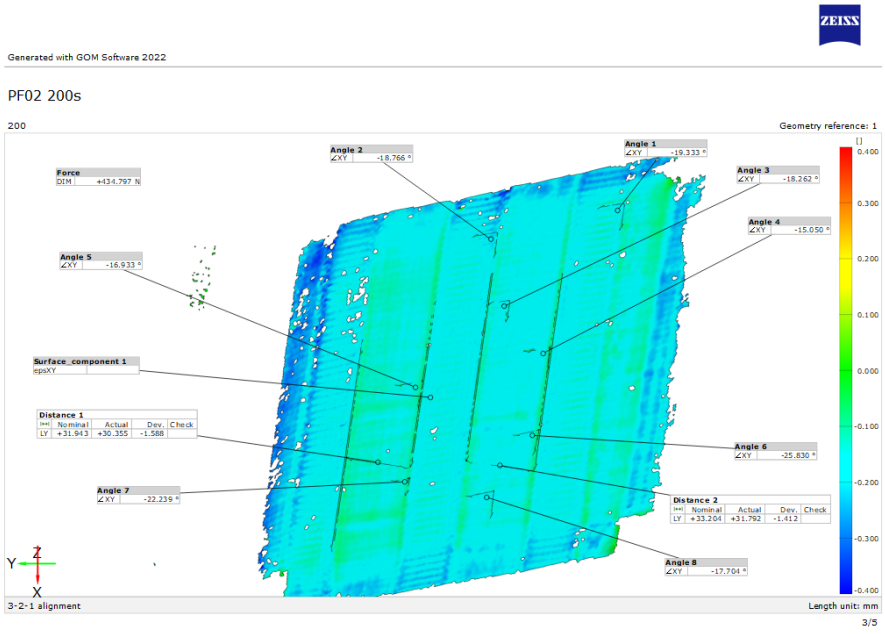

Figure C.12: PF02 after 200s

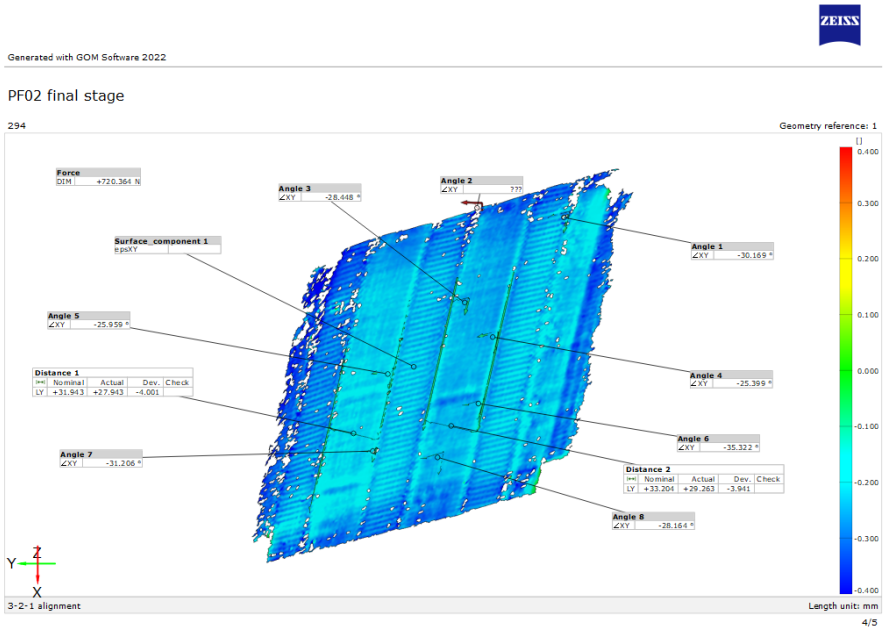

Figure C.13: PF02 after 300s - end of test

The graph in figure C.14 illustrates the force-angle behaviour of specimen PF02 measured with the DIC system. $Angle_i$ reported in the graph below, are different points along the specimen where the angle change has been measured (figure C.10). The reference angle is 90 degrees as warp and weft have this orientation when no shear stresses are being applied, the difference between 90 degrees and the deformed angle is the shear angle which is represented in the curve below.

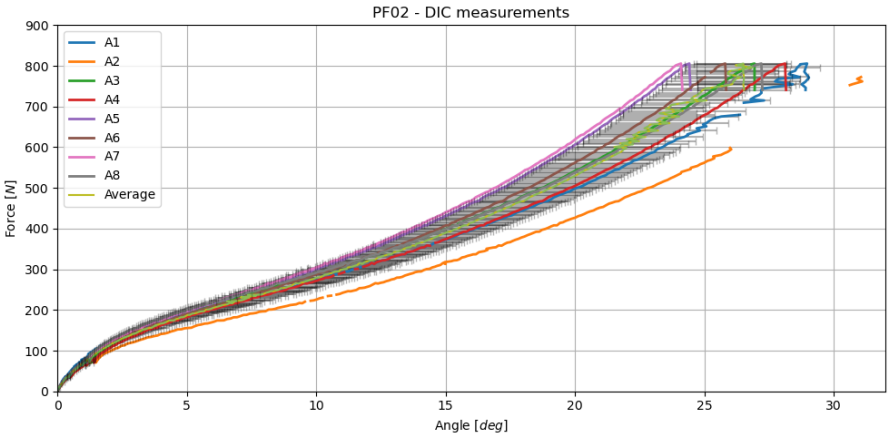

Figure C.14: PF02 DIC response: all $Angle_i$ are different points along the specimen where the angle change has been measured (figure C.10)

Usually, the interesting limit angle for textiles is where wrinkles start to appear. In the case of the studied material, the limit angle is limited by the space needed for the OPV strips in order to avoid their damage. Hence the measure of the shortening of the floating part of the weave.

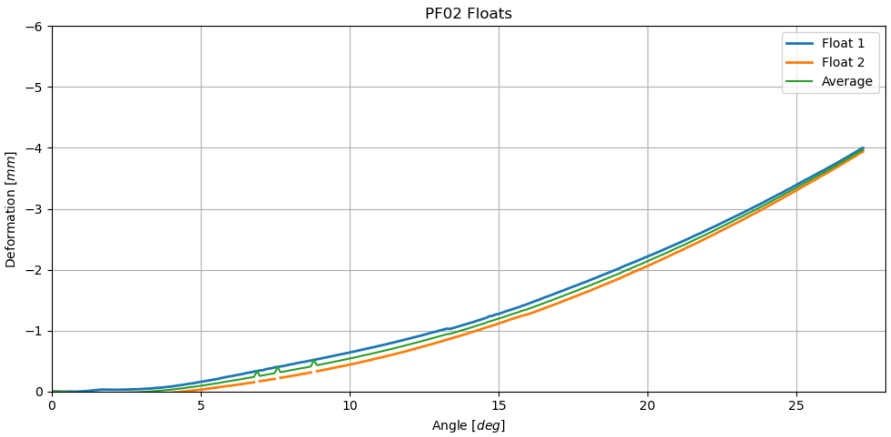

Figure C.15: PF02 DIC response: all $Float_i$ are different points along the upper and lower float of the specimen, where the length change has been measured (figure C.10)

The deformation-angle graph in figure C.15 represents the shortening in of the weave floats. It is noticeable in this case too how the curve starts with an upwards curvature up to around 7.5 degrees followed by a downward curvature, which is the opposite seen on graph C.14.

The initial width of PF02 float is 32 and 33 mm (starting from the left float on figure C.10), as the width of OPV strips is 25mm the maximum feasible shortening width is 7mm. The average float deformation (*Float AVG*), of 7mm corresponds to an angle of 27 degrees which is considered the limit angle for PF02. This is considered a conservative limit as from observing figure C.15 one can notice none of the floats has reached 7mm.

PF03

In figures, C.16 - C.19 warp direction corresponds to y-axis, while weft corresponds to x-axis. The colour scale refers to the major strain along the specimen.

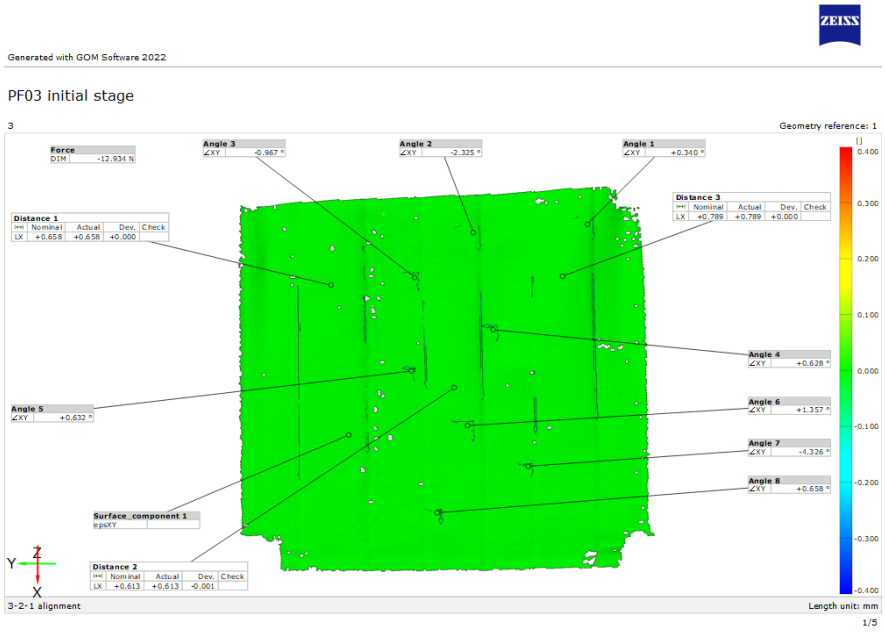

Figure C.16: PF03 initial stage

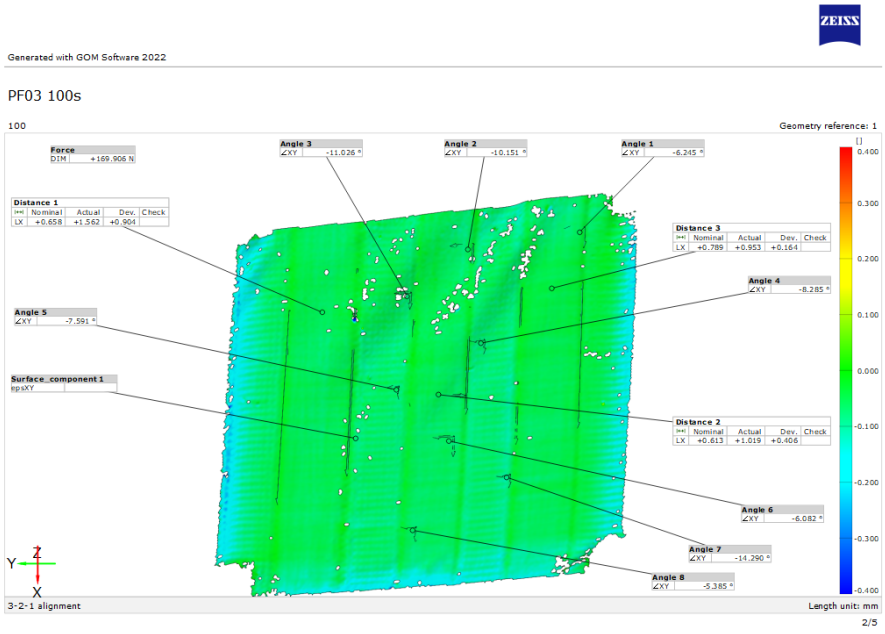

Figure C.17: PF03 after 100s

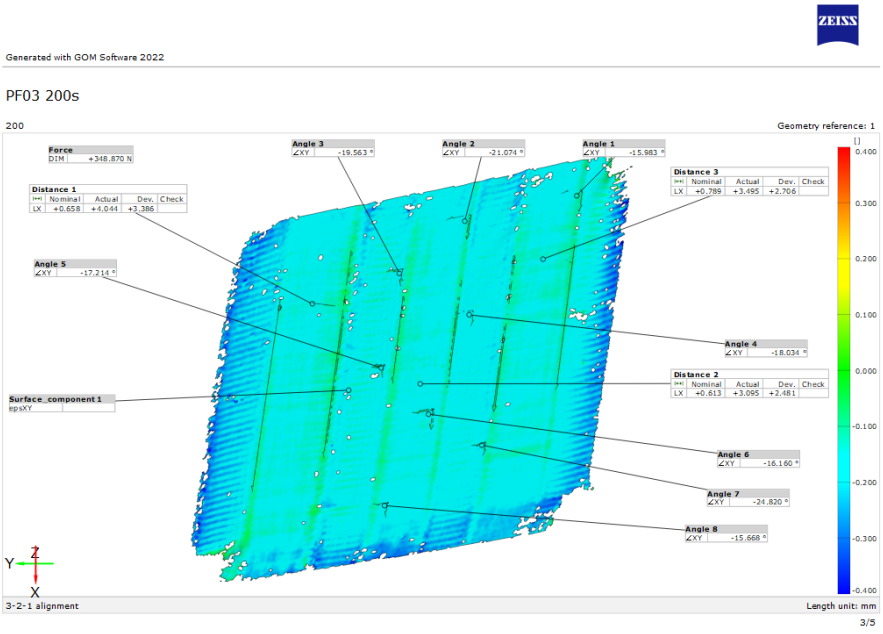

Figure C.18: PF03 after 200s

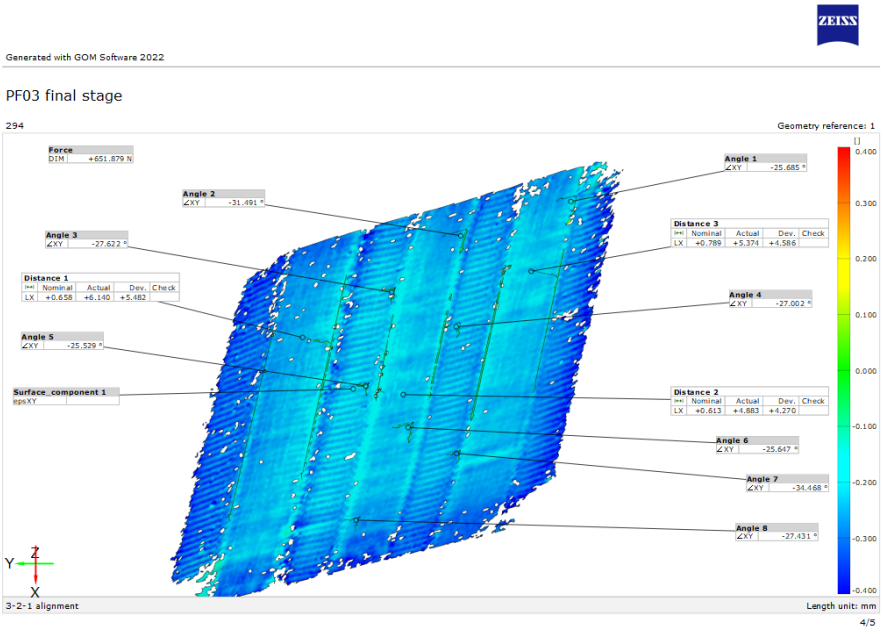

Figure C.19: PF03 after 300s - end of test

The graph in figure C.20 illustrates the force-angle behaviour of specimen PF03 measured with the DIC system. $Angle_i$ reported in the graph below, are different points along the specimen where the angle change has been measured (figure C.16). The reference angle is 90 degrees as warp and weft have this orientation when no shear stresses are being applied, the difference between 90 degrees and the deformed angle is the shear angle which is represented in the curve below.

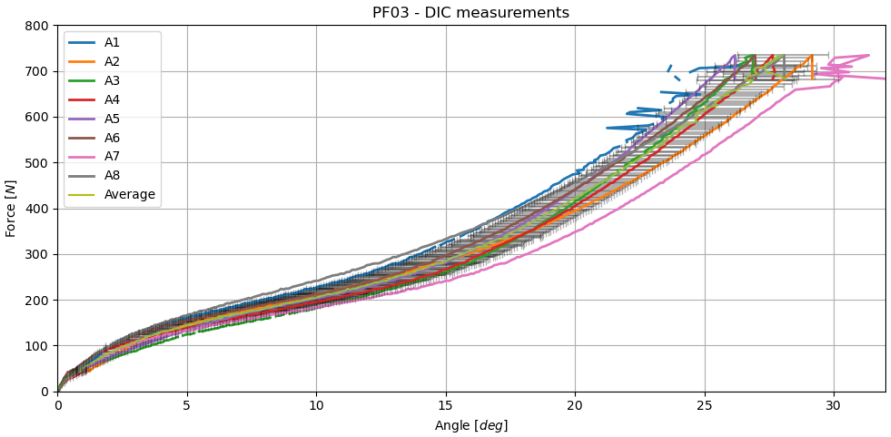

Figure C.20: PF03 DIC response: all $Angle_i$ are different points along the specimen where the angle change has been measured (figure C.16)

Usually, the interesting limit angle for textiles is where wrinkles start to appear. In the case of the studied material, the limit angle is limited by the space needed for the OPV strips in order to avoid their damage. Hence the measure of the shortening of the floating part of the weave.

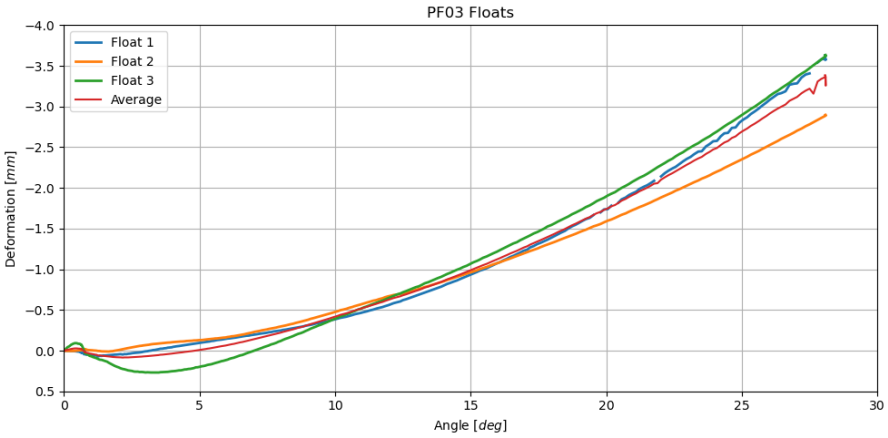

Figure C.21: PF03 DIC response: all $Float_i$ are different points along the upper and lower float of the specimen, where the length change has been measured (figure C.16)

The deformation-angle graph in figure C.21 represents the shortening in of the weave floats. It is noticeable in this case too how the curve starts with an upwards curvature up to around 7.5 degrees followed by a downward curvature, which is the opposite seen on graph C.20.

The initial width of PF03 float is 28 and 28 mm (starting from the left float on figure C.16), as the width of OPV strips is 25mm the maximum feasible shortening width is 3mm. The average float deformation (*Float AVG*), of 3mm corresponds to an angle of 26 degrees which is considered the limit angle for PF03. It is noticeable from C.21 that the distance increases before starting to decrease which is a sign of initial wrinkles in the specimen. Thus this test can not be considered valid.

Conclusion

An overview of all specimens follows. Figure C.22 represents the response of all specimens measured the DIC system. The angle change has been measured in eight different points for each specimen, the average of all measured points of each specimen (PF01:PF03) has been considered.

As seen for PF01, the force vs. angle graph on figure C.22 increases gradually, starting with a downwards curvature until around 7.5 degrees followed by an upwards curvature.

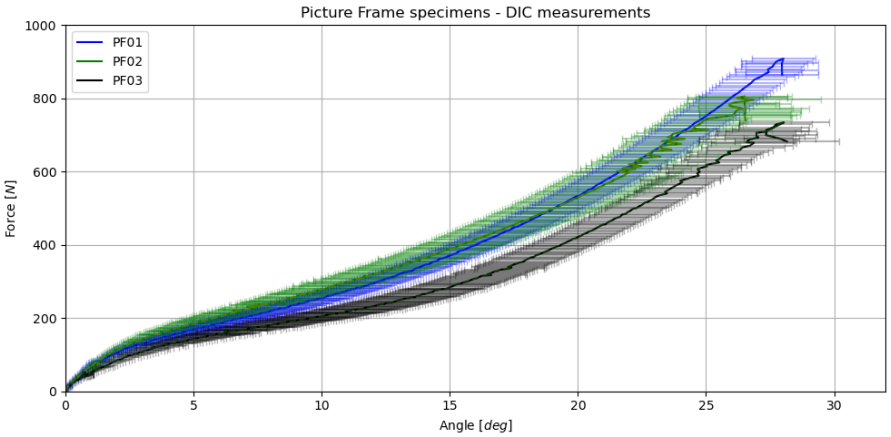

Figure C.22: Angle response of all specimens measured with DIC system

The limit angle is defined by the space needed for the OPV strips in order to avoid damaging of the system. In case of large shear deformations, the OPV can undergo compression stresses due to the shortening of the float length. An overview of the float deformation is given in figure C.23. The shown data regard the average of each specimen and the average of specimens PF01 and PF02. PF03 has been disregarded for conclusive data (PF AVG12) as it contained initial wrinkles due to an inappropriate pre-tension at the starting phase.

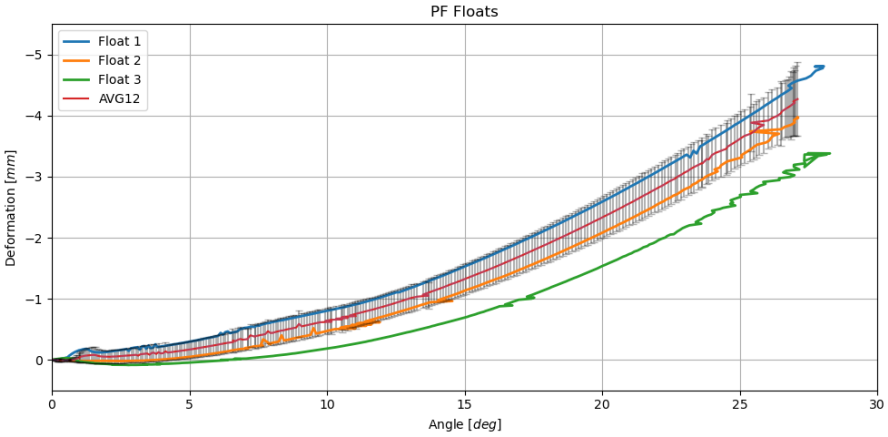

Figure C.23: Average float shortening of all specimens

The deformation vs. angle graph in figure C.23 represents the shortening of the weave floats. The initial average width of all floats is 30 mm, as the width of OPV strips is 25mm the maximum feasible shortening width is 5mm. The average float deformation of specimens PF01 and PF02 (*PF AVG12*) is considered representative of all specimens. The limit of 5mm has not been reached during testing, meaning up to 27 degrees of shearing angle the OPV strips will not undergo any compressive stress.

D

Python Code: Regression Analysis

```
# -*- coding: utf-8 -*-
"""
Created on Sat Dec 10 22:35:31 2022

@author: Stephanie
"""

import numpy as np
import matplotlib.pyplot as plt
import pandas as pd

from sklearn.linear_model import LinearRegression
from sklearn.preprocessing import PolynomialFeatures
from sklearn.metrics import mean_squared_error
from sklearn.model_selection import train_test_split
from sklearn.metrics import r2_score


data = pd.read_excel(
    r"E:\04 Thesis\regression\bilinear\PFs_Regression.xlsx").dropna()
angle = data['Angle12']
x = angle.to_numpy().reshape(-1, 1)
force = data['Ts12']
y = force.to_numpy()

# Create an instance of a linear regression model and fit it to the data with the fit() function:
model = LinearRegression(fit_intercept=False).fit(x, y)

# Obtain the coefficient of determination by calling the model with the score() function, then print
r_sq = model.score(x, y)
print('coefficient of determination:', r_sq)
# Print the Intercept:
print('intercept:', model.intercept_)
# Print the Slope:
print('slope:', model.coef_)
# Predict a Response:
y_pred = model.predict(x)
poly_mse = mean_squared_error(y, y_pred)

################################################## REGR PART 2
```

```
data2 = pd.read_excel(
    r"E:\04 Thesis\regression\bilinear\PFs_Regression2.xlsx").dropna()
angle2 = data2['Angle12']
x2 = angle2.to_numpy().reshape(-1, 1)
force = data2['Ts12']
y2 = force.to_numpy()

y2_int=0.626107

# Create an instance of a linear regression model and fit it to the data with the fit() function:
model = LinearRegression(fit_intercept=False).fit(x2, y2-y2_int )

# Obtain the coefficient of determination by calling the model with the score() function, then print
r_sq = model.score(x2, y2-y2_int)
print('coefficient of determination:', r_sq)
# Print the Intercept:
print('intercept:', model.intercept_)
# Print the Slope:
print('slope:', model.coef_)
# Predict a Response:
y_pred2 = model.predict(x2) + y2_int
poly_mse2 = mean_squared_error(y2, y_pred2)


plt.figure(figsize=(10, 6))
plt.title(" Linear Regression", size=15)
plt.scatter(x, y)
plt.plot(x, y_pred, c="red")
plt.scatter(x2, y2)
plt.plot(x2, y_pred2, c="red")
plt.xlabel('Angle [deg]')
plt.ylabel('Ts [N/mm^2]')
plt.show()
```